

ABSTRACT

Title of Document: Self-Assembled Photoresponsive and Thermo-responsive Fluids with Tunable Rheology

Rakesh Kumar, Doctor of Philosophy, 2009

Directed By: Professor Srinivasa R. Raghavan, Department of Chemical and Biomolecular Engineering

Fluids whose rheological properties can be tuned by light or heat (termed as photorheological (PR) or thermorheological (TR) fluids, respectively) have attracted a lot of attention as they can be useful in numerous applications such as drug delivery, coatings, sensors, and valves for microfluidic devices. However, current formulations of these fluids suffer from several limitations: in particular, they often require synthesis of complex organic molecules by elaborate procedures, and this limits the widespread use of these fluids. In this dissertation, we seek to develop and investigate new classes of PR and TR fluids based on organic molecules that are readily available and quite inexpensive. Since no new synthesis is required, these systems could prove to be more attractive for a variety of applications.

In the first part of this study, we describe a new aqueous photorheological (PR) fluid based on the zwitterionic surfactant, erucyl dimethyl amidopropyl betaine (EDAB) and the photosensitive molecule, ortho-methoxy cinnamic acid (OMCA). EDAB/OMCA fluids exhibit photogelling, i.e., a large (~ 10,000 fold) increase in viscosity upon exposure to UV radiation. We show that this photogelling is caused by the growth of long

wormlike micelles in the sample. This structural change, in turn, is induced by the UV-induced isomerization of OMCA molecules from their *trans* to *cis* form. Evidence from zeta-potential studies, small-angle neutron scattering (SANS), and rheology are used to systematically reveal the molecular and microstructural mechanism for our results.

In the second part of this study, we turn our attention to non-aqueous solvents and demonstrate a new class of PR fluids using such solvents. The PR effect here relies on transformations of “reverse” micellar structures formed by a well-known lipid (lecithin) in conjunction with *para*-coumaric acid (PCA). Lecithin/PCA fluids exhibit a substantial decrease in viscosity upon exposure to UV light (i.e., photothinning). Initially, the molecules self-assemble into long wormlike micelles, leading to highly viscoelastic fluids. Upon UV irradiation, PCA is photo-isomerized from *trans* to *cis*. This change in geometry induces a transition from long to short micelles. In turn, the solution viscosity is decreased by more than three orders of magnitude. Small-angle neutron scattering (SANS) is used to confirm the dramatic reduction in micellar length.

In the last study, we report a class of aqueous fluids whose viscosity increases upon heating (i.e., thermo-thickening). These fluids are mixtures of telechelic associating polymers (HEURs) and a type of supramolecules called cyclodextrins (CDs) in water. Interestingly, we observe this behavior only with a particular type of CDs, called α -CDs, and not with the other common CD types, i.e., β - and γ -CDs. These results are explained in terms of a competition between the hydrophobic end-caps and the hydrophilic backbone of the polymer for complexation with α -CD molecules. We have also

investigated the effect of amphiphiles (single-tailed surfactants and double-tailed lipids) on the thermo-thickening. The addition of lipids substantially enhances the thermo-thickening behavior, which is explained to be due to an enhancement of the connectivity of hydrophobic junctions by lipid vesicles.

Self-Assembled Photoresponsive and Thermoresponsive Fluids with Tunable Rheology

By

Rakesh Kumar

Dissertation submitted to the Faculty of the Graduate School of the
University of Maryland, College Park, in partial fulfillment
of the requirements for the degree of
Doctor of Philosophy
2009

Advisory Committee:

Prof. Srinivasa R. Raghavan, Dept. of Chemical and Biomolecular Engineering, Chair

Prof. Richard V. Calabrese, Dept. of Chemical and Biomolecular Engineering

Prof. Ganesh Sriram, Dept. of Chemical and Biomolecular Engineering

Prof. Daniel E. Falvey, Dept. of Chemistry and Biochemistry

Prof. Edo Waks, Dept. of Electrical and Computer Engineering

© Copyright by
Rakesh Kumar
2009

Dedication

This dissertation is dedicated to my beloved parents, Shri. Satya Pal Garg and Smt. Nirmala Garg, for their unwavering support for me through all the challenges I've encountered in pursuit of my goals. For my entire life they have encouraged me to always better myself and to challenge myself continually.

Acknowledgements

First and most important, I would like to express my sincere gratitude to my advisor, Dr. Srinivasa Raghavan, for his excellent guidance, unlimited encouragement and patience. He was a great mentor, providing guidance when needed while also allowing enough space to grow on my own as a researcher. He is full of energy and has this special quality of motivating you even when nothing is going right. His attitude towards my shortcomings or occasions when I turned up with half baked ideas or documents in the course of this research has been extremely constructive with prompt suggestions about what would be a way to improve or better way to proceed. I have grown in many ways under his guidance; including improvements in my knowledge and in my writing and presentation skills. On a personal level, I value his friendship and admire his dedication. Thanks for caring.

I would like to thank Dr. Sriram, Dr. Anisimov, Dr. Waks, Dr. Calabrese, Dr. Falvey, Dr. Isaacs, and Dr. Shapiro for serving on my PhD proposal and defense committees, and providing me with valuable suggestions and corrections that have greatly enhanced the quality of my dissertation. I would also like to thank Dr. Waks and Dr. Shapiro for the illuminating discussions and collaborations involving different aspects of my research.

A truly outstanding quality of the chemical engineering department at U. Maryland is its terrific staff. Many thanks to N. Kay Morris, Sue Pleyo, Olivia Noble, Ginette Villeneuve, Patricia Lorenzana, Mike McNicholas, Kathy Lopresti, Faye Levine, Debbie

Snyder, and Julie Holbrook. Every interaction with them brought a smile to my face. Without them I would have been lost.

I am grateful to all of my colleagues in the Complex Fluids and Nanomaterials group: Jae-Ho Lee, Bani Cipriano, Shih-Hung Tung, Hee-Young Lee, Aimee Ketner, Jennifer Hong, Matt Dowling, Chao Zhu, Oluwatosin Ogunsola, Peter Thomas, Kunshan Sun, George Chacko, Khyati Tiwari, Dr. Seung-Won Ko, Elijah George, Vishal Javvaji, Veidhes Basrur, and Chi-Wei Hung. I cherish the friendships I made by joining this great group of people. I would like to thank them for their many insightful and amusing discussions. A special thanks to my friend, Hee-Young Lee, for his positive words and encouragement during the difficult times as well as for our countless “stress relieving smoking seasons”. I would also like to thank my friends & first year homework gang: Aimee, Erin, Jenn, and Ayan. I would always remember our adventures with a smile on my face. Also I would like to acknowledge all the undergraduate students who assisted me through this work, notably: Adil, Alex, Ben, Christine, Golnaz, and Tony.

I want to thank my family for their support and countless sacrifices. My parents raised me to believe that I could achieve anything I set my mind to. My family members: Lovely, Meena, Shaveta, Abu, Mandeep, Shishir, and Prashant, who have been there for me through every crisis, and are an endless source of great joy and love.

I would also like to thank my buddies: Raghu, Jishnu, Kapil, Chandru, Ayan, and Bhargav, who have provided endless support, encouragement, laughter, and food throughout this entire educational process.

I would also like to express my sincere gratitude to my mentors at IIT Kharagpur, Prof. S. Ray, and at NCL Pune, Dr. BD Kulkarni and Dr. VK Jayaraman, for their inspiration and support during difficult times. Without their help and encouragement, I would have never embarked on this educational journey.

Finally, I would like to acknowledge NIST for facilitating the SANS experiments and Dr Ghandehari's lab at UM, Baltimore for facilitating the zeta-potential studies. This work was partially funded by a seed grant from the Small Smart Systems Center (SSSC) at UMD and a CAREER award from NSF-CTS.

TABLE OF CONTENTS

Dedication	ii
Acknowledgements	iii
Table of Contents	vi
List of Figures	viii
1. Introduction and Overview	1
1.1. Problem Statement	1
2.2. Proposed Approach	3
2. Background	6
2.1. Self-Assembly of Surfactants	6
2.2. Wormlike Micelles	8
2.3. Reverse Self-Assembly	12
2.4. Reverse Wormlike Micelles	13
2.5. Photoresponsive Molecules	14
2.6. Cyclodextrins	17
2.7. Associating Polymers	18
2.8. Characterization Techniques – I. Rheology	20
2.9. Characterization Techniques – II. SANS	22
2.10. Characterization Techniques – III. UV-Vis Spectroscopy	25
3. A New Class of Aqueous Photogelling Fluids	27
3.1. Introduction	27
3.2. Experimental Section	31
3.3. Results and Discussion	33
3.4. Conclusions	48

4. “Smart” Non-Aqueous Photothinning Fluids	50
4.1. Introduction	50
4.2. Experimental Section	52
4.3. Results and Discussion	54
4.4. Conclusions	65
5. Aqueous Thermo-Thickening Fluids	66
5.1. Introduction	66
5.2. Experimental Section	69
5.3. Results and Discussion	71
5.4. Conclusions	85
6. Conclusions and Recommendations	87
6.1. Conclusions	87
6.2. Recommendations for Future Work	89
6.2.1. Reversible PR Fluids	89
6.2.2. Microfluidic Devices Incorporating PR / TR Fluids.....	89
6.2.3 Methods for Writing and Erasing Patterns in Gels with Light	90
7. References	94

LIST OF FIGURES

Figure 1.1. Schematic illustrating the working principle of a stimulus-responsive fluid that can reversibly change its flow properties upon exposure to light or heat. The flow properties are dependent upon the internal structure in the fluid.

Figure 2.1. Schematics depicting the connection between the geometry of amphiphilic molecules and the structures they form in water. The hydrophilic heads of the amphiphiles are shown in blue and the hydrophobic tails in red.

Figure 2.2. Schematic showing the structure of an individual wormlike micelle as well as the entanglement of micellar chains into a transient network.

Figure 2.3. Schematic illustrating different routes for preparing wormlike micelles.

Figure 2.4. Schematics depicting the connection between the geometry of amphiphilic molecules and the structures they form in oil. The hydrophilic heads of the amphiphiles are shown in blue and the hydrophobic tails in red.

Figure 2.5. Structure of reverse wormlike micelles and their entangled network. The micelles have a locally cylindrical structure, as shown by the close-up.

Figure 2.6. Photoisomerization of stilbene (top) and azobenzene (bottom) upon irradiation by light. In case of azobenzene, the *cis* to *trans* isomerisation can also be induced by heat.

Figure 2.7. Truncated cone-shaped conformation of β -CD.

Figure 2.8. Architecture of a telechelic associating polymer and the structures formed by its self-assembly in aqueous solution.

Figure 2.9. Schematic of a SANS experiment (adapted from www.gkss.de).

Figure 3.1. Composition of photogelling fluids described in this Chapter. The fluids consist of the zwitterionic surfactant, EDAB and the organic derivative, OMCA. When EDAB is combined with *trans*-OMCA, the result is a low-viscosity fluid. Upon UV irradiation, *trans*-OMCA is photoisomerized to *cis*-OMCA, which causes a substantial rise in fluid viscosity. The viscosity rise is associated with the growth of EDAB micelles.

Figure 3.2. UV-Vis spectra of *trans*-OMCA before irradiation, *trans*-OMCA after UV irradiation, and *cis*-OMCA. Each sample is an aqueous solution containing 1 mM of the corresponding additive. The drop in absorbance and blue shift in the *trans*-OMCA curve after UV irradiation indicate that the molecule has been photoisomerized to its *cis* form.

Figure 3.3. Zero-shear viscosity η_0 of 50 mM EDAB + OMCA mixtures as a function of the OMCA concentration. Data are shown for samples containing either *trans*-OMCA or

cis-OMCA and for *trans*-OMCA samples after 20 min of UV irradiation. As shown by the arrow, the high *trans*-OMCA samples undergo photogelling, i.e., they experience a significant light-induced increase in viscosity.

Figure 3.4. Photographs and dynamic rheological data (frequency spectra) for a sample containing 50 mM EDAB + 130 mM *trans*-OMCA (A) before and (B) after UV irradiation. Before irradiation, the sample is water-like and shows a purely viscous response in dynamic rheology. After UV irradiation for 30 min, the sample is gel-like and shows a strongly viscoelastic response. Note that the latter sample does not flow easily out of the tilted vial and also note the presence of trapped bubbles in the fluid.

Figure 3.5. Steady-shear rheology of a 50 mM EDAB + 130 mM *trans*-OMCA sample before irradiation and after UV irradiation for various periods of time (as indicated on the plot). The sample is observed to switch from a low-viscosity, Newtonian fluid to a highly viscous, shear-thinning fluid with progressive irradiation.

Figure 3.6. SANS data and analysis for EDAB/*trans*-OMCA mixtures before and after 30 min of UV irradiation. Plots (a) – (c) show scattering spectra (intensity I vs. wave vector q) for three samples, each with 50 mM EDAB and with OMCA concentrations of 150, 170, and 190 mM, respectively. Plot (d) presents analysis of the data for the 190 mM OMCA sample using the IFT method. See text for details.

Figure 3.7. Zeta-Potential of 2.5 mM EDAB + OMCA mixtures as a function of the OMCA concentration. Data are shown for *trans*-OMCA, *cis*-OMCA, and *trans*-OMCA samples after 30 min of UV irradiation. Lines through the data are guides for the eye.

Figure 3.8. Mechanism for photogelling in EDAB samples. Addition of *trans*-OMCA increases the effective headgroup charge due to adsorption of the counterions, and this leads to short micelles. When *trans*-OMCA is photoisomerized to *cis*-OMCA, the *cis* isomer desorbs from the micelles, effectively lowering the headgroup charge. As a result, the micelles grow into long, wormlike structures, and the viscosity thereby increases substantially (photogelling).

Figure 3.9. Cycling of viscosity by UV irradiation and sample composition. The initial sample (50 mM EDAB + 130 mM of *trans*-OMCA) is exposed to UV light for 40 min, causing a 10,000-fold rise in viscosity. Then, 50 mM of *trans*-OMCA is added, which drops the viscosity back to its original value. The resulting sample is then irradiated again for 40 min, which induces a 50-fold increase in viscosity. Finally, addition of a further 50 mM of *trans*-OMCA again decreases the viscosity back to its original value.

Figure 4.1. Molecular structures of the *trans* isomers of *p*-coumaric acid (PCA), *m*-coumaric acid (MCA), and *o*-coumaric acid (OCA). Their polarities are in order: PCA > MCA > OCA.

Figure 4.2. UV-Vis spectra of *trans*-PCA before irradiation and after UV irradiation. The sample contains 1mM PCA and 5 mM lecithin in cyclohexane. The drop in absorbance

and slight blue shift in the *trans*-PCA curve after UV irradiation indicate that the molecule has been photoisomerized to its *cis* form. Lecithin was added to dissolve PCA in cyclohexane and it does not have any significant effect on PCA spectra.

Figure 4.3. Photographs of a sample containing 100 mM lecithin + 110 mM *trans*-PCA in cyclohexane (A) before and (B) after UV irradiation. Before irradiation, the sample is highly viscoelastic and holds its own weight along with a magnetic stir bar in an inverted vial. After UV irradiation for 30 min, the sample is transformed into a low-viscosity fluid that flows very easily and does not entrap air bubbles.

Figure 4.4. Effect of UV irradiation on the rheology at 25°C of a sample containing 100 mM lecithin + 110 mM *trans*-PCA in cyclohexane (A) Dynamic rheological data, before and after UV irradiation for 30 min; (B) Steady-shear rheological data before and after UV irradiation for varying periods of time (as indicated on the plot). The sample is observed to switch from a highly viscoelastic, shear-thinning response to a low-viscosity, Newtonian response upon UV irradiation.

Figure 4.5. Zero shear viscosity η_0 of lecithin + *trans*-PCA in Cyclohexane at 25°C as a function of P_0 , the molar ratio of PCA to lecithin, with the lecithin concentration held constant at 100 mM. Data are shown for samples before (red circles) and after 30 min of UV irradiation (blue squares).

Figure 4.6. Zero shear viscosity η_0 of lecithin + *trans*-PCA in six different organic solvents, before and after UV irradiation. The lecithin concentration is fixed at 100 mM, while the [PCA]:[lecithin] molar ratios P_0 are those corresponding to the maximum viscosity in each solvent. After UV irradiation for 30 min, all samples showed a substantial drop in viscosity, i.e., photothinning.

Figure 4.7. SANS data and analysis for lecithin/*trans*-PCA/cyclohexane mixtures before and after 30 min of UV irradiation. Plots (a) – (b) show scattering spectra (intensity I vs. wave vector q) for three samples, each with 100 mM lecithin and with PCA concentrations of 60 and 70 mM, respectively. Plot (d) presents analysis of the data for the 60 mM PCA sample using the IFT method. See text for details.

Figure 4.8. Mechanism for photothinning in lecithin/PCA/oil samples. The polar *trans*-PCA forms H-bonds with lecithin headgroups, increasing the effective headgroup area. This favors growth of reverse wormlike micelles and thereby leads to a high viscosity. When *trans*-PCA is photoisomerized, the less polar *cis*-PCA has only a weak H-bonding tendency, and thus unbinds from the headgroups. The lowered headgroup area favors the shortening of micelles, and in turn the sample viscosity drops (photothinning).

Figure 5.1. Schematics of (a) the RM825 associating polymer and (b) the cyclodextrins (CDs) studied.

Figure 5.2. Zero-shear viscosity η_0 at room temperature (25°C) for 5% RM825 + CD mixtures as a function of the CD concentration. Data are shown for α -, β -, and γ -CD. In all cases, the viscosity drops with increasing [CD].

Figure 5.3. Viscosity as a function of temperature for solutions containing 7% RM825 and 14 mM of α -, β -, or γ -CD. The complex viscosity η^* is shown; similar results are available for the steady-shear viscosity. The viscosity decreases with temperature for the β - and γ -CD samples whereas the sample with α -CD shows an increase in viscosity with temperature (thermo-thickening).

Figure 5.4. Thermo-thickening responses for different compositions of RM825 and α -CD. (a) Constant polymer concentration (5%), varying [α -CD]. (b) Different [polymer] and [α -CD] such that the solutions have approximately the same viscosity at room temperature.

Figure 5.5. SANS data at low (25°C) and high (50°C) temperatures for solutions containing 5% RM825 and different concentrations of α -CD. The solid lines through each curve are fits to equation 5.1.

Figure 5.6. Correlation lengths ξ obtained from fits of equation 5.1 to the SANS data in Figure 5.5. The values are shown as functions of the α -CD concentration and for the two different temperatures. Lines through the data are guides for the eye.

Figure 5.7. Viscosity vs. temperature for solutions of 6% RM825 + 12 mM α -CD in the absence and presence of the cationic surfactant, CTAB. In the presence of CTAB, the response shifts from thermo-thickening to thermo-thinning.

Figure 5.8. Viscosity vs. temperature for solutions of 6% RM825 + 12 mM α -CD in the absence and presence of vesicles of the lipid, lecithin. The presence of lecithin vesicles accentuates the thermo-thickening response.

Figure 5.9. Viscosity vs. temperature for solutions of 5% Borchigel PW25 + 10 mM α -CD in the absence and presence of 10 mM lecithin vesicles. This HEUR/ α -CD mixture also shows thermo-thickening and lecithin vesicles again enhance the effect.

Figure 5.10. (a) Mechanism for thermo-thickening in HEUR/ α -CD mixtures. At low T , the hydrophobes on HEUR chain ends are capped by α -CDs and the viscosity is hence low. Upon heating, some of the α -CDs detach from the hydrophobes and bind to the PEO backbone of the HEUR chains. The liberated hydrophobes associate with each other and thereby enhance the solution viscosity. (b) Mechanism for the enhancement of thermo-thickening by lipid vesicles. The vesicles do not bind to the α -CD and the solution has a low viscosity at low T . Upon heating, some hydrophobes get freed and these can either associate with each other or with the bilayers of the vesicles. The vesicles, in effect, increase the connectivity of HEUR chains and this further enhances the viscosity.

Figure 6.1. Reversible switching of SP to MC regulated by UV and visible light.

Figure 6.2. Reversibly creating and erasing spatial patterns on a SP-doped gel by irradiating through a mask.

Figure 6.3. Reversibly writing and erasing on SP-doped gel by simple green-light laser pointer.

Chapter 1

Introduction and Overview

1.1 Problem Statement

Recently there has been a lot of interest in fluids whose rheological properties can be controlled by external field e.g., heat, electrical or magnetic field, pH, and light.¹⁻¹⁴ This extensive attention to field-driven rheology modulation is motivated by the potential of such fluids in a variety of applications such as drug delivery, wound covering, cancer therapy, sensors, microfluidics or MEMS devices, paints, coatings, personal care products, and traditional mechanical engineering applications like dampers, shock absorbers, and brakes.¹⁻¹⁴ Owing to their obvious potential, many researchers have been working on developing a variety of new stimuli-responsive fluids and many breakthroughs have been made. However, most of these fluids suffer from many serious shortcomings. These include, for example, a lack of precise spatial control over stimuli (critical in microscale or nanoscale applications), aggregation and instability with time in some stimuli-responsive systems,⁴⁻⁶ and issues like poor biodegradability and poor resilience in the case of thermogelling systems used for drug delivery.² Therefore, there is plenty of scope and motivation for further continued research and development in this field of stimuli-driven rheology modulation.

This dissertation seeks to develop and investigate new formulations of stimuli-responsive fluids whose rheological properties can be tuned by *light* or *heat*. These fluids

are termed as *photorheological* (PR) fluids if the stimulus used is light and *thermorheological* (TR) fluids if the stimulus used is temperature. The working principle will be to exploit molecular self-assembly, i.e., the spontaneous aggregation of surfactant or polymer molecules when placed in a solvent, as illustrated by Figure 1.1. On the left, the molecules present in the fluid self-assemble into discrete spherical nanostructures, which impart a low viscosity to the sample. Under the action of the stimulus (light or temperature), the self-assembly is switched such that the molecules form a connected network of chains, and the sample, in turn, exhibits a high viscosity. Thus the transition in macroscopic properties (rheology) is coupled to those at the nanostructural and molecular levels. In principle, these transitions would be reversible as well.

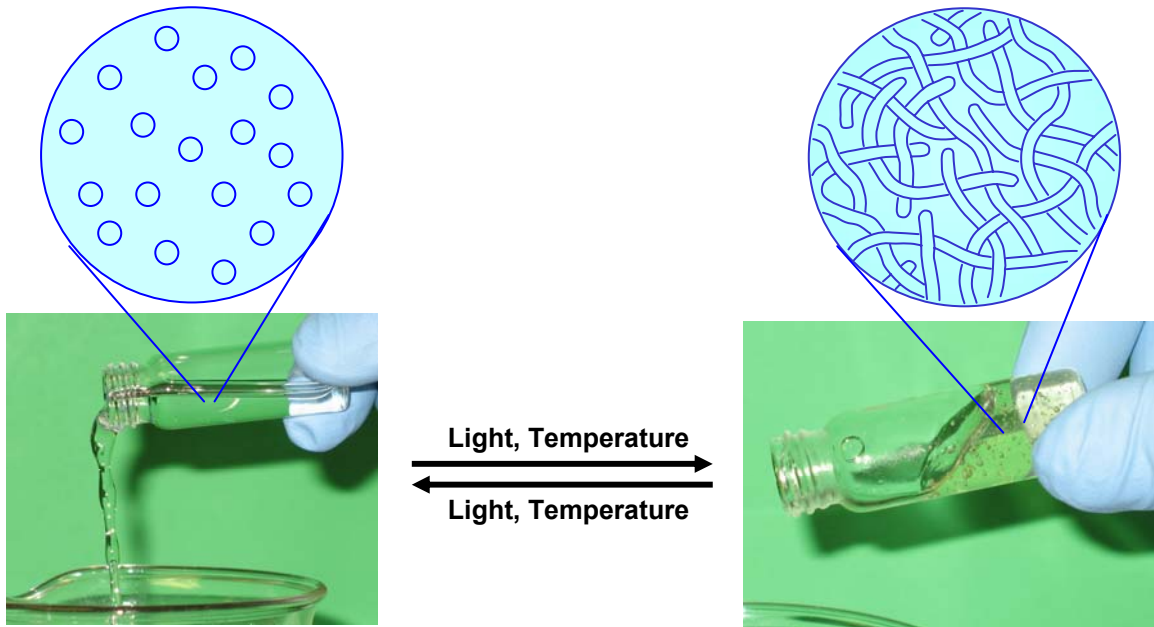


Figure 1.1. Schematic illustrating the working principle of a stimulus-responsive fluid that can reversibly change its flow properties upon exposure to light or heat. The flow properties are dependent upon the internal structure in the fluid.

One important motivation for our work is that the PR and TR fluids that are currently available are accessible only to a few research groups. This is so because such fluid formulations usually rely on complicated organic molecules that need to be specially synthesized in the laboratory. Particularly in the case of PR fluids, the synthesis procedures for these molecules (e.g., photosensitive surfactants or polymers bearing an azobenzene or stilbene moiety) tend to be difficult and cumbersome.^{9,10,12-14} Even in the case of TR fluids, the molecules involved are often not commercially available, or if they are, they tend to be very expensive.¹⁻³ Thus, the high cost and/or labor-intensive synthesis procedures make current PR and TR fluids unattractive for commercial exploitation. If simple and inexpensive routes could be found for making such fluids, it would open the door for a great deal of application-oriented research (e.g., microfluidics valves, sensors), both in academia as well as industry.

1.2 Proposed Approach

In this study, we will develop new formulations of PR and TR fluids based on simple, readily available, and inexpensive molecules. Further, we wish to gain a better fundamental understanding of the PR and TR effects at three different length scales:

- **Molecular (Sub-Nano) Scales:** What transitions in molecular geometry or structure occur upon application of the stimulus? We will use UV-Vis spectroscopy to probe such molecular changes.
- **Nano-Micro Scales:** What transitions in self-assembled structure (type, size, shape, surface charge) occur upon application of the stimulus? We will use scattering techniques and zeta potential measurements to study these aspects.

- **Macro Scale:** How do the macroscopic rheological properties change upon application of the stimulus? How fast do these changes occur? We will use both steady and dynamic rheological techniques to study our samples. Ultimately, we will correlate the changes occurring at each length scale to obtain a comprehensive picture of our system.

The rest of this dissertation is organized as follows. **Chapter 2** provides a detailed background on molecular self-assembly and characterization techniques. In **Chapter 3**, we present a novel PR formulation made simply by mixing a commercially available surfactant and a photoadditive in water. This PR fluid exhibits a 10,000-fold increase in viscosity upon irradiation by UV light i.e., a *photogelling* effect. **Chapter 4** extends the concepts developed in Chapter 3 to the discovery of non-aqueous PR fluids in organic solvents. The fluids exhibit a rapid and controllable decrease in viscosity upon exposure to UV radiation (i.e., photothinning). Finally, in **Chapter 5**, we report a TR system in which the viscosity increases significantly upon heating (i.e., thermo-thickening). A variety of techniques, including UV-Vis spectroscopy, rheological measurements, and small-angle neutron scattering (SANS) are used in all of above mentioned studies. Details of these techniques are also given in Chapter 2.

The significance of this work is that it seeks to overcome current limitations in the field of stimuli-driven rheology modulation. We hope that the availability of new, simple PR and TR fluid formulations will help to popularize these fluids both in academia and industry. We anticipate that the new directions we set forth in this field will

be further explored by other researchers, and this increased research will ultimately lead to practical applications for PR and TR fluids in both existing as well as emerging technologies.

Chapter 2

Background

This dissertation is concerned with stimuli-responsive self-assembled fluids whose rheological properties can be tuned by light or heat. In this chapter, we will discuss the fundamentals of amphiphile self-assembly in aqueous and non-aqueous media. In addition, we will describe the basic properties of cyclodextrins, associating polymers, and of photo-induced transitions in molecules. We will finish with a brief discussion of characterization techniques such as rheology, small-angle neutron scattering (SANS), and UV-Vis spectroscopy.

2.1 Self-Assembly of Surfactants

Surfactants (also referred to as detergents or lipids) are molecules that combine both a hydrophilic moiety (head) and a hydrophobic moiety (tail) into a single molecule. Figure 2.1 depicts typical surfactant molecules with blue hydrophilic heads and red hydrophobic tails. When added to a polar solvent such as water, surfactants spontaneously aggregate into various types of structures, the most common of which are micelles. This process of spontaneous aggregation is known as self-assembly. For surfactants to form micelles, their concentration should be higher than a certain threshold concentration known as critical micelle concentration (CMC). Self-assembly is a thermodynamically driven process i.e., it involves a minimization of the Gibbs free energy of the system. The crucial driving force for this process is the hydrophobic effect,

i.e., the gain in entropy of water molecules when surfactant hydrophobes are removed from water and buried in a micelle.

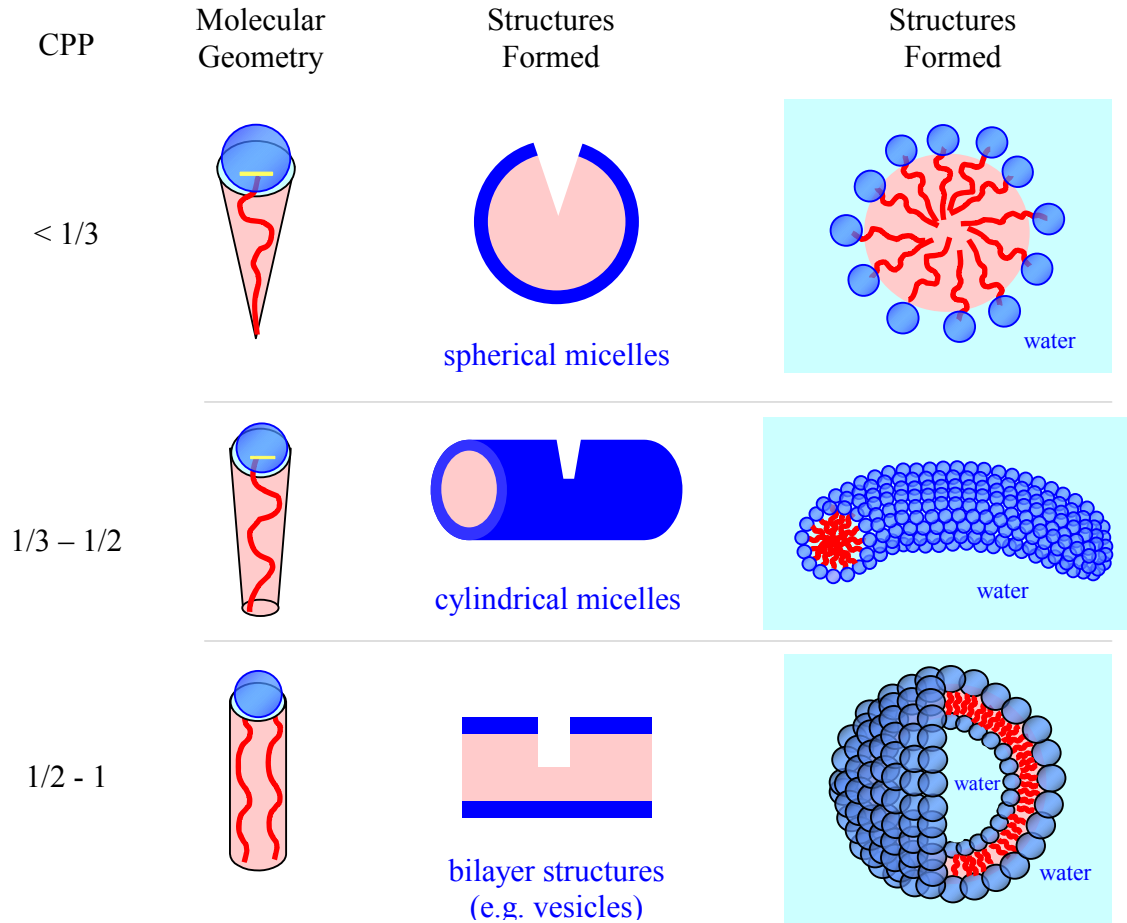


Figure 2.1. Schematics depicting the connection between the geometry of amphiphilic molecules and the structures they form in water. The hydrophilic heads of the amphiphiles are shown in blue and the hydrophobic tails in red.

The size and shape of self-assembled structures depends on the molecular structure and charge of the surfactant, its concentration in solution, and also on the physico-chemical conditions like temperature, ionic strength and salt concentration. A variety of shapes are possible for micelles such as spherical or cylindrical, and

intermediate shapes like oblate or prolate ellipsoids. Apart from micelles, surfactants can self-assemble into other structures such as bilayers or vesicles. The size of these structures can also vary from a few nanometers to several microns. How can one predict the kind of structure that will be formed by a surfactant in a given solution? Qualitative predictions can be made based on the net geometry of the surfactant molecules. The geometrical quantity dictating this correlation is known as the critical packing parameter (CPP), defined as:¹⁵

$$\text{CPP} = \frac{a_{\text{tail}}}{a_{\text{hg}}} \quad (2.1)$$

where a_{tail} is the average cross-sectional area of the hydrophobic tail and a_{hg} is the effective cross-sectional area of the hydrophilic head.¹⁶⁻¹⁸ The larger the CPP, the more curved the aggregate, as shown in Figure 2.1. In particular, for $\text{CPP} \sim \frac{1}{3}$ (molecules shaped like a cone), surfactants tend to assemble into spherical micelles in water, whereas for CPP between $\frac{1}{3}$ and $\frac{1}{2}$ (molecules shaped like truncated cones), cylindrical micelles are expected. Finally, for molecules shaped like cylinders, i.e., having $a_{\text{tail}} \approx a_{\text{hg}}$ and a $\text{CPP} = 1$, bilayer structures (vesicles) are likely to be formed.

2.2 Wormlike Micelles

As mentioned above, surfactants self assemble into cylindrical micelles around a $\text{CPP} = \frac{1}{2}$. Under specific conditions, these cylindrical micelles can grow into “polymer-like” elongated and flexible chains, and they are then known as wormlike or threadlike micelles (Figure 2.2).^{19,20} In general, these wormlike micelles have a diameter similar to spherical micelles (5-10 nm) while their end-to-end length (referred to as the contour length) can be as long as a few microns (i.e., > 1000 nm).²⁰⁻²⁴ Similar to a solution of

flexible polymers, wormlike micelles tend to become entangled in solution. This entanglement results in a transient network of chains (Figure 2.2) and in turn, the solution becomes highly viscous and displays remarkable viscoelastic or elastic properties. The term viscoelastic implies that the solution has both viscous (or liquid-like) character and elastic (or solid-like) character.

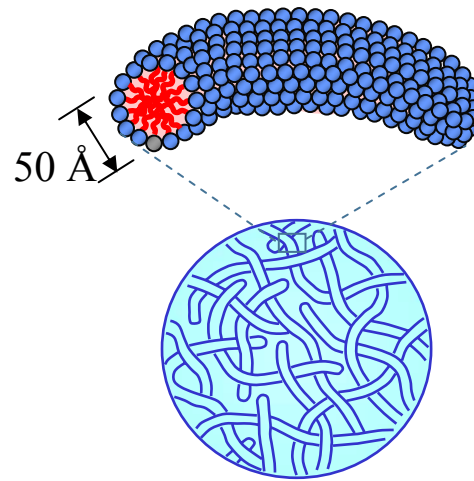


Figure 2.2. Schematic showing the structure of an individual wormlike micelle as well as the entanglement of micellar chains into a transient network.

Another characteristic property of wormlike micellar solutions is their flow-birefringence i.e., when a vial containing a wormlike micellar solution is shaken and observed under crossed-polarizers, we see bright streaks of light in the sample. Birefringence (also known as double refraction) refers to a difference in refractive indices of a material along mutually perpendicular directions. It is a characteristic property of anisotropic materials such as liquid crystals.²⁵ For wormlike micelles, flow or shear causes the chains to align along the direction of shear, thus making the sample

temporarily anisotropic. Note that wormlike micelles do not show birefringence at rest, i.e., the chains are randomly oriented at rest and the solution is completely isotropic.

Wormlike micelles can be formed by a variety of surfactants such as cationic, anionic, nonionic, and zwitterionic.^{19,20} In general, charged surfactants do not self-assemble into long wormlike micelles by themselves. They form wormlike micelles in the presence of co-surfactants, opposite charged or non-ionic surfactants, salts or appropriate counterions (Figure 2.3).

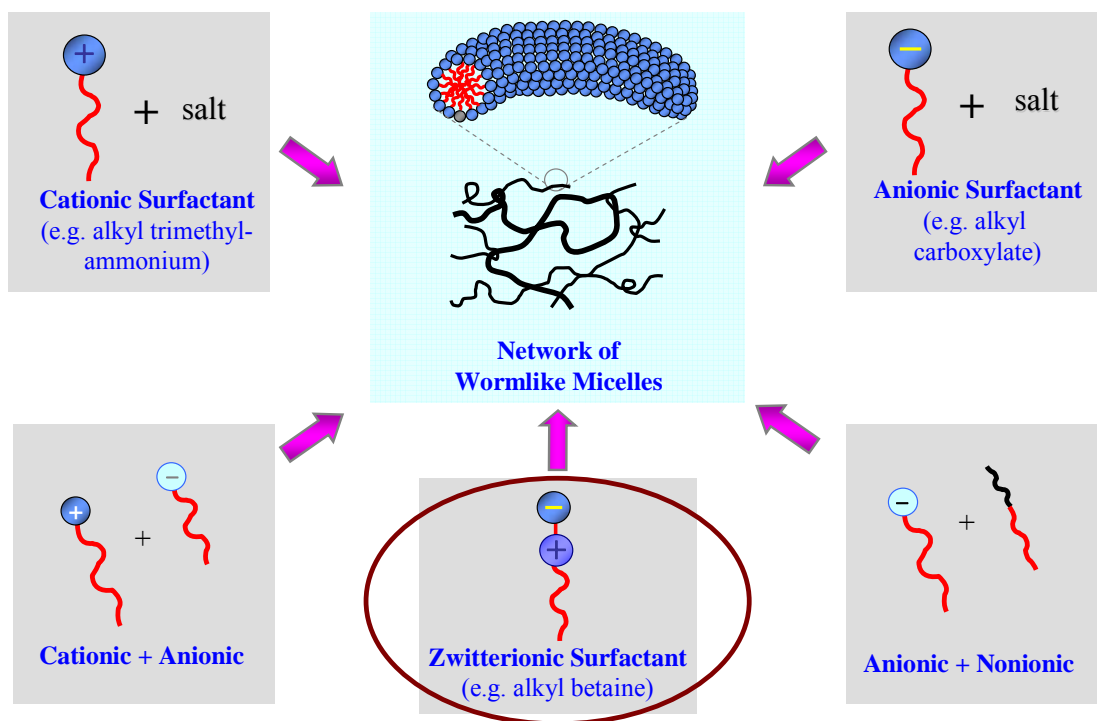


Figure 2.3. Schematic illustrating different routes for preparing wormlike micelles.

The most well known wormlike micellar systems are based on cationic surfactants with a long hydrophobic tail, such as cetyl trimethylammonium bromide (CTAB).^{22,26-30}

CTAB is a surfactant with 16-carbon tail and a cationic headgroup. Ionic surfactants such as CTAB have strong electrostatic repulsions between the head groups, which cause the effective area of the head to be large. Therefore the molecule has a cone like geometry i.e., $CPP = 1/3$ and in turn forms spherical micelles. The addition of salt screens the electrostatic repulsion between the charged head groups, which results in a reduction in the effective headgroup area and in turn the CPP increases from $1/3$ to $1/2$. This increase in the CPP induces a conversion from spherical to cylindrical micelles, which then grow uniaxially to become worms.

Unlike the cationic surfactants discussed above, *zwitterionic* surfactants can assemble into long wormlike micelles without addition of salt or other chemicals.^{20,24,31-36} The reason for this lies in the nature of the surfactant headgroup. Zwitterionic surfactants contain both positive and negative charges in their head group. For example, one class of zwitterionic surfactants called *betaines* have a positively charged quaternary ammonium group and a negatively charged carboxylate group.³⁶ The proximity of the positive and negative charges means that the net charge on the surfactant headgroup is quite low. A low charge implies weak headgroup repulsions, and therefore a smaller effective headgroup area (a_{hg}). As a result, zwitterionic surfactant molecules have a geometry close to a truncated cone and tend to assemble into wormlike micelles on their own. In Chapter 3, we will use a zwitterionic betaine surfactant to form wormlike micelles.

2.3 Reverse Self-Assembly

Molecular self-assembly can also occur in a variety of organic solvents in addition to water. Generally, the organic solvent must be either highly polar or highly non-polar to allow self-assembly of amphiphiles. Self-assembled structures formed in highly non-polar solvents have a reversed geometry compared to those in water. For example, in a reverse micelle (Figure 2.4), the hydrophobic tails (depicted in red) stick out into the oil, while the hydrophilic headgroups (blue) are shielded from the oil phase by being buried in the interior of the micelle.

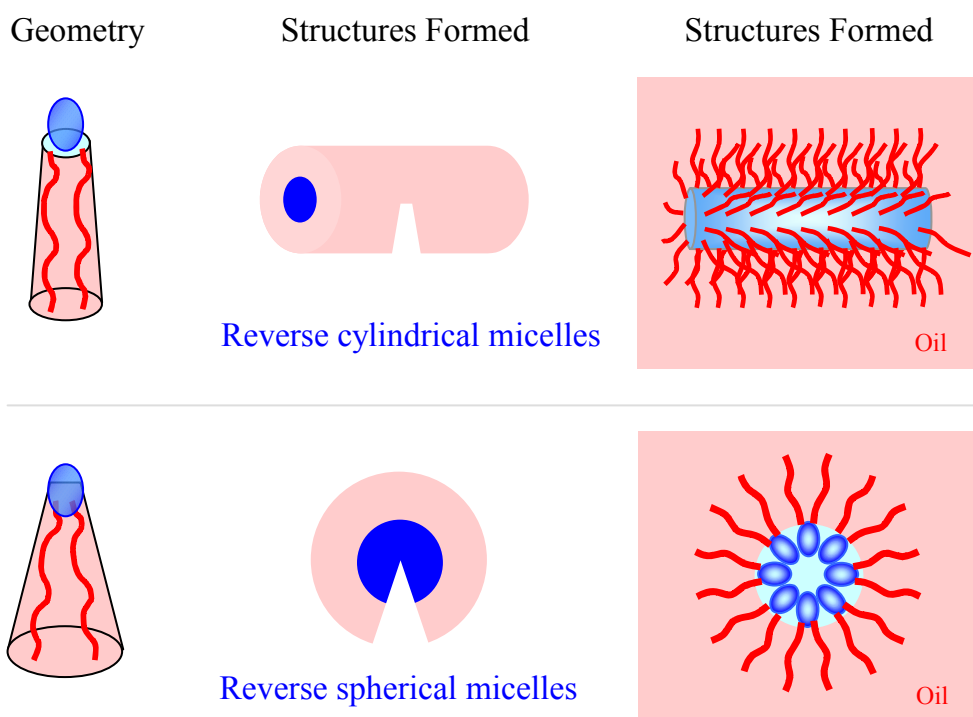


Figure 2.4. Schematics depicting the connection between the geometry of amphiphilic molecules and the structures they form in oil. The hydrophilic heads of the amphiphiles are shown in blue and the hydrophobic tails in red.³⁷

From the viewpoint of molecular geometry, the CPP values for amphiphiles in non-polar solvents need to be greater than 1, which implies that the molecule has a large tail area and a small headgroup area. In the limit of a CPP much larger than 1, the molecules will assemble into reverse spherical micelles, as depicted at the bottom of Figure 2.4. If there is a slight reduction in the tail group area or increase in head group area, the CPP will move closer to 1. This in turn will cause a transition from reverse spherical micelles to reverse cylindrical micelles, depicted at the top of Figure 2.4. As reverse cylinders grow into very long and flexible chains, they become “reverse wormlike micelles”, and these are discussed in the next section.

2.4 Reverse Wormlike Micelles

Similar to wormlike micelles in water, it is also possible to form reverse wormlike micelles in oil. Figure 2.5 shows the structure of these reverse wormlike micelles; again, note that the hydrophobic tails are directed outward and the hydrophilic heads inward.

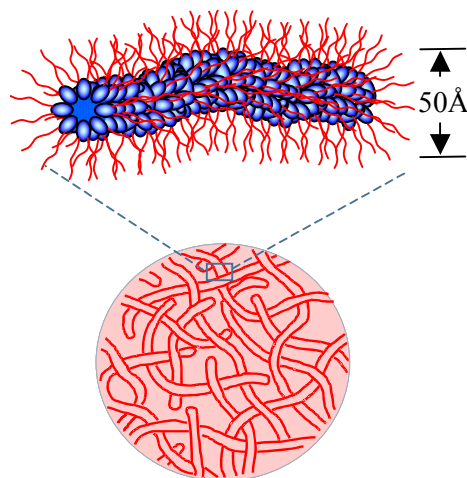


Figure 2.5. Structure of reverse wormlike micelles and their entangled network.³⁸ The micelles have a locally cylindrical structure, as shown by the close-up.³⁷

Only a few amphiphilic formulations have been reported to contain reverse worms,³⁹⁻⁴³ most of which are based on the phospholipid, lecithin. Lecithin tends to assemble into reverse spherical structures when added to non-polar solvents, such as alkanes and cycloalkanes. Upon the addition of a small amount of certain highly polar solvents such as water, the reverse spheres will grow uniaxially into reverse wormlike micelles.⁴¹ The water is believed to sit at the micellar interface and form hydrogen bonds with the phosphate headgroup of the lecithin, thus bridging the lecithin molecules together.⁴⁴⁻⁴⁵ The hydrogen bonds are thus the driving force for the growth of these reverse wormlike micelles. From a geometric standpoint, the water causes an increase in the CPP by increasing the area of the lecithin headgroup, and this in turn causes the transition from spherical to wormlike reverse micelles.

2.5 Photoresponsive Molecules

Photoresponsive molecules go through a chemical transformation upon irradiation by light at certain wavelengths. We are especially interested in light-induced changes in the geometry of molecules in the absence of chemical reactions. In particular, we are interested in photoisomerisation processes (e.g., a *trans* to *cis* photoisomerization). Such transitions occur in molecules having a C-C double bond or an N-N double bond e.g., stilbenes, phenylalkenes, and azobenzenes.

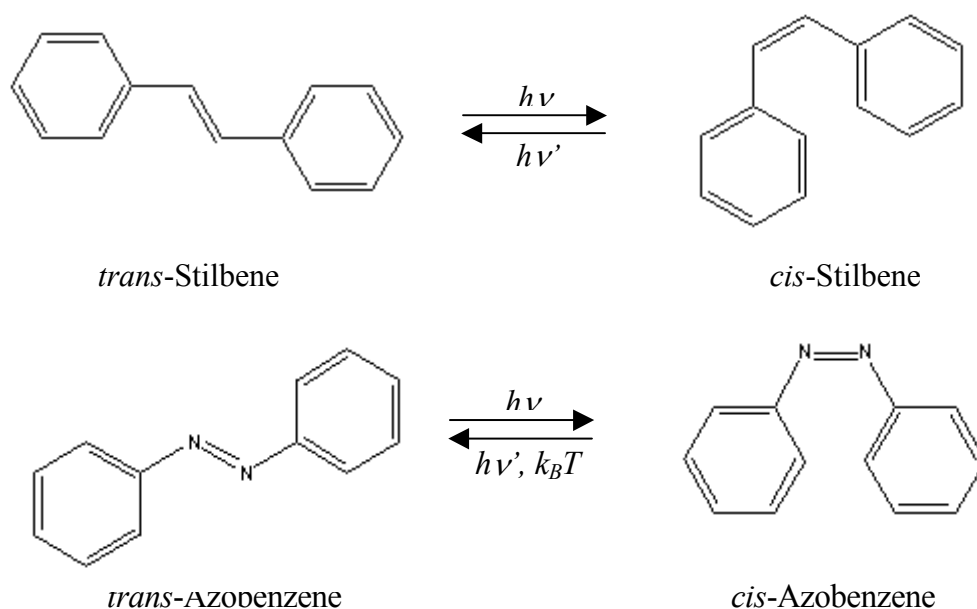


Figure 2.6. Photoisomerization of stilbene (top) and azobenzene (bottom) upon irradiation by light. In case of azobenzenes, the *cis* to *trans* isomerisation can also be induce by heat.

- Stilbenes:** Stilbene (IUPAC name; 1,2-diphenylethylene) has a C-C double bond with phenyl groups on each carbon atom (Figure 2.6). In the *trans* form, the phenyl groups are on opposite sides of the double bond, while in the *cis* form, they are on the same side of the double bond. Under ambient conditions (ground state) the *trans* and *cis* isomers are separated by an energy barrier that impedes rotation about the C-C double bond.^{46,47} However, upon irradiation by UV light, the *trans*-stilbene molecule goes from its ground state to an excited state as an electron is transferred from the pi bonding (π) to the pi anti-bonding (π^*) orbital.^{47,48} In the excited state, the energy barrier for rotation about the C-C double bond is reduced. Thus, when the molecules fall back to the ground state, they return in equal amounts of *cis*- and *trans*-stilbene. Further UV irradiation converts more of the remaining *trans* isomers to *cis*. At

equilibrium (or more precisely, the “photostationary state”), the predominant isomer will be *cis* (e.g., > 80%), but a fraction of *trans* isomers will always remain. In comparison with the *trans*, the *cis* isomer generally absorbs light at shorter wavelengths: for example, the absorption peak is at 254 nm for *cis*-stilbene compared to 313 nm for *trans*-stilbene. In turn, when *cis*-stilbene is irradiated with UV light at 254 nm, it tends to isomerize back to its *trans* form.

- **Azobenzenes**: Azobenzenes (IUPAC name: 1,2-phenyldazene) are another class of photosensitive molecules. As shown in Figure 2.6, azobenzene has an N-N double bond with a phenyl group on each nitrogen. Azobenzene compounds generally have two absorption peaks: a high-intensity peak at UV wavelengths and a low intensity peak in the visible range of the wavelength spectrum.^{49,50} When *trans*-azobenzene is irradiated with UV light ($330 < \lambda < 380$ nm), it isomerizes to its *cis* form with the photostationary state corresponding to approximately 80% *cis* and 20% *trans*. On the other hand, when *cis*-azobenzene is irradiated with visible light ($\lambda > 420$ nm), it isomerizes back to a mostly *trans* form.⁵¹ Furthermore, the *cis* to *trans* transition of azobenzene can also be carried out by heat instead of light.
- **Phenylalkenes**: These are molecules with a single phenyl ring attached to a C-C double bond. For example, cinnamic acid (IUPAC name: 3-phenyl-2-propenoic acid), has a phenyl ring on one carbon of the double bond and a carboxylic acid group on the other carbon. Cinnamic acid derivatives tend to have two absorption peaks, both in the UV range: a low-intensity peak at longer wavelengths and a higher intensity

peak at shorter wavelengths. The absorption peaks of *trans* and *cis*-cinnamic acid fall within a few nm of each other (280 nm for *cis* and 283 nm for *trans*).⁵² However, the absorbance is much lower for the *cis* isomer over the entire spectrum. UV irradiation can thus induce a *trans* to *cis* isomerization of cinnamic acid, but the reverse *cis* to *trans* isomerization cannot be accomplished with light. In our work in Chapter 3, we will use a cinnamic acid derivative, viz. ortho-methoxy cinnamic acid (OMCA) that also can be transformed from its *trans* to *cis* isomer upon UV irradiation, but reverse photoisomerization is not possible.

2.6 Cyclodextrins

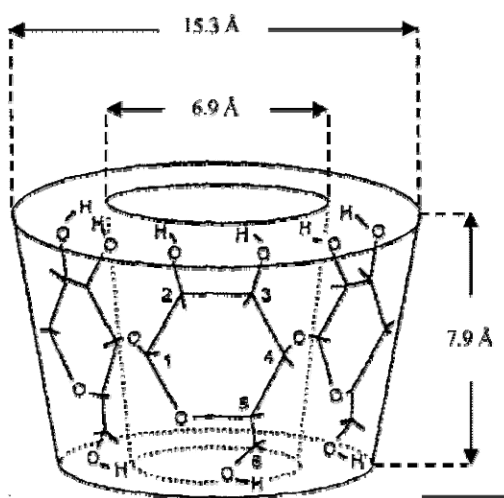


Figure 2.7. Truncated cone-shaped conformation of β -CD.⁵³

Cyclodextrins (CDs) are cyclic oligosaccharides containing D-(+) glucopyranose units attached by α -(1,4) glucosidic bonds, as shown in Figure 2.7.⁵⁴ They are rigid, truncated cone-shaped structures, with an internal cavity of size 5 to 8 Å depending upon the number of glucopyranose units. The wide side of the truncated cone is bordered by

the secondary hydroxyl groups (2-OH and 3-OH), while the primary hydroxyl groups (6-OH) are on the narrow side. The molecule is stiffened by hydrogen bonding between the 2-OH and 3-OH groups around its outer rim. Note that all hydroxyl groups are located on the outside of the molecular cavity, thereby making the outer surface hydrophilic. On the other hand, no hydroxyl groups are located in the inner cavity, which is thus hydrophobic. CDs thus have hydrophilic outer surfaces and hydrophobic inner cavities. Because of their unique structure, CDs can form host-guest inclusion complexes with various hydrophobic guest molecules or hydrophobic parts of these molecules.⁵³⁻⁶¹ Note that the bonding between the CD and the guest is through non-covalent interactions. Table 2.1⁶² lists the properties of the three naturally occurring CDs, which are labeled α -, β -, and γ -CDs. These natural CDs are produced from starch by enzymatic degradation. In our research, we will use CDs to create new TR fluids, as described in Chapter 5.

Type of CD	Number of glucose units	Cavity diameter Å	Molecular Weight	Solubility in water (g/L)
α	6	4.7-5.3	972	145
β	7	6-6.5	1135	18.5
γ	8	7.5-8.3	1297	232

Table 2.1. Properties of the three naturally occurring cyclodextrins.⁶²

2.7 Associating Polymers

The term “associating polymer” generally refers to a water-soluble polymer bearing hydrophobic groups either on its ends or along the backbone.^{63,64} When the

hydrophobes are present on the chain ends, the structure is called telechelic.⁶⁴ An example is the hydrophobic ethoxylated urethane (HEUR) architecture, where the backbone is composed of poly(ethylene oxide) (PEO) and this is linked to hydrophobic end-caps (typically *n*-akyl moieties) through urethane spacers (Figure 2.8).⁶⁴ As their name indicates, associating polymers associate in aqueous solution through their hydrophobes. This results in “flower micelles” that have a hydrophobic core surrounded by a corona of looping PEO segments.^{63,64} Adjacent flower micelles also get connected through bridging PEO segments, and this leads to a transient network of such micelles.⁶⁴ In turn, the viscosity of the solution is appreciably enhanced. The ability to thicken water at low concentrations makes associating polymers the rheology modifiers of choice in a variety of applications including paints and coatings, consumer products etc.⁶⁴ In our research, we will use associating polymers to create new TR fluids, as described in Chapter 5.

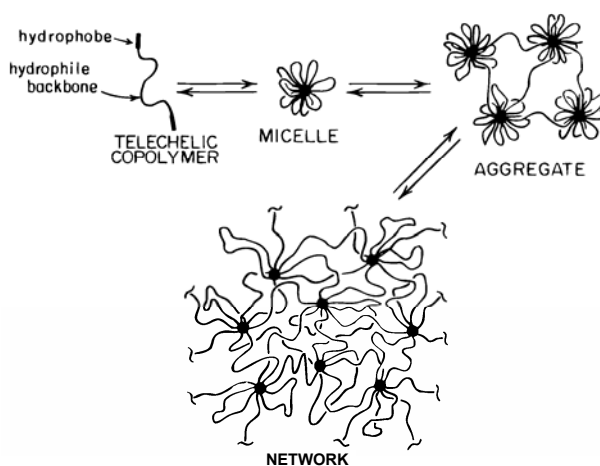


Figure 2.8. Architecture of a telechelic associating polymer and the structures formed by its self-assembly in aqueous solution.⁶⁵

2.8 Characterization Technique – I: Rheology

The main focus of this proposal is on the stimuli-driven modulation of rheological properties. Rheology is formally defined as the study of the deformation and flow in materials.^{66,67} Rheological measurements are useful in characterizing complex fluids and soft materials and they help to correlate the microstructure to the macroscopic flow properties of the material.²⁵ Measurements can be performed under steady or dynamic shear. In the case of steady shear, the sample is subjected to a constant shear-rate $\dot{\gamma}$ and the response is measured as a shear-stress σ . The (apparent) viscosity η is calculated as the ratio of the shear stress to shear rate ($\eta = \sigma / \dot{\gamma}$). A plot of η vs. shear rate is called the flow curve of the material. Several fluids show a Newtonian behavior in their flow curve at low shear rates i.e., in this regime, the viscosity is *independent* of shear rate. The viscosity in this “Newtonian plateau region” is called the zero-shear viscosity η_0 , and it corresponds to the viscosity of the sample in the limit of $\dot{\gamma} \rightarrow 0$.⁶⁷

Rheological experiments can also be conducted in dynamic or oscillatory shear, where the sample is subjected to a sinusoidal strain $\gamma = \gamma_0 \sin(\omega t)$. Here γ_0 is the strain-amplitude and ω is the frequency of the oscillations. The sample response will be in the form of a sinusoidal stress $\sigma = \sigma_0 \sin(\omega t + \delta)$, which is shifted by a phase angle δ relative to the strain waveform. The stress can be decomposed into two components using trigonometric identities, the first being in-phase with the sinusoidal strain, and the second being out-of-phase by 90° :

$$\sigma = \gamma_0 \left[G'(\omega) \sin(\omega t) + G''(\omega) \cos(\omega t) \right] \quad (2.2)$$

where G' is the **Elastic** or **Storage Modulus** and G'' is the **Viscous** or **Loss Modulus**. The dynamic experiment ultimately yields plots of G' and G'' as functions of ω (usually plotted on a double-log scale), which are collectively called the frequency spectrum of the material. Such a plot is useful because it shows how the viscoelasticity of the material varies with timescale, which in turn is a signature of the microstructure.⁶⁶

The physical interpretation of G' and G'' are as follows. The elastic modulus G' is obtained from the in-phase component of the stress, and provides information about the elastic nature of the material. G' is also called the storage modulus since elastic behavior implies the storage of deformational energy. The viscous modulus G'' is extracted from the out-of-phase component of the stress, and it characterizes the viscous nature of the material. G'' is also known as the loss modulus since viscous deformation results in the dissipation of energy. G' and G'' are meaningful only if the dynamic rheological measurements are taken in the “linear viscoelastic” or LVE regime.⁶⁷ The LVE regime corresponds to low imposed strains, such that the stress response is linearly proportional to the strain. In that case, G' and G'' will be independent of strain amplitude and will be functions only of the frequency ω – the moduli will then be true material properties.

An important advantage of dynamic rheology is that it enables the characterization of the material’s microstructure without disrupting it. Since only small-amplitude strains are used (within the LVE regime), the net deformation imposed on the sample is minimal. Thus, the linear viscoelastic moduli reflect the microstructure present in the sample at rest.⁶⁶ In contrast, steady-shear rheology measures material properties

under continuous flow conditions, which correspond to relatively large deformations. Therefore, dynamic rheological parameters can be correlated with static microstructures and steady-shear rheological measurements correspond to flow-induced changes in the microstructure.

2.9 Characterization Technique – II: SANS

Scattering techniques are very useful for probing the structures of materials on the micro- and nanometer scale.⁶⁸ The basic principle behind these techniques is that the intensity of scattered radiation from a structured fluid is a function of the size, shape, and interactions of the “particles” present. We will use small-angle neutron scattering (SANS) to study our samples as it is useful in probing structure over size scales on the order of a few nm. In SANS, the contrast between the solvent and the “particles” is achieved by switching the hydrogen in the solvent molecules with deuterium, for example using D₂O instead of H₂O. SANS experiments require a nuclear reactor to generate neutrons and we are fortunate to have one of the premier facilities for SANS nearby at the National Institute of Standards and Technology (NIST) in Gaithersburg, MD.

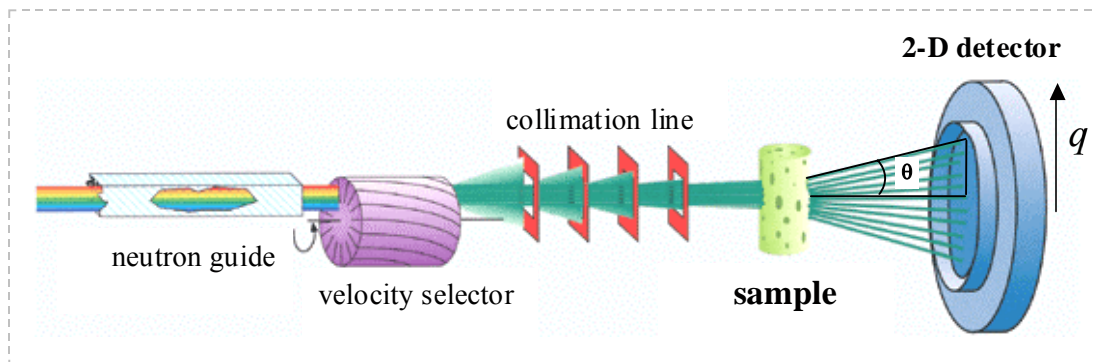


Figure 2.9. Schematic of a SANS experiment (adapted from www.gkss.de).

The basic geometry of a SANS experiment is illustrated in Figure 2.9. A nuclear reactor emits neutrons, which then pass through a velocity selector set for a particular wavelength and wavelength spread. These neutrons then pass through several collimating lenses and into the sample placed in the sample chamber. Finally, a 2-D detector collects the neutrons scattered by the sample. Using calibration standards, the collected 2-D data is corrected and placed on an absolute scale. This data is then spherically averaged to give a plot of the scattered intensity I vs. wave vector q . The wave vector is defined as: ⁶⁸

$$q = \frac{4\pi}{\lambda} \sin\left(\frac{\theta}{2}\right) \quad (2.3)$$

Here, λ is the wavelength of the incident radiation and θ is the scattering angle. q can be considered an inverse length scale, with high q corresponding to small structures, and low q to large structures in the sample.

For a structured fluid containing n_p particles per unit volume, the intensity $I(q)$ can be expressed as follows: ⁶⁸

$$I(q) = n_p \cdot P(q) \cdot S(q) \quad (2.4)$$

where $P(q)$ is referred to as the form factor and $S(q)$ as the structure factor. $S(q)$ is the scattering that arises from *interparticle* interactions and thus reflects the spatial arrangement of the particles in the sample. $P(q)$ is the scattering that arises from *intraparticle* interferences, and thus is a function of the particle size and shape. When the particles are in dilute solution (i.e., n_p is small), the interparticle interactions become negligible and therefore the structure factor $S(q) \rightarrow 1$. The SANS intensity $I(q)$ can then be modeled purely in terms of the form factor $P(q)$, i.e., the sizes and shapes of the

particles. The form factors for several different particle geometries have been developed, which can be fit to the data to extract structural information about the particles. However, one must make an *a priori* assumption about the type of structures present to select a particular form factor. But a good fit to the data does not necessarily mean the model is correct, i.e., many models may fit the same data, especially if they have a large number of variable parameters.

The shortcomings with the “straight modeling” approach have led to the development of an alternate method of analysis that requires no *a priori* knowledge about the scatterers. This is the Indirect Fourier Transform (IFT) method, and here a Fourier transformation is done on the scattering intensity $I(q)$ to give the pair distance distribution function $p(r)$ in real space. $I(q)$ and $p(r)$ are related by the following equation:¹⁷

$$I(q) = 4\pi \int_0^{\infty} p(r) \frac{\sin(qr)}{qr} dr \quad (2.5)$$

The $p(r)$ function provides structural information about the scatterers in the sample. In particular, the largest dimension of the scattering entities can be estimated. The simplest form of the IFT technique is valid only for non-interacting scatterers.¹⁷ Before implementing the IFT methodology, it is useful to first subtract the incoherent background from the scattering data. This background can be estimated from the asymptotic slope of a Porod plot ($I(q) \cdot q^4$ vs q^4). A software package is commercially available to perform the IFT calculation on the data with subtracted background. In Chapter 3 and 4, we will use the IFT approach to analyze our SANS data on stimuli-responsive micellar systems.

2.10 Characterization Technique – III: UV-Vis Spectroscopy

UV-Vis absorption spectroscopy is an analytical technique used to study molecules that adsorb radiation in the ultraviolet (200 to 400 nm) and visible (400 to 800 nm) regions of the electromagnetic radiation spectrum.⁵² Generally, when a molecule absorbs radiation, the energy gained is proportional to the energy of the incident photons. In the UV-Vis range, the absorbed energy typically acts to move electrons into higher energy levels.⁵² A given molecule does not absorb energy continuously throughout a spectral range because the absorbed energy is quantized; therefore, the molecule will absorb at the wavelengths that provide the exact amount of energy necessary to promote it to the next higher energy level.⁵² Therefore, each compound will have a unique UV-Vis absorption spectrum. UV-Vis can thus serve as a convenient analytical technique for a variety of compounds, especially those that have an aromatic group.

A typical UV-Vis experiment involves placing a solution containing a low concentration of solute (10^{-5} to 10^{-2} M) in a cuvette, which is then placed in the sample cell of a UV-Vis spectrometer. Light is broken down into its component wavelengths in the spectrometer and passed through the sample. The absorption intensity is measured for each wavelength and a UV-Vis spectrum (plot of absorbance vs. wavelength) is produced for the sample. UV-Vis spectroscopy can be used as a quantitative analytical method to determine the concentration of a solute in solution. This can be done using the Beer-Lambert law:⁵²

$$A = \varepsilon \cdot c \cdot \ell \quad (2.6)$$

where A is the measured absorbance at a particular wavelength, c is the concentration of the solute in mol/L, ℓ is the path length of the sample, and ε is the molar extinction coefficient or molar absorptivity at that wavelength. UV-Vis spectroscopy has an important role to play in the study of photoresponsive systems. For example, different photoisomers have different UV-Vis spectra, enabling their easy identification. Also, the peak absorption wavelength is generally the wavelength at which the compound is irradiated to induce a phototransition.

Chapter 3

A New Class of Aqueous Photogelling Fluids

The results presented in this chapter have been published in the following journal article: Rakesh Kumar and Srinivasa R. Raghavan, “*Photogelling fluids based on light-activated growth of zwitterionic wormlike micelles.*” *Soft Matter* 5, 797-803 (2009).

3.1 Introduction

As described in Chapter 1, interest in stimuli-responsive fluids and materials has been building considerably over the past two decades. A stimulus of particular focus has been light, and among the various material properties that one seeks to modulate using light are the rheological properties (such as viscosity).^{9,69} Accordingly, several groups,^{9,12-14,69,70} including ours,⁷¹ have sought to create fluids whose viscosity can be modulated by irradiation with light at a given wavelength. Such fluids could properly be termed *photorheological* (PR) fluids,^{71,72} a term that was originally introduced into the literature by Wolff and co-workers⁷² in the late 1980s. Much of the interest in developing PR fluids has been due to their potential to be used in microscale applications, such as microvalves or flow sensors within MEMS or microfluidic devices.⁷¹ In such applications, the use of light as a modulating field can be particularly advantageous since light can be directed at a precise spot with resolution of a few micrometers.

Our approach to PR fluids has differed from those of others in an important way. The focus of other groups has largely been on synthesizing novel light-sensitive organic molecules, such as new classes of photoresponsive surfactants^{9,12,13} or polymers,^{14,70} and using these to create the PR fluids. While these studies have demonstrated impressive rheology-modulation with light, the light-sensitive molecules underlying these systems have remained accessible only to the select groups that are capable of synthesizing them. We have instead sought to create PR fluids from simple, existing molecules that would be available to any chemistry laboratory. In a recent study,⁷¹ we have shown that such an idea is feasible: specifically, we reported PR fluids that were mixtures of two widely available chemicals: the cationic surfactant, cetyl trimethylammonium bromide (CTAB) and the photoisomerizable molecule, *trans*-ortho-methoxy-cinnamic acid (OMCA). We showed that CTAB/OMCA fluids undergo *photothinning*, i.e., a rapid and controllable decrease in viscosity (factors of 1000 to 10,000) upon exposure to UV radiation.⁷¹ This viscosity change was not reversible by light, i.e., the viscosity could be decreased but not increased. Despite this limitation, our study did show that dramatic light-triggered rheological changes are possible in simple systems. From a mechanistic standpoint, the molecular change (*trans-cis* isomerization of OMCA) underlying the phenomenon was connected to changes in the microstructure (reductions in the size of wormlike micelles), and thereby to the drop in viscosity.⁷¹

In this Chapter, we describe a new class of PR fluids that exhibit *photogelling*, i.e., a 10,000-fold *increase* in viscosity upon UV irradiation. These fluids again consist of two commercial compounds: the zwitterionic surfactant, erucyl dimethyl amidopropyl

betaine (EDAB) and the same photoadditive as before, i.e., OMCA. The main results, as indicated by Figure 3.1, are that certain mixtures of EDAB and OMCA form fluids with a low viscosity (similar to water). Upon UV irradiation, OMCA is converted from its *trans* to its *cis* form,⁷¹ and in turn, these fluids are transformed into highly viscous, gel-like samples. We will show that the rheological changes correlate with a transition from short to long, “wormlike” micelles^{19,73}. In other words, the light-induced change in OMCA geometry *activates the axial growth* of cylindrical micelles into long, flexible chains that undergo physical entanglement, producing a viscoelastic fluid. Although the photogelling cannot be reversed by light (see discussion later), we will show that the viscosity *can* be decreased by further addition of OMCA. Thus, a combination of light and sample composition can be used to cycle the viscosity between high and low states.

A few further points are worth mentioning at this stage. First, the change from a photothinning system (our earlier study) to the photogelling system described here is not a trivial one. Specifically, photogelling requires the use of a zwitterionic surfactant that is capable of forming wormlike micelles (“worms” for short) (see Section 2.2).^{35,74} Although zwitterionic surfactants, including EDAB, are popular in industry due to their low skin irritation and biodegradability,²⁴ they have not been investigated in detail by academic researchers. Most academic studies on wormlike micelles have utilized cationic surfactants like CTAB, and for those surfactants to form worms it is well known that salts (either inorganic or organic) must be added.^{19,73} On the other hand, EDAB is a long (C₂₂-tailed) zwitterionic surfactant that can form worms even in the absence of salt – in fact, inorganic salts like NaCl have no influence on worm formation.⁷⁴ These aspects on the

rheology of EDAB worms were brought to light in our recent paper⁷⁴ that may be considered a precursor to the present study.

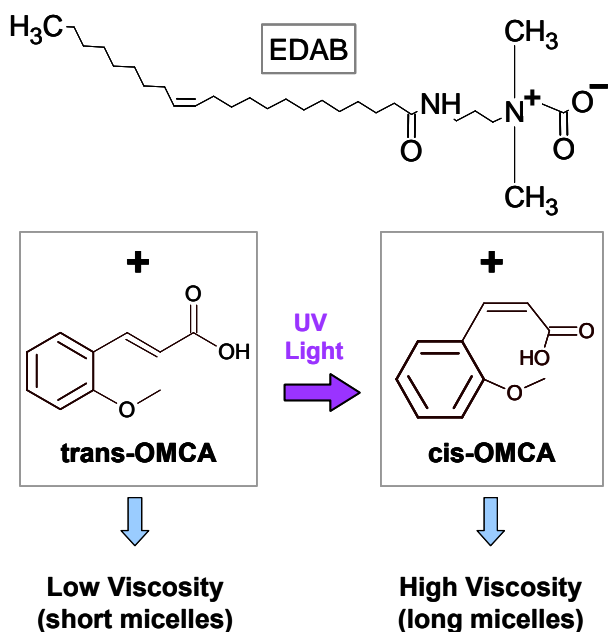


Figure 3.1. Composition of photogelling fluids described in this Chapter. The fluids consist of the zwitterionic surfactant, EDAB and the organic derivative, OMCA. When EDAB is combined with *trans*-OMCA, the result is a low-viscosity fluid. Upon UV irradiation, *trans*-OMCA is photoisomerized to *cis*-OMCA, which causes a substantial rise in fluid viscosity. The viscosity rise is associated with the growth of EDAB micelles.

It is worth reiterating that EDAB and similar betaine surfactants are commercially available,⁷⁴ allowing researchers in any lab to replicate our results and to use photogelling fluids for applications of interest. Interestingly, from an applications standpoint, photogelling is likely to be more useful than photothinning – one potential application would be in capillary electrophoresis, where a photogelling carrier fluid can be loaded into the capillary while it is thin and later transformed into a gel-like state by UV irradiation. Also, in the context of biomolecular applications such as bioseparations,

EDAB-based PR fluids may indeed be formulated using physiological buffer solutions. Note that the background electrolyte in such buffers does not influence micelle formation in the case of EDAB or other zwitterionics,^{35,74} but would do so in the case of cationic surfactants.^{19,73}

Finally, we wish to elaborate a bit more on the mechanism underlying the photogelling reported in this paper (a detailed discussion is given later). The key to the mechanism is that (a) EDAB is zwitterionic; and (b) the *trans* isomer of OMCA tends to bind and intercalate into EDAB micelles, whereas the *cis* isomer does not. When binding occurs, an effective charge is imparted to EDAB headgroups, which translates into short micelles. On the other hand, when the *cis* isomer unbinds and exits the micelle, the effective charge is reduced, causing micellar growth (see Figure 3.8 later). Indeed, we have been able to verify this mechanism through a combination of small-angle neutron scattering (SANS) and zeta-potential measurements. SANS is a sensitive probe for the dimensions of the micelles, while zeta-potential probes the net surface charge on the micelles. In sum, the photoinduced rheological transitions reported in this paper can be sensibly explained by the coupling of events occurring at the molecular, microstructural, and macroscopic scales.

3.2 Experimental Section

Materials. The EDAB surfactant was a commercial product manufactured by Rhodia Inc, Cranbury, NJ. EDAB is a zwitterionic surfactant of the betaine type (see structure in Figure 3.1), with the molecule having both a positively charged dimethylammonium

moiety and a negatively charged carboxylate group. Further details about the sample are given in our earlier paper; as an aside, the critical micelle concentration (CMC) of EDAB is very low: $\sim 1 \mu\text{M}$.⁷⁴ OMCA in its *trans* form was purchased from Acros Chemicals, while the *cis* form was purchased from TCI America (each isomer was greater than 98% in purity). Ultra-pure deionized water from a Millipore water-purification system was used in preparing samples for rheological characterization, while D₂O (99.95% deuteration, from Cambridge Isotopes) was used for the SANS studies. Solutions containing OMCA were buffered to a pH of 10 using equimolar amounts of sodium carbonate and sodium bicarbonate. Weighed quantities of EDAB were added to these solutions to reach the final sample compositions. Samples were stirred continuously under mild heat until they became homogeneous. The solutions were then left to equilibrate overnight at room temperature before conducting any experiments.

Sample Response Before and After UV Irradiation. EDAB/OMCA samples were irradiated with UV light from a Oriel 200 W mercury arc lamp. A dichroic beam turner with a mirror reflectance range of 280 to 400 nm was used to access the UV range of the emitted light. Samples (5 mL) were placed in a Petri dish with a quartz cover and were irradiated for a specific duration under stirring. Due to the nature of the OMCA spectra, (see Figure 3.2) irradiated samples did not undergo any changes when stored under ambient conditions, which made it easy to conduct subsequent tests.

Rheological Studies. Steady and dynamic rheological experiments were performed on an AR2000 stress controlled rheometer (TA Instruments, Newark, DE). Samples were

run at 25°C on a cone-and-plate geometry (40 mm diameter, 2° cone angle) or a couette geometry (rotor of radius 14 mm and height 42 mm, and cup of radius 15 mm). Dynamic frequency spectra were obtained in the linear viscoelastic regime of each sample, as determined by dynamic stress-sweep experiments.

Small Angle Neutron Scattering (SANS). SANS measurements were made on the NG-7 and NG-3 (30 m) beamlines at NIST in Gaithersburg, MD. Neutrons with a wavelength of 6 Å were selected. Three sample-detector distances were used to obtain data over a range of wave vectors from 0.004 to 0.4 Å⁻¹. Samples were studied in 2 mm quartz cells at 25°C. Scattering spectra were corrected and placed on an absolute scale using NIST calibration standards. The data are shown as plots of the absolute intensity I versus the wave vector $q = 4\pi\sin(\theta/2)/\lambda$, where λ is the wavelength of incident neutrons and θ the scattering angle.

SANS Data Analysis. SANS data were analyzed by the Indirect Fourier Transform (IFT) method, which requires no *a priori* assumptions on the nature of the scatterers.⁷⁵ Here, a Fourier transformation of the scattering intensity $I(q)$ is performed to obtain the pair distance distribution function $p(r)$ in real space. $p(r)$ provides structural information about the scatterers, such as their maximum dimension. IFT analysis was implemented using the commercial PCG software package.

Zeta Potential. The zeta potential of EDAB/OMCA micelles was measured for dilute solutions using a Zetasizer 3000HS (Malvern Instruments). The electrophoretic mobility

was measured and converted into the zeta potential using the Smoluchowski equation.⁷⁶ Prior to use with our samples, the instrument was calibrated using zeta potential transfer standards. Each reported value is an average over 9 independent measurements.

3.3 Results and Discussion

UV-Vis spectra for *trans* and *cis*-OMCA are presented in Figure 3.2. These experiments were done with aqueous solutions containing 1 mM of each derivative along with a slight excess of base. Figure 3.2 shows that the absorption peaks for the *trans* form are centered at 270 nm and 312 nm while the *cis* form has absorption peaks at 254 and 293 nm. Note that the *trans* form has much higher absorbance than the *cis* form over the entire UV range. As discussed in section 2.3, UV irradiation should cause a *trans* to *cis* photoisomerisation of OMCA. To test this, we irradiated the *trans*-OMCA solution with UV light (< 400 nm) for 1 min and recorded UV-Vis spectra after irradiation. Indeed, Figure 3.2 confirms this – the irradiated sample shows peaks at 257 and 300 nm and its spectrum is close to that of the pure *cis* compound. Actually, the irradiated sample corresponds to a photostationary state of about 83% *cis* isomers: i.e., its spectrum can be obtained by superposing those for pure *cis* and *trans* in a ratio of 83:17. The nature of the spectra of *trans* and *cis*-OMCA in Figure 3.2 shows that reverse photoisomerisation (i.e., *cis* to *trans*) is not possible as *cis*-OMCA has much lower absorption than *trans*-OMCA over the entire wavelength range. Also, the OMCA spectra show negligible absorbance in the visible range – this inertness to visible light makes handling and storage of OMCA samples quite easy. Furthermore, we verified that OMCA spectra were unaffected by the presence of EDAB in solution.

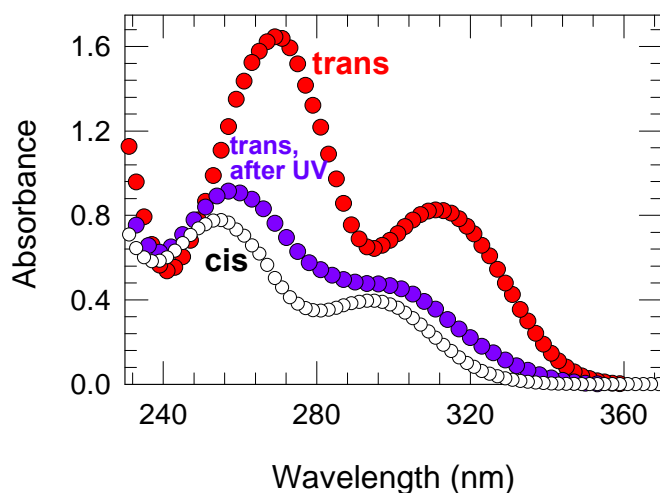


Figure 3.2. UV-Vis spectra of *trans*-OMCA before irradiation, *trans*-OMCA after UV irradiation, and *cis*-OMCA. Each sample is an aqueous solution containing 1 mM of the corresponding additive. The drop in absorbance and blue shift in the *trans*-OMCA curve after UV irradiation indicate that the molecule has been photoisomerized to its *cis* form.

We next discuss the differences between *trans* and *cis*-OMCA when combined with solutions of EDAB. As mentioned earlier, OMCA is available commercially in both its *trans* and *cis* forms, permitting separate studies with each isomer. When EDAB alone is added to water at a concentration of 50 mM, it turns it into a gel-like fluid. The rheology of EDAB samples at various concentrations has been reported in detail in our previous paper.⁷⁴ Figure 3.3 shows that a 50 mM EDAB solution (no OMCA) has a low-shear viscosity of about 300 Pa.s. When *cis*-OMCA is added to the EDAB solution, it has negligible effect on the rheology and the viscosity stays practically unchanged over the entire range of *cis*-OMCA concentrations (unfilled points). In contrast, the addition of *trans*-OMCA lowers the viscosity of EDAB solutions: about 130 mM of *trans*-OMCA reduces the viscosity to a value close to that of water (1 mPa.s). This result is similar to that reported in our earlier paper,⁷⁴ where we had studied the effects of adding salts to

EDAB solutions. While simple, inorganic salts like NaCl were not found to have an effect on EDAB solution rheology, aromatic salts like sodium salicylate (NaSal) and sodium hydroxy-naphthalene-carboxylate (NaHNC) both reduced the viscosity. The viscosity reduction was much higher for the more hydrophobic counterion, i.e., NaHNC compared to NaSal.⁷⁴ The mechanism underlying such viscosity reduction is discussed later in the paper.

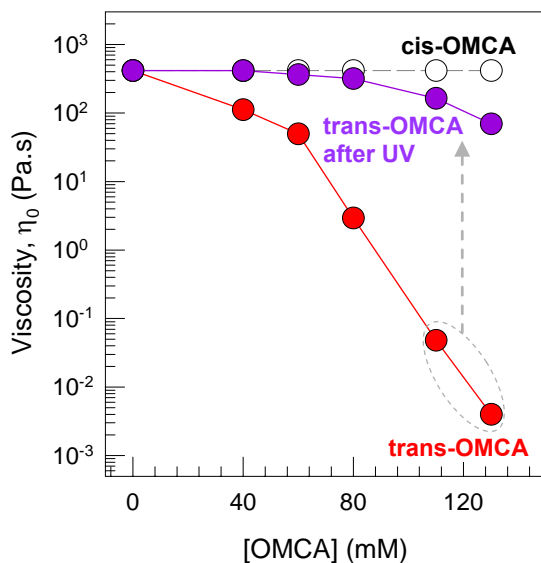


Figure 3.3. Zero-shear viscosity η_0 of 50 mM EDAB + OMCA mixtures as a function of the OMCA concentration. Data are shown for samples containing either *trans*-OMCA or *cis*-OMCA and for *trans*-OMCA samples after 20 min of UV irradiation. As shown by the arrow, the high *trans*-OMCA samples undergo photogelling, i.e., they experience a significant light-induced increase in viscosity.

For the moment, we will highlight the effect of UV irradiation on EDAB + *trans*-OMCA samples. As discussed above, *trans*-OMCA gets photoisomerized to *cis*-OMCA upon UV irradiation. It is therefore of interest to examine the changes in the rheology of EDAB + *trans*-OMCA solutions upon UV irradiation. Accordingly, we irradiated each of the above samples for 20 min and then recorded their rheological response. Note that,

following irradiation, the samples remained unaltered when stored under ambient conditions (exposure to visible light has no effect because both OMCA isomers have no measurable absorbance in the visible range of the spectrum⁷¹). Thus, irradiated samples could be conveniently tested by rheometry, and their zero-shear viscosity η_0 values are shown in Figure 3.3. All samples exhibit an increase in η_0 , with the increase being particularly significant (factor of 10,000 or more) for samples having a high *trans*-OMCA content. The latter samples will be the focus of the rest of the paper, and we will describe their light-induced transformation as “photogelling”.

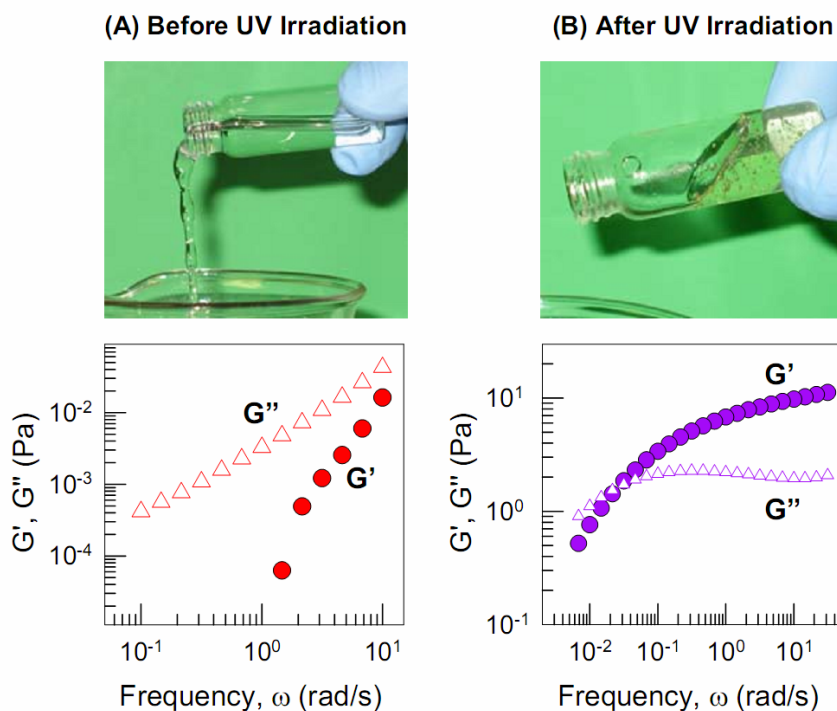


Figure 3.4. Photographs and dynamic rheological data (frequency spectra) for a sample containing 50 mM EDAB + 130 mM *trans*-OMCA (A) before and (B) after UV irradiation. Before irradiation, the sample is water-like and shows a purely viscous response in dynamic rheology. After UV irradiation for 30 min, the sample is gel-like and shows a strongly viscoelastic response. Note that the latter sample does not flow easily out of the tilted vial and also note the presence of trapped bubbles in the fluid.

Figure 3.4 shows photographs and dynamic rheological data on a photogelling sample consisting of 50 mM EDAB and 130 mM *trans*-OMCA. Before UV irradiation, the sample is a freely flowing, low-viscosity liquid that readily pours out of the vial. Upon UV irradiation, it is clear that the sample has been converted into a viscoelastic, gel-like fluid (note the presence of entrapped bubbles). Flow-birefringence, i.e., bright streaks of light under crossed polarizers, was also seen when this gel-like sample was shaken. No such flow-birefringence was evident before UV irradiation. As is well-known, strong viscoelasticity and flow-birefringence are characteristic properties of surfactant samples that contain wormlike micelles, i.e., long and flexible micellar chains with a cylindrical cross-section.^{19,73} Thus visual evidence points to the existence of wormlike micelles in the sample after UV irradiation.

The above visual observations are fully consistent with the dynamic rheological data shown in Figure 3.4. The data are presented as plots of the elastic modulus G' and viscous modulus G'' vs. the angular frequency ω . The sample before irradiation behaves like a viscous liquid over the entire range of frequencies (i.e., in this case, $G'' > G'$, with both moduli being strong functions of frequency). On the other hand, the irradiated sample shows a strongly viscoelastic response, i.e. the response is elastic over most of the frequency range ($G' > G''$, plateau in G'), whereas it is viscous at very low frequencies or long time scales. The frequency at which G' and G'' intersect is an estimate for the longest relaxation time of the sample, which is about 100 s in this case. This relaxation time is more than a factor of 1000 higher than that of the unirradiated sample. Note that

the irradiated material is gel-like, but not a “true” gel – if so, the relaxation time would be infinite and the moduli would never intersect.

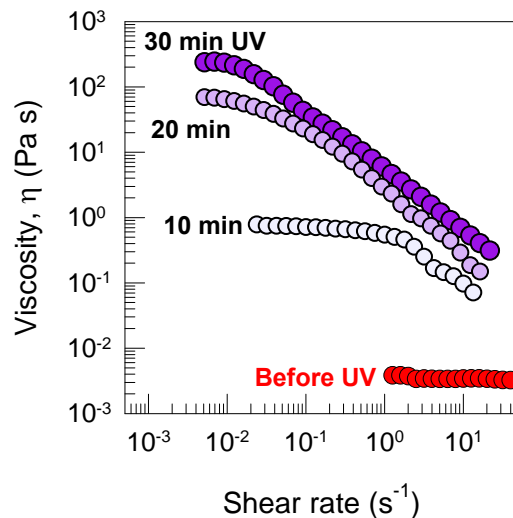


Figure 3.5. Steady-shear rheology of a 50 mM EDAB + 130 mM *trans*-OMCA sample before irradiation and after UV irradiation for various periods of time (as indicated on the plot). The sample is observed to switch from a low-viscosity, Newtonian fluid to a highly viscous, shear-thinning fluid with progressive irradiation.

The light-induced rheological changes are also evident under steady-shear rheology. Figure 3.5 shows viscosity vs. shear rate plots for the 50 mM EDAB + 130 mM *trans*-OMCA sample after various intervals of UV irradiation. Before UV irradiation, the sample is a low-viscosity, Newtonian fluid. After 10 min of irradiation, the zero-shear viscosity η_0 is increased by two orders of magnitude and the sample shows shear-thinning at high shear rates. After 20 min, η_0 is further increased by another two orders of magnitude and the sample becomes strongly shear-thinning. After 30 min, η_0 is close to that of a 50 mM EDAB sample with *cis*-OMCA and no further increase in η_0 occurs with longer irradiation. The viscosity increase is thus tunable via the irradiation time. It should be noted that the *rate-limiting step for photogelling is the rate of absorption of UV light*

by the sample (the photoisomerization itself occurs in milliseconds).⁷¹ In turn, light absorption depends on the intensity of the UV lamp, the sample volume, and the experimental geometry (path length). Rapid transitions can be easily achieved for small sample volumes confined in thin channels.

The results thus far have shown a significant light-induced viscosity increase (photogelling) in EDAB+*trans*-OMCA samples and have been attributed to a transition from short to long wormlike micelles. To confirm this hypothesis, we resorted to SANS. Samples were made in D₂O for SANS experiments to attain the required contrast between micellar structures and solvent (the switch from H₂O to D₂O had no effect on the sample rheology). Figure 3.6 shows SANS spectra for 50 mM EDAB solutions at three different *trans*-OMCA concentrations: 150, 170, and 190 mM, respectively. Data are shown both before and after UV irradiation for 30 min. All samples show a significant rise in low- q scattering intensity upon irradiation. This rise in low- q intensity indicates an increase in micellar size. For the 170 and 190 mM *trans*-OMCA samples (Figure 3.6b and 3.6c), before irradiation, there is a plateau in the low- q intensity, suggesting the presence of spherical micelles (or ellipsoids with nearly equal long and short axes). On the other hand, after irradiation, there is a q^{-1} decay of the intensity at low q , which is indicative of scattering from long cylindrical chains.⁷⁷ There is also no appreciable change in the intensity at high q upon UV irradiation, which implies that the micellar radius remains the same before and after irradiation.

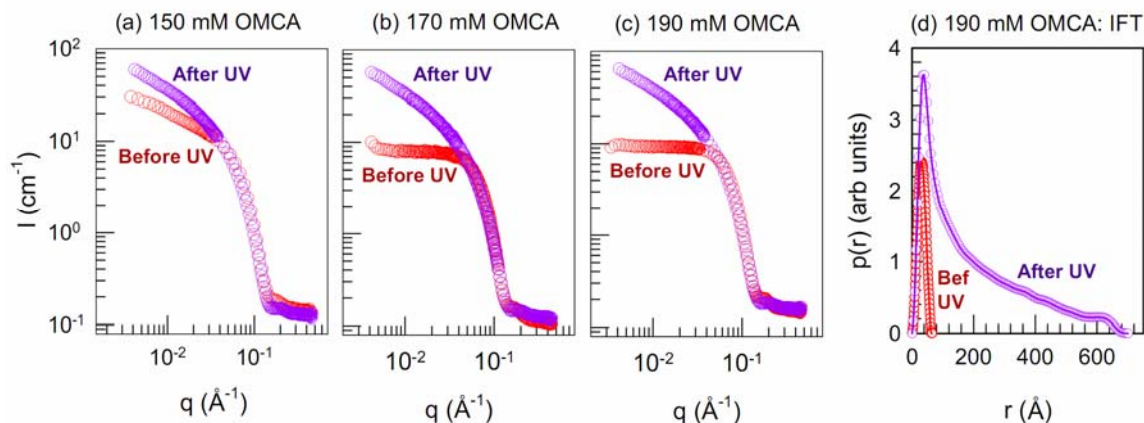


Figure 3.6. SANS data and analysis for EDAB/*trans*-OMCA mixtures before and after 30 min of UV irradiation. Plots (a) – (c) show scattering spectra (intensity I vs. wave vector q) for three samples, each with 50 mM EDAB and with OMCA concentrations of 150, 170, and 190 mM, respectively. Plot (d) presents analysis of the data for the 190 mM OMCA sample using the IFT method. See text for details.

Further quantitative information from the SANS data can be obtained by modeling it through the Indirect Fourier Transform (IFT) method.⁷⁵ Using IFT, we can analyze our SANS data without assuming *a priori* the nature of the scatterers, e.g., whether micelles are long or short, cylindrical or spherical. IFT modeling of the SANS data from the 50 mM EDAB + 190 mM *trans*-OMCA sample yielded the pair distance distribution functions $p(r)$ shown in Figure 3.6d. Before irradiation, $p(r)$ is symmetrical with a narrow peak. This symmetry suggests small spherical micelles with a diameter of about 65 \AA (the diameter corresponds to the point where $p(r)$ meets the x-axis).⁷⁸ In contrast, after irradiation $p(r)$ is asymmetrical and decreases to zero around 700 \AA . This $p(r)$ function is characteristic of long cylindrical micelles.⁷⁹ The point where $p(r)$ meets the x-axis is a lower estimate for the contour length of the cylinders, i.e., 700 \AA in this case. Thus, the SANS data confirm that the microstructural basis for photogelling involves the light-induced growth of cylindrical micelles.

The key question now is to connect the light-induced microstructural transition (short to long micelles) with the transitions occurring at the molecular level. As discussed in our earlier study, we have confirmed that the main effect of light at the molecular level is to induce a *trans* to *cis* photoisomerization of OMCA.^{71,80} Other photoinduced effects associated with cinnamic acid or its derivatives such as photodimerization⁸⁰ have been ruled out using high-performance liquid chromatography (HPLC).⁷¹ We had also shown that *trans*-OMCA is significantly more hydrophobic than *cis*-OMCA. One piece of evidence in this regard was the solubility of the two isomers in deionized water: while the solubility of *cis*-OMCA was 8.6 mM, that of *trans*-OMCA was only 0.26 mM i.e., more than a factor of 30 less.⁷¹ This finding is consistent with other studies that have found the *trans* isomer to be more hydrophobic than the *cis* isomer for a variety of other compounds.^{12,13} In the present context, the hydrophobicity of *trans*-OMCA implies that it will readily bind (intercalate) into EDAB micelles, whereas the more hydrophilic *cis*-OMCA will be more likely to remain in solution.

The tendency of *trans*-OMCA to bind to EDAB micelles while *cis*-OMCA does not is central to our proposed mechanism. We further postulate that counterion binding regulates micellar growth through its effect on micellar surface (headgroup) charge. As stated in the Introduction, EDAB is a zwitterionic surfactant, and the low charge on the EDAB headgroup (coupled with the long C₂₂ tail length) facilitates the formation of worms.⁷⁴ If an anionic counterion like *trans*-OMCA were to bind to EDAB worms, the result would be to impart a net negative charge to the headgroup. The resulting charge repulsions would expand the EDAB headgroup area.⁷⁶ In turn, the molecular geometry

would now favor the formation of short cylinders or spheres rather than long cylinders (worms). The micelles would thereby tend to become much shorter, explaining the low viscosity of EDAB+*trans*-OMCA samples.

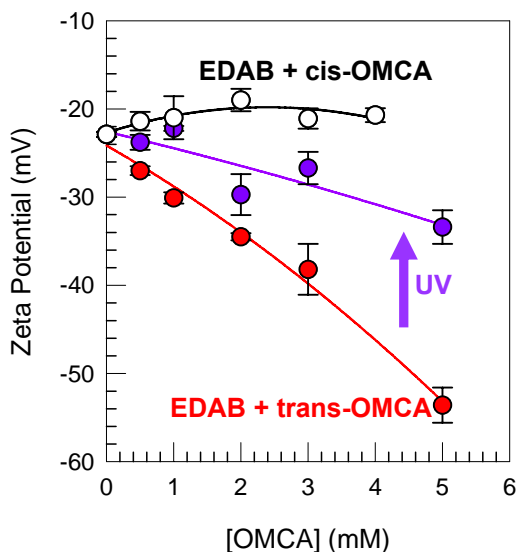


Figure 3.7. Zeta-Potential of 2.5 mM EDAB + OMCA mixtures as a function of the OMCA concentration. Data are shown for *trans*-OMCA, *cis*-OMCA, and *trans*-OMCA samples after 30 min of UV irradiation. Lines through the data are guides for the eye.

In order to test our above hypothesis, we turn to zeta potential measurements (Figure 3.7). The zeta potential quantifies the surface charge densities of colloidal particles. We studied the surface charge on EDAB micelles before and after adding OMCA. The concentrations were kept low (2.5 mM EDAB and 0 to 5 mM of *trans*- and *cis*-OMCA) in order to minimize the effects of micelle size, shape, and intermicellar interactions.⁷⁶ Significantly, the zeta-potential results show the very same trends seen previously in the viscosity data (compare Figures 3.3 and 3.7). In Figure 3.7, we note that the zwitterionic EDAB micelles have a low surface charge and hence a low zeta potential

of -22.9 mV. When *cis*-OMCA is added to the solution, the zeta potential is practically unchanged, indicating that the *cis* isomer is not bound to the micelles. However, with increasing amounts of *trans*-OMCA, the zeta potential becomes more and more negative: the values go from -22.9 to -53.6 mV as *trans*-OMCA is increased from 0 to 5 mM. The implication is that *trans*-OMCA binds (intercalates) into EDAB micelles, thereby making their surface more negative. Finally, we show results for EDAB/*trans*-OMCA samples after 20 min of UV irradiation. In all cases, the irradiated samples show less negative zeta potentials, indicating that the surface charge on the micelles has been lowered. This is fully consistent with the idea that photoisomerization of *trans*-OMCA to *cis*-OMCA leads to unbinding of the latter from EDAB micelles.

The zeta potential data validate our hypothesis that counterion binding and the resulting electrostatic effects are the underlying basis for photogelling in the present system. The key point is that *trans*-OMCA has a much greater affinity for EDAB micelles than *cis*-OMCA. The reason for this has to do with the greater hydrophobicity of *trans*-OMCA (see above) and also its favorable geometry.⁷¹ With regard to geometry, the hydrophobic and hydrophilic parts of *trans*-OMCA are well separated, allowing the counterion to intercalate its hydrophobic parts (aromatic ring, methyl group) into the micelle interior while exposing its hydrophilic part (carboxylate anion) to the water outside. On the other hand, the methyl and carboxylate groups are located very close to each other in the case of *cis*-OMCA, which makes it difficult for the counterion to bind in a way that would be favorable to the entire molecule. Therefore, from a geometry

standpoint also, one expects *trans*-OMCA to have a much stronger tendency to bind (intercalate) into zwitterionic micelles than *cis*-OMCA.

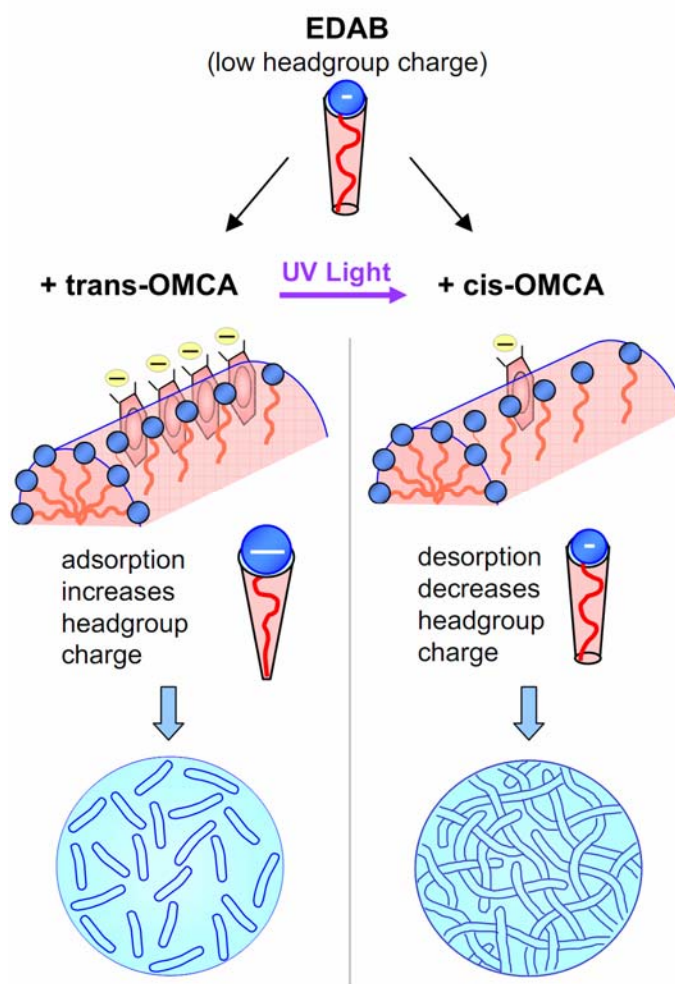


Figure 3.8. Mechanism for photogelling in EDAB samples. Addition of *trans*-OMCA increases the effective headgroup charge due to adsorption of the counterions, and this leads to short micelles. When *trans*-OMCA is photoisomerized to *cis*-OMCA, the *cis* isomer desorbs from the micelles, effectively lowering the headgroup charge. As a result, the micelles grow into long, wormlike structures, and the viscosity thereby increases substantially (photogelling).

Taken together, photogelling can be explained based on the schematics shown in Figure 3.8. At the molecular level, *trans*-OMCA binds to EDAB micelles, increasing the charge on the headgroup and thereby the effective headgroup size. The effective

geometry thus goes from a truncated cone in the case of EDAB to a cone shape in the case of EDAB+*trans*-OMCA. As a result, small micelles (spheres or short cylinders) are formed. When *trans*-OMCA is photoisomerized to *cis*-OMCA, the latter unbinds and exits the micelles. The headgroup charge is decreased to its original low value, and the molecular geometry reverts to a truncated cone shape. Accordingly, the micelles grow into long cylinders and the increase in their contour length L sharply increases the timescale for worm reptation or dis-entanglement ($t_{\text{rep}} \sim L^3$).⁷³ This explains why longer worms lead to a viscosity increase (photogelling).

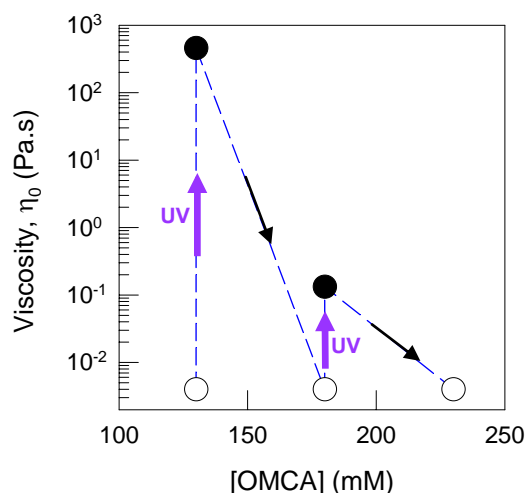


Figure 3.9. Cycling of viscosity by UV irradiation and sample composition. The initial sample (50 mM EDAB + 130 mM of *trans*-OMCA) is exposed to UV light for 40 min, causing a 10,000-fold rise in viscosity. Then, 50 mM of *trans*-OMCA is added, which drops the viscosity back to its original value. The resulting sample is then irradiated again for 40 min, which induces a 50-fold increase in viscosity. Finally, addition of a further 50 mM of *trans*-OMCA again decreases the viscosity back to its original value.

Finally, we discuss the reversibility of the viscosity changes in EDAB/OMCA systems. As explained earlier, a reverse *cis* to *trans* photoisomerization is not possible with OMCA because the absorbance of the *cis* isomer is lower than that of the *trans* over

most of the UV and visible wavelength ranges. Nevertheless, photogelling in EDAB/OMCA fluids can indeed be reversed by a composition change. Specifically, after the sample has been photogelled, we can reduce its viscosity by adding more *trans*-OMCA to it. This is shown in Figure 3.9, where the viscosity is taken along multiple cycling steps: in each step, the upward cycle is caused by UV irradiation at constant composition while the downward cycle is caused by a composition change. Such viscosity cycling can be done up to 2 times.

The above ability to cycle the viscosity demonstrates several things: first, it shows that the viscosity change is indeed connected to self-assembly phenomena, not covalent bond formation or other irreversible processes. Second, the reason this works is very much consistent with our postulated mechanism. Take cycle 1 as an example: during the upward cycle, *trans*-OMCA bound to the micelles is converted to *cis*-OMCA, which desorbs from the micelles. Then, more *trans*-OMCA is added to the solution, which binds to the micelles and increases their charge, lowering the viscosity. In the next cycle, the process is repeated, etc. Note that cycling cannot be done indefinitely because the photo-conversion of *trans* to *cis* only proceeds up to a photostationary state of 80% *cis*.⁷¹ Also, samples with more *trans*-OMCA require longer times to increase their viscosity, which is why the “high” viscosity is lower in the second cycle than the first (the same irradiation time was used for all samples). At any rate, using the above methodology, it is indeed possible to go back and forth between high and low viscosity states, and this is an aspect that could be useful in certain applications.

From an applications standpoint, we should reiterate that the present photoresponsive fluid based on a zwitterionic surfactant offers some advantages over those based on ionic surfactants. In particular, photogelling EDAB/OMCA fluids are quite tolerant to the addition of other components, such as electrolytes, macromolecules, or nanoparticles. An application that could be of interest for photogelling fluids is in capillary electrophoresis, as mentioned in the Introduction. Other applications are bound to arise once photogelling fluids are more widely studied; again, the facile preparation of these fluids from inexpensive commercial ingredients should allow new investigators to venture into this field.

3.4 Conclusions

We have shown that UV irradiation can induce a dramatic increase in viscosity (i.e., photogelling) in EDAB/OMCA mixtures. The step-by-step mechanism for this phenomenon is as follows: (1) EDAB, a zwitterionic surfactant (low head group charge, long tail) forms long wormlike micelles in water, which gives rise to a very high viscosity. (2) When OMCA is in its *trans* form, it binds strongly to EDAB due to its high hydrophobicity and favorable geometry. The binding of these anionic counterions, in turn, increases the headgroup charge and thereby headgroup repulsions. This causes a dramatic reduction in micelle size, and thus in solution viscosity. (3) Upon irradiation by UV light, *trans*-OMCA is isomerized to *cis*-OMCA. The *cis* isomer has a much weaker interaction with EDAB since its geometry and lesser hydrophobicity do not favor binding at the micellar interface. Thus, the *cis* isomer tends to desorb from the micellar interface,

allowing the spherical micelles to transform back into long wormlike micelles. The solution viscosity thereby increases by more than four orders of magnitude.

Chapter 4

“Smart” Non-Aqueous Photothinning Fluids

4.1 Introduction

In the previous Chapter, we described an aqueous PR fluid that was prepared using common, inexpensive chemicals rather than complicated organic molecules. In this Chapter, we turn our attention to the design of PR fluids based on organic (non-polar) solvents. We continue to emphasize simplicity in our approach, i.e., we will use chemicals that can be purchased from commercial vendors rather than molecules that must be synthesized in the laboratory by labor-intensive routes. Our approach is to be contrasted with previous studies on non-aqueous PR fluids – in all those cases, new photo-responsive molecules were synthesized and used. For example, Eastoe et al.⁸¹ synthesized a stilbene-based photo-surfactant and used it to develop a photoresponsive organogel in toluene. Similarly, Shinkai and co-workers⁸² synthesized an azobenzene-modified cholesterol and created photoresponsive organogels with this molecule in a range of organic solvents. While these past approaches were indeed novel and successful, they cannot be replicated by other researchers who lack skills in organic synthesis. Our goal is to develop non-aqueous PR formulations that can be replicated easily and at low cost in any laboratory in the world.

The mechanism behind the aqueous PR fluids in Chapter 3 involved changes in the sizes of micelles in water. By analogy, non-aqueous PR fluids could be based on changes in the sizes of “reverse” micelles (the term “reverse” refers to micelles in organic

solvents, see Section 2.3). From a rheological standpoint, the structures that can impart high viscosity to organic solvents are the reverse wormlike micelles described in Section 2.4.⁸³⁻⁸⁷ These reverse worms are long, flexible cylindrical chains with the nonpolar surfactant tails on the outside and the polar surfactant heads on the inside of the cylinder. While there is a vast literature on reverse worms, most studies have focused on only one or two formulations (mixtures) of amphiphilic molecules.^{37,83-87} To create photoresponsive reverse worms, one thus has to either tweak an existing formulation or create a new one.

The approach we have taken in this study is to devise a new formulation for reverse worms using a photoresponsive organic molecule, viz. *para*-coumaric acid (PCA). When the *trans* form of PCA is added to a non-viscous organosol of lecithin in solvents such as cyclohexane or *n*-decane, the solution becomes highly viscous and viscoelastic. Upon irradiation with UV light, *trans*-PCA is photoisomerized to *cis*-PCA, which causes the sample to revert to a low viscosity, Newtonian fluid. We use SANS to show that the microstructural changes responsible for these rheological effects are the growth of reverse micelles from spheres to worms in the presence of *trans*-PCA and the shrinking of worms back to spheres in the presence of *cis*-PCA. As for why it is the *trans* isomer that causes micellar growth, we believe the answer lies in the higher polarity of this isomer, which translates into a superior hydrogen-bonding capability.^{88,89} Interestingly, among the *trans*- isomers of coumaric acid (Figure 4.1), only the *para* form induces growth of reverse micelles; the *meta* and *ortho* forms do not. This is again indicative of the higher polarity of *trans*-PCA.⁹⁰

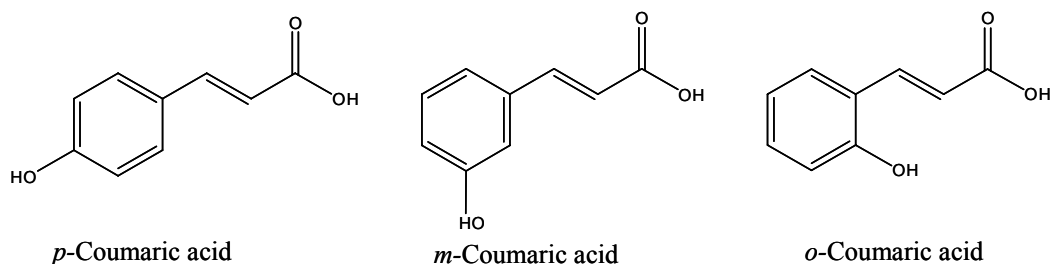


Figure 4.1. Molecular structures of the *trans* isomers of *p*-coumaric acid (PCA), *m*-coumaric acid (MCA), and *o*-coumaric acid (OCA). Their polarities are in order: PCA > MCA > OCA.⁹⁰

4.2 Experimental Section

Materials. Soybean lecithin (95% purity) was purchased from Avanti Polar Lipids, Inc., and used as received. The *trans* isomers of *para*-, *meta*-, and *ortho*-coumaric acids (denoted as PCA, MCA, and OCA, respectively) were purchased from Sigma-Aldrich and used as received (each was > 98% in purity). Cyclohexane, iso-octane, and isopropyl palmitate were purchased from EM Sciences, Fisher and TCI, respectively. *n*-hexane, 1-hexene, and *n*-decane were purchased from Sigma-Aldrich. Deuterated cyclohexane (99.5% D) was obtained from Cambridge Isotopes. Samples were prepared by dissolving weighed amounts of lecithin and the chosen coumaric acid in a given organic solvent. They were then heated to ~ 65°C under continuous stirring for ~ 1 h till the solutions became homogeneous. The samples were then stirred continuously for 24 h and then left to equilibrate overnight in a dessicator at room temperature before any experiments were conducted.

Sample Response Before and After UV Irradiation. Samples were irradiated with UV light from an Oriel 200 W mercury arc lamp. To access the desired wavelength of emitted light, a dichroic beam turner with a mirror reflectance range of 280 to 400 nm was used along with a < 400 nm filter. To nullify the effects of atmospheric moisture, samples (5 mL) were placed in borosilicate glass vials with their caps on and were irradiated through vial walls for a specific duration under stirring. Irradiated samples did not undergo any changes when stored in the dark under ambient conditions (to be additionally careful, we covered sample vials with aluminium foil), which made it easy to conduct subsequent tests. UV-Vis spectroscopy before and after irradiation were carried out using a Varian Cary 50 spectrophotometer.

Rheological Studies. Steady and dynamic rheological experiments were performed on an AR2000 stress controlled rheometer (TA Instruments, Newark, DE). Samples were run at 25°C on a cone-and plate geometry (40-mm diameter, 2° cone angle). A solvent trap was used to minimize organic solvent evaporation. Frequency spectra were conducted in the linear viscoelastic regime of the samples, as determined from dynamic strain sweep measurements. For the steady shear experiments, sufficient time was allowed before data collection at each shear rate so as to ensure that the viscosity reached its steady-state value.

Small Angle Neutron Scattering (SANS). SANS measurements were made on the NG-7 (30 m) beamline at NIST in Gaithersburg, MD. Neutrons with a wavelength of 6 Å were selected. The distances between sample chamber and detector were 1.2 m and 15 m. The

range of scattering vector q was 0.004~0.4 \AA^{-1} . Samples were prepared with deuterated cyclohexane and studied in 1 mm quartz cells at 25°C. Scattering spectra were corrected and placed on an absolute scale using calibration standards provided by NIST. Data are shown for the radially averaged intensity I vs the wave vector $q = (4\pi/\lambda) \sin(\theta/2)$, where λ is the wavelength of incident neutrons and θ the scattering angle.

SANS Data Analysis. SANS data were analyzed by the Indirect Fourier Transform (IFT) method, which requires no *a priori* assumptions on the nature of the scatterers. Here, a Fourier transformation of the scattering intensity $I(q)$ is performed to obtain the pair distance distribution function $p(r)$ in real space. $p(r)$ provides structural information about the scatterers, such as their maximum dimension. IFT analysis was implemented using the commercial PCG software package.

4.3 Results and Discussion

We first studied mixtures of lecithin and the *trans*-coumaric acids (PCA, MCA and OCA; structures in Figure 4.1) in cyclohexane. All three coumaric acids were insoluble in cyclohexane when added directly; however, all could be dissolved in the presence of lecithin. Initial experiments showed that, among the three, only PCA increased the viscosity of lecithin solutions. We believe this result is due to the greater polarity of PCA, as will be discussed later.⁹⁰ Further experiments were done solely on lecithin/PCA mixtures.

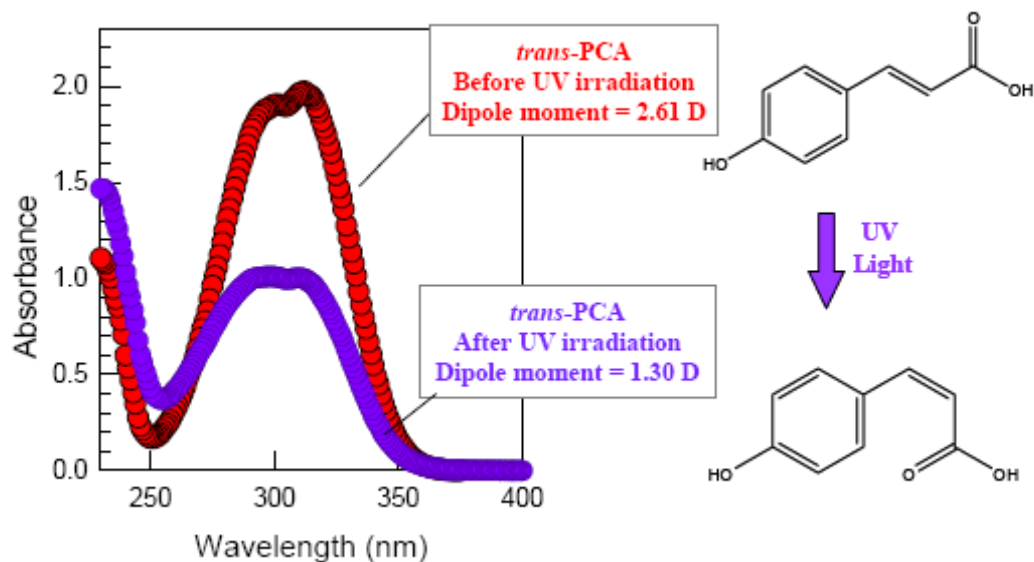


Figure 4.2. UV-Vis spectra of *trans*-PCA before and after UV irradiation. The sample contains 1 mM PCA and 5 mM lecithin in cyclohexane. The drop in absorbance and slight blue shift in the curve after UV irradiation indicate that the *trans*-PCA has been photoisomerized to its *cis* form. Lecithin was added to dissolve PCA in cyclohexane and it does not have any significant effect on the PCA spectra.

PCA is known to undergo photoisomerization about its double bond.⁹¹ To confirm that this occurs in the presence of lecithin, we recorded UV-Vis spectra on mixtures of 1 mM *trans*-PCA and 5 mM lecithin in cyclohexane (Figure 4.2). The sample shows an absorbance peak in the UV range (at 312 nm), which is evidently due to the *trans*-PCA. We then irradiated the above solution with UV light (280-400 nm) and then recorded the spectrum again. The new spectrum (violet curve) shows a drop in peak intensity and a slight blue shift in the peak position to a lower wavelength ~ 300 nm. This change in the spectrum is consistent with a UV-induced photoisomerization from *trans* to *cis*-PCA. Similar data have been reported for a variety of cinnamic acid derivatives.^{52,71,91,92} We should mention that the presence of lecithin had no effect on PCA spectra; similar data were obtained for solutions of PCA alone in solvents like ethanol and water.

The above UV-Vis spectra also imply that the reverse photoisomerization of PCA (i.e., *cis* to *trans*) is not possible because *cis*-PCA has a lower absorbance than *trans*-PCA over most of their spectra. Although the *cis* form has a slightly higher absorbance for wavelengths below 260 nm, reverse isomerization by irradiation at these wavelengths is difficult to achieve in practice because the absorbances are too close for the two isomers. Similar conclusions have been reached by other researchers.^{71,91,92} Another notable fact from Figure 4.2 is that both isomers of PCA have negligible absorbances in the visible range of their spectra. Thus, exposure to visible light has no effect on PCA samples, and UV-irradiated samples remain unaltered when stored under ambient conditions.

(A) Before UV Irradiation



(B) After UV Irradiation

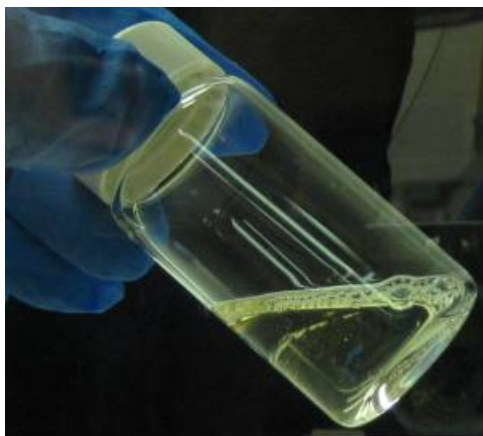


Figure 4.3. Photographs of a sample containing 100 mM lecithin + 110 mM *trans*-PCA in cyclohexane (A) before and (B) after UV irradiation. Before irradiation, the sample is highly viscoelastic and holds its own weight along with a magnetic stir bar in an inverted vial. After UV irradiation for 30 min, the sample is transformed into a low-viscosity fluid that flows very easily and does not entrap air bubbles.

With the knowledge that PCA can indeed be photoisomerized, we now consider the macroscopic effects of UV irradiation on lecithin/*trans*-PCA samples in cyclohexane.

The lecithin concentration was fixed at 100 mM and varying amounts of PCA were tested. At PCA concentrations approximately equimolar to the lecithin, the fluid became appreciably viscoelastic and gel-like. An example is shown in Figure 4.3a for a sample with 110 mM PCA – in this case the sample holds its weight for some time in the inverted vial. Note that the magnetic stirrer bar remains trapped in the sample. Flow-birefringence i.e., bright streaks of light under crossed polarizers, was also seen when this gel-like sample was shaken. Next, consider the same sample after UV irradiation for 30 min. The sample (Figure 4.3b) is now transformed into a free-flowing, low-viscosity fluid. It flows easily upon tilting the vial and bubbles rise to the liquid surface rapidly. No flow-birefringence was seen in this case. We refer to the above macroscopic changes as “photothinning”, i.e., conversion from a gel-like state to a thin, flowing liquid.

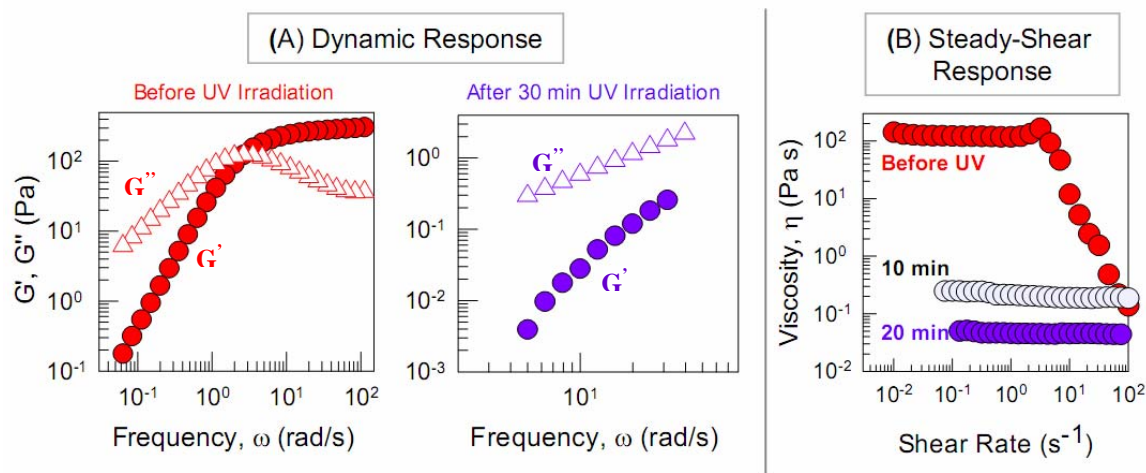


Figure 4.4. Effect of UV irradiation on the rheology at 25°C of a sample containing 100 mM lecithin + 110 mM *trans*-PCA in cyclohexane (A) Dynamic rheological data, before and after UV irradiation for 30 min; (B) Steady-shear rheological data before and after UV irradiation for varying periods of time (as indicated on the plot). The sample is observed to switch from a highly viscoelastic, shear-thinning response to a low-viscosity, Newtonian response upon UV irradiation.

The above visual observations are quantified through dynamic and steady-shear rheological experiments on the same sample as in Figure 4.3. First we discuss the data from dynamic rheology (Figure 4.4a), which is a more sensitive probe of the structure in complex fluids. The data are shown as plots of the elastic modulus G' and the viscous modulus G'' as functions of angular frequency ω . Before irradiation, the lecithin/trans-PCA sample in cyclohexane exhibits a viscoelastic response typical of reverse wormlike micelles. That is, at high frequencies or short time scales, the behavior is elastic with $G' > G''$, whereas at low frequencies or long time scales, the behavior is viscous ($G'' > G'$, with both moduli strongly dependent on frequency). After 30 min of irradiation with UV light, the sample exhibits a purely viscous response ($G'' \gg G'$) over the entire range of frequencies, which suggests that the original worms have been considerably shortened.

The corresponding steady-shear rheological data are plotted in Figure 4.4b with data being shown for different periods of UV irradiation. Before irradiation, the sample shows a non-Newtonian and shear-thinning response: the viscosity tends to a plateau at low shear-rates followed by a precipitous drop at higher shear-rates. After only 10 min of UV irradiation, the sample response is converted to a nearly Newtonian one (i.e., constant viscosity, independent of shear-rate) and the value of the viscosity is lowered by nearly two orders of magnitude. After 10 more min of irradiation (total 20 min), the viscosity is further lowered by an order of magnitude. Further irradiation beyond 20 min has negligible effect on the viscosity. Thus the extent of the viscosity drop (photothinning) can be controlled by the irradiation time. As mentioned in Chapter 3, the rate limiting

step for the viscosity change is the absorption of UV light by the sample and we can shorten this timescale by using higher intensity lamps or smaller sample volumes.

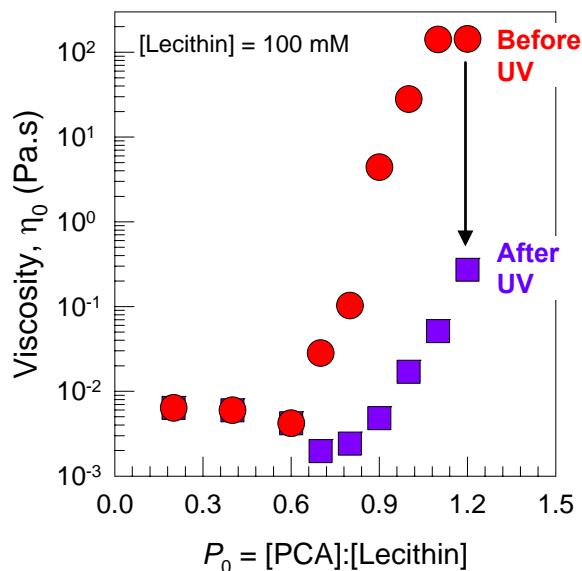


Figure 4.5. Zero shear viscosity η_0 of lecithin + *trans*-PCA in Cyclohexane at 25°C as a function of P_0 , the molar ratio of PCA to lecithin, with the lecithin concentration held constant at 100 mM. Data are shown for samples before (red circles) and after 30 min of UV irradiation (blue squares).

We now consider the effect of UV on a range of lecithin/PCA compositions in cyclohexane, with the [lecithin] fixed at 100 mM. The molar ratio of PCA:lecithin, denoted by P_0 , is the x-axis in Figure 4.5; note that the sample in Figures 4.3 and 4.4 corresponded to a P_0 of 1.1. The y-axis shows the zero-shear viscosity (η_0), which is the viscosity in the limit of low shear-rates, both before and after irradiation with UV light for 30 min. First, consider the behavior of lecithin/PCA/cyclohexane mixtures before irradiation. At low P_0 values (< 0.6), the samples have a low η_0 , effectively identical to that of a lecithin/cyclohexane solution without any PCA. Thereafter, as P_0 is increased

from 0.6 to 1.2, η_0 grows by 5 orders of magnitude, implying the formation and growth of reverse worms. However, further addition of PCA (i.e., $P_0 > 1.2$) causes the mixture to phase-separate into two isotropic liquid phases. Thus, we find that addition of PCA causes a rapid increase in viscosity up to a maximum, followed by phase separation. The same pattern was observed earlier in a study on lecithin-bile salt mixtures in cyclohexane, where again the bile salt induced growth of lecithin reverse worms.⁹³ Now, we consider the effect of UV irradiation on the viscosity of the above samples. A drop in η_0 occurs for all the viscous lecithin/PCA samples ($P_0 > 0.6$), with the drop being particularly large (factor of 1000 or more) for samples near the peak viscosity ($P_0 \sim 1$ to 1.2). Thus the magnitude of photothinning can be modulated via the sample composition.

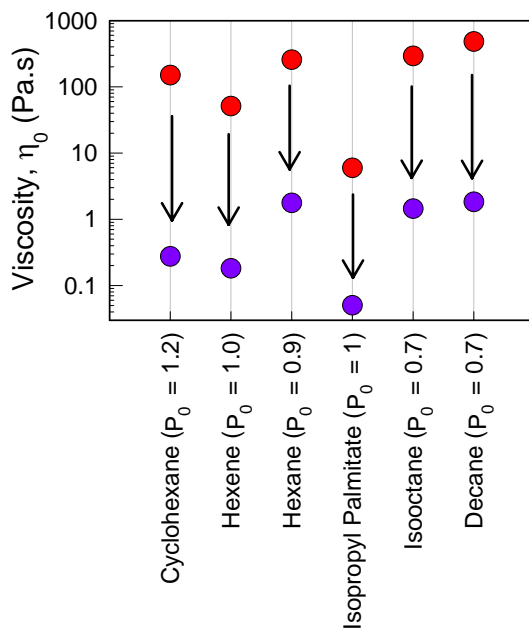


Figure 4.6. Zero shear viscosity η_0 of lecithin + *trans*-PCA in six different organic solvents, before and after UV irradiation. The lecithin concentration is fixed at 100 mM, while the [PCA]:[lecithin] molar ratios P_0 are those corresponding to the maximum viscosity in each solvent. After UV irradiation for 30 min, all samples showed a substantial drop in viscosity, i.e., photothinning.

Having demonstrated photothinning in cyclohexane, we were interested in extending these results to other organic solvents. A number of solvents were studied and it was found that a variety of nonpolar solvents (*n*-alkanes, cycloalkanes, alkenes, fatty acid esters) could be rendered viscoelastic by mixtures of lecithin and PCA. In all cases, the viscosity increased up to a certain [PCA]:[lecithin] molar ratio P_0 , followed by phase separation. For a [lecithin] of 100 mM, the value of P_0 at the onset of phase separation varied from 0.7 to 1.2 depending on the solvent. To compare the photoresponse between solvents in a uniform way, we picked a sample close to the maximum viscosity; the corresponding P_0 values are indicated in Figure 4.6. The results show significant UV-induced drops in zero-shear viscosity η_0 (i.e., photothinning) for each of the six different solvents. The viscosity is reduced by factors ranging from 100 to 1000 in these samples.

The results so far suggest that the combination of lecithin and *trans*-PCA forms reverse worms in nonpolar liquids, leading to viscoelasticity. When *trans*-PCA is converted to *cis*-PCA by exposure to UV light, it induces the worms to shorten considerably and so the viscosity drops. To confirm the above microstructural picture, we conducted SANS experiments. Samples were made in deuterated cyclohexane to amplify the contrast between the micelles and the solvent; these samples were identical to those made in cyclohexane. Figure 4.7a and 4.7b show SANS spectra (I vs. q) for two samples, both with 100 mM lecithin and with PCA concentrations of 60 and 70 mM, respectively. Data are provided both before and after UV irradiation for 30 min. In both cases, the spectra before irradiation have a shape reminiscent of cylindrical structures (slope close to -1 at low q).⁷⁷ Also, in both cases, a drop in the scattered intensity at low q is found

after irradiation, which qualitatively signals a decrease in micelle length (overall size). On the other hand, the data at high q are unaffected by irradiation, indicating a constant diameter for the micelles.

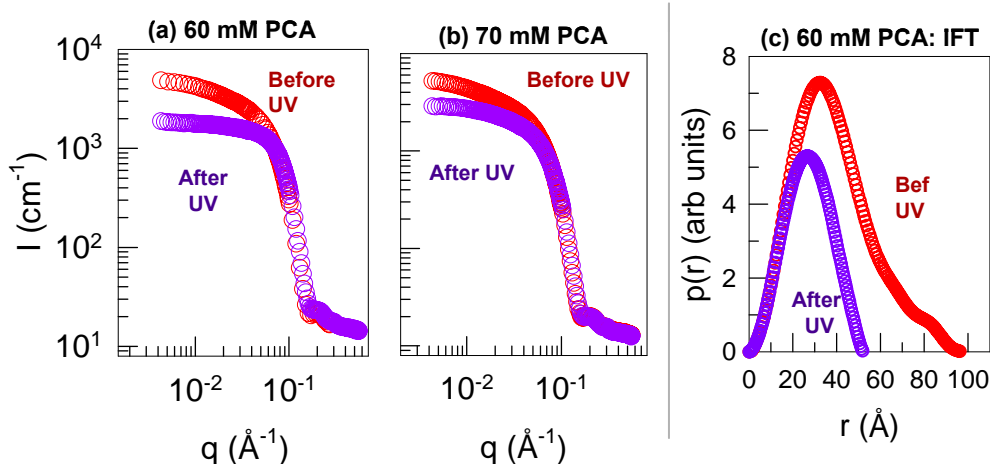


Figure 4.7. SANS data and analysis for lecithin/*trans*-PCA/cyclohexane mixtures before and after 30 min of UV irradiation. Plots (a) – (b) show scattering spectra (intensity I vs. wave vector q) for three samples, each with 100 mM lecithin and with PCA concentrations of 60 and 70 mM, respectively. Plot (d) presents analysis of the data for the 60 mM PCA sample using the IFT method. See text for details.

To glean more quantitative information, we modeled the SANS data using the IFT method, which permits analysis of the data without *a priori* assumptions on the nature of the scatterers. Figure 4.7c shows the pair distribution functions $p(r)$ obtained from IFT modeling of the SANS data from the 60 mM PCA sample. The $p(r)$ before irradiation is asymmetrical and drops to zero around 95 Å. This shape of the $p(r)$ function is characteristic of cylindrical micelles, with 95 Å being a lower estimate for their contour length.⁷⁹ On the other hand, the $p(r)$ after irradiation is nearly symmetrical and this shape suggests ellipsoidal micelles with nearly equal length and diameter.⁷⁸ The point where $p(r)$ meets the x-axis gives the micelle diameter, which is about 55 Å in this case. Thus,

the analysis confirms a reduction in micelle size upon irradiation. Similar results are obtained by analyzing the data from the 70 mM PCA sample as well (not shown).

Mechanism for Photothinning. We have used SANS to confirm that reverse worms exist in lecithin/PCA/oil samples and that the worms shorten upon UV irradiation. The questions that still need to be addressed are: (1) why does PCA induce growth of reverse worms whereas its isomers (MCA and OCA) do not; and (2) why do the worms shorten when PCA is converted from *trans* to *cis*.

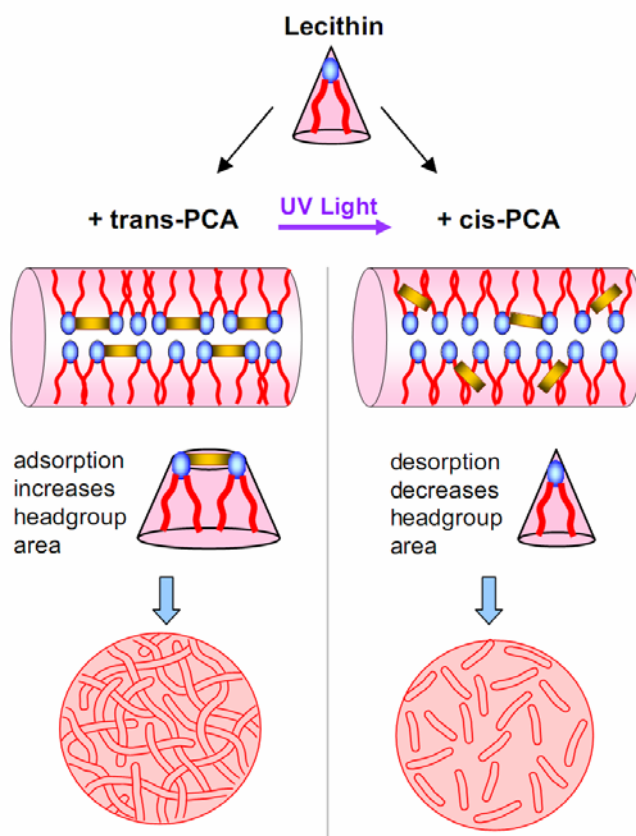


Figure 4.8. Mechanism for photothinning in lecithin/PCA/oil samples. The polar *trans*-PCA forms H-bonds with lecithin headgroups, increasing the effective headgroup area. This favors growth of reverse wormlike micelles and thereby leads to a high viscosity. When *trans*-PCA is photoisomerized, the less polar *cis*-PCA has only a weak H-bonding tendency, and thus unbinds from the headgroups. The lowered headgroup area favors the shortening of micelles, and in turn the sample viscosity drops (photothinning).

We believe the answers to the above questions lie in the polarities and by extension the hydrogen-bonding (H-bonding) capabilities, of the different moieties. It is known that the polarities and H-bonding tendencies of the *trans* isomers follow the order PCA > MCA > OCA.⁹⁰ In turn, H-bonding is critical to the growth of reverse micelles. The only additives that are currently known to induce growth of lecithin micelles are water and bile salts such as sodium deoxycholate (SDC).^{84-86,93} Both these additives form H-bonds with lecithin headgroups and thereby increase the headgroup area without affecting the tail area. The resultant change in molecular geometry favors the growth of cylindrical micelles at the expense of spherical micelles.⁹³ We believe that *trans*-PCA functions in a similar manner. In other words, the hydroxyl (-OH) groups of *trans*-PCA form H-bonds with lecithin headgroups, as shown by Figure 4.8, and this leads to axial growth of cylindrical lecithin micelles.

Next, we tackle the effects of UV irradiation. It is evident that PCA does undergo a UV-induced photoisomerization from *trans* to *cis*. There are numerous studies on this topic and our own UV-Vis data (Figure 4.2) are consistent with such a transition.^{89,91} The two isomers of PCA are also known to substantially differ in their polarity.^{88,89} Indeed, the *trans* form of PCA is reported to have a dipole moment almost double that of the *cis* form.⁸⁹ We believe the lower polarity, and by extension, H-bonding ability of *cis*-PCA relative to *trans*-PCA is the key to explaining the photothinning behavior.⁸⁸ As depicted in Figure 4.8, when the weakly polar *cis*-PCA is formed by UV irradiation, it will tend to unbind from the lecithin headgroups. As a result, the headgroup area will decrease to its original low value, and this will favor shortening of the reverse worms – in turn,

explaining the drop in viscosity. The above mechanism offers a tentative, but plausible, framework within which to interpret our results.

4.4 Conclusions

In this study, we have shown that PR fluids can be made using nonpolar organic liquids and using two simple, inexpensive components, lecithin and PCA. The combination of lecithin with the *trans* form of PCA gives rise to reverse worms and thereby to viscoelastic fluids. The underlying mechanism is believed to be the ability of *trans*-PCA to form H-bonds with the headgroups of lecithin, which thereby alters the molecular geometry to one favoring growth of reverse worms. Upon UV irradiation, PCA undergoes a photoisomerization from *trans* to *cis*. The *cis* moiety, being considerably less polar, is incapable of H-bonding with lecithin – as a result, the micelles revert to much smaller sizes, leading to a substantial drop in viscosity. Such photothinning behavior has been achieved for samples in a range of organic solvents including *n*-alkanes, alkenes, and fatty acid esters.

Chapter 5

Aqueous Thermo-Thickening Fluids

5.1 Introduction

In this Chapter, we report a new class of thermorheological (TR) fluids in which the viscosity increases significantly upon heating (i.e., thermo-thickening). These fluids are mixtures of associating polymers and cyclodextrins in water. As discussed earlier in Section 2.7, the term “associating polymer” generally refers to a water-soluble polymer bearing hydrophobic groups either on its ends or along the backbone.^{63,64} When the hydrophobes are present on the chain ends, the structure is called telechelic.⁶⁴ An example is the hydrophobic ethoxylated urethane (HEUR) architecture, where the backbone is composed of poly(ethylene oxide) (PEO) and this is linked to hydrophobic end-caps (typically *n*-alkyl moieties) through urethane spacers (Figure 5.1).⁶⁴ As their name indicates, associating polymers associate in aqueous solution through their hydrophobes. This results in “flower micelles” that have a hydrophobic core surrounded by a corona of looping PEO segments.^{63,64} Adjacent flower micelles also get connected through bridging PEO segments, and this leads to a transient network of such micelles.⁶⁴ In turn, the viscosity of the solution is appreciably enhanced. The ability to thicken water at low concentrations makes associating polymers the rheology modifiers of choice in a variety of applications including paints and coatings, consumer products etc.⁶⁴

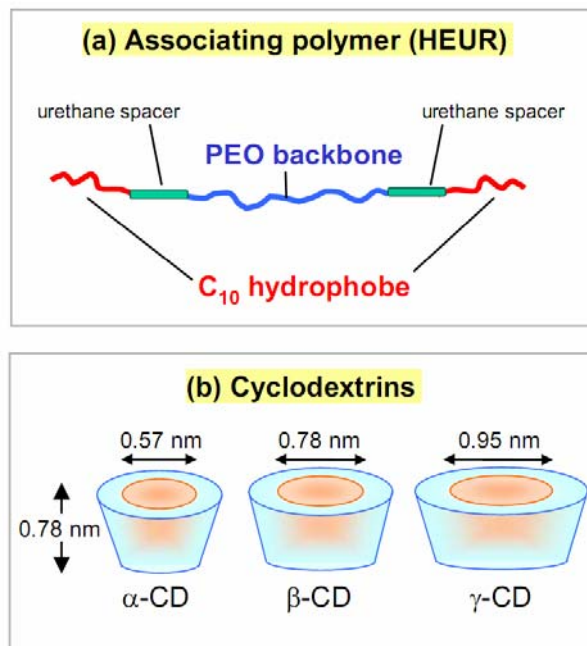


Figure 5.1. Schematics of (a) the RM825 associating polymer and (b) the cyclodextrins (CDs) studied.

Cyclodextrins (CDs) are a class of supramolecules known for their ability to modulate hydrophobic interactions between associating polymers (see Section 2.6).^{54,55} These molecules are doughnut-shaped cyclic oligomers of glucose with the inner cavity of the doughnut being hydrophobic while the exterior is hydrophilic.⁵⁴ Three types of CDs commonly occur in nature: α -, β - and γ -CD, and these correspond to six-, seven- and eight- membered glucose rings, respectively (Figure 5.1).⁵⁴ When CD molecules are added to an aqueous solution of associating polymers, the hydrophobic cavities of the CDs envelop and sequester the hydrophobes on the polymer chains.^{55-61,94,95} The hydrophobes are thereby prevented from associating with each other, and in turn, the solution viscosity is drastically reduced. Subsequent addition of surfactants to the above solutions can restore the viscosity: this is because the surfactants compete with the polymer hydrophobes for complexation with the CDs.^{57,60,61}

The focus of this study is the effect of temperature on solution viscosity. In the case of associating polymers, the viscosity typically drops exponentially upon heating.^{58,63,95} The variation of the zero-shear viscosity η_0 with temperature can then be depicted on an Arrhenius plot, which is a semilog plot of η_0 vs. $1/T$, where T is the absolute temperature.^{58,63} The slope of the straight line on this plot can be used to estimate the flow-activation energy E_a for the system. Mixtures of associating polymers and CDs, which tend to exhibit lower viscosities than the polymer alone, have also been studied as functions of temperature.^{58,61,95} In those cases also, a further drop in viscosity or other rheological properties is generally found upon heating, and again the data follow the Arrhenius relationship (with one exception,⁹⁵ see below).

In this Chapter, we report that mixtures of telechelic associating polymers (HEURs) and CDs can show *increases* in viscosity upon heating over a wide range of temperatures. As discussed above, this trend is unusual in the case of associating polymers. Indeed, an increase in viscosity upon heating (also called “thermo-thickening” or “thermo-gelling”) is observed in only a few classes of complex fluids, whether based on polymers,⁹⁶⁻⁹⁸ surfactants,^{99,100} or other hybrid supramolecules¹⁰¹. The majority of complex, structured fluids decrease in viscosity upon heating. Thus, thermo-thickening in HEUR/CD fluids is definitely worthy of study. Interestingly, we observe this behavior only with α -CDs and not with β - and γ -CDs. We have also investigated the effect of amphiphiles (single-tailed surfactants and double-tailed lipids) on the thermo-thickening. Strikingly, we find that the addition of lipids accentuates the thermo-thickening behavior whereas single-tailed surfactants have the opposite effect.

To our knowledge, there is only one other study that has reported comparable results and that is a recent one by Tam *et al.*⁹⁵ These authors studied mixtures of telechelic associating polymers and α -CDs and found that, depending on the concentration of α -CD, the solution viscosity either decreased monotonically with temperature or showed a modest increase over a range of temperatures. These results were explained in terms of a competition between the hydrophobic end-caps and the hydrophilic backbone of the polymer for complexation with α -CD molecules. In the present study, we explore thermo-thickening in HEUR/ α -CD mixtures in more detail using both rheological techniques and small-angle neutron scattering (SANS). We also explain how lipids accentuate this effect by virtue of their self-assembly into vesicle structures.

5.2 Experimental Section

Polymers. The associating polymer (HEUR) used in most of the studies was a gift from the Rohm & Haas Co. and is denoted by RM-825. This polymer has an overall molecular weight of about 25,000 and the hydrophobic end-caps are linear C₁₀ alkyl chains. The same polymer has been employed in several previous studies in the literature.^{102,103} The polymer was supplied as a purified wax and was used as received. In addition to RM-825, a few studies were also done with commercial associating polymers manufactured by OMG Borchers GmbH. One such polymer is denoted by BorchGel PW25 and this was supplied as a solution of ~ 25 wt% polymer in a 4:6 mixture of water:propylene glycol. The polymer was dried to constant weight in a vacuum oven for 48 h and the resulting solid material was used for making samples. Note that, while the BorchGel polymers are

known to be HEURs, no further information on molecular weight or hydrophobe length were provided by the manufacturer.

Cyclodextrins, Surfactants, and Other Materials. α -, β -, and γ -CDs (> 98% purity) were purchased from TCI America. The surfactants, cetyl trimethylammonium bromide (CTAB) and sodium dodecyl sulfate (SDS) (both > 99% purity) were purchased from Sigma-Aldrich. Lecithin (> 98% purity) was obtained from Avanti Polar Lipids.

Sample Preparation. Ultra-pure deionized water from a Millipore water-purification system was used in preparing samples for rheological characterization, while D₂O (99.95% deuteration, from Cambridge Isotopes) was used for the SANS studies. The samples without lecithin were prepared by dissolving weighed amounts of polymer, cyclodextrins and/or CTAB in water. The samples were heated to ~ 65°C under continuous stirring for about an hour till the solutions became homogeneous. Samples were then stirred continuously for one day and then left to equilibrate overnight at room temperature before any experiments were conducted. For samples containing lecithin, solutions were prepared by adding the lecithin to water and subsequently vortex mixing for 10 min. A Branson 1510 sonicator was then used for 2 hrs at 40 kHz to make vesicles. Weighted quantities of polymer and cyclodextrins were then added to the vesicle solutions and the mixture was stirred for one hour using a magnetic stirrer bar at ~ 65 °C. Thereafter, samples were stirred continuously overnight at room temperature to ensure that the final sample was completely homogeneous.

Rheological Studies. Steady and dynamic rheological experiments were performed on an AR2000 stress controlled rheometer (TA Instruments, Newark, DE). Samples were run on a cone-and-plate geometry (40-mm diameter, 4° cone angle) or a couette geometry (rotor of radius 14 mm and height 42 mm, and cup of radius 15 mm). For steady shear experiments at different temperatures, experiments were performed 1 hour after equilibrating loaded sample to desired temperature. Dynamic frequency spectra were obtained in the linear viscoelastic regime of each sample, as determined by dynamic strain-sweep experiments. For temperature sweep studies, we used a heating rate of 1 °C/min at a constant frequency of 10 sec⁻¹ and strain of 1%.

Small Angle Neutron Scattering (SANS). SANS measurements were made on the NG-7 and NG-3 (30 m) beamlines at NIST in Gaithersburg, MD. Neutrons with a wavelength of 6 Å were selected. Three sample-detector distances were used to obtain data over a range of wave vectors from 0.004 to 0.4 Å⁻¹. Samples were studied in 2 mm quartz cells at 25°C and 50°C. Scattering spectra were corrected and placed on an absolute scale using NIST calibration standards. The data are shown as plots of the absolute intensity I versus the wave vector $q = 4\pi\sin(\theta/2)/\lambda$, where λ is the wavelength of incident neutrons and θ the scattering angle.

5.3 Results and Discussion

HEUR + CD: Rheological Studies. First we present data on mixtures of a telechelic HEUR and different CDs at room temperature (25°C). The HEUR is RM-825 with a molecular weight around 25,000 and with linear C₁₀ alkyl chains as the hydrophobic end-

caps.^{102,103} A 5 wt% solution of RM-825 in deionized water showed a moderate viscosity. Under steady-shear rheology, the solution exhibited a Newtonian (shear-invariant) response with a constant viscosity of ~ 5 Pa.s over a range of shear-rates from 0.01 to 200 s^{-1} . The addition of all three CDs (α -, β -, and γ -) lowered the viscosity while the response remained Newtonian. The rheology of each sample can therefore be represented by a single value of the viscosity, denoted by η_0 , and this is shown in Figure 5.2 as a function of the CD concentration (note that the viscosity-axis is on a logarithmic scale).

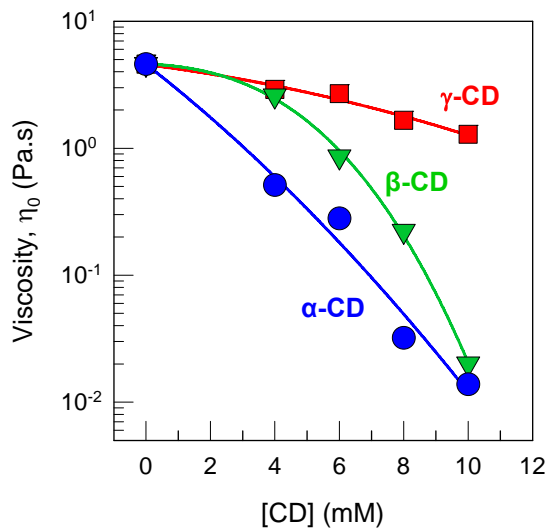


Figure 5.2. Zero-shear viscosity η_0 at room temperature (25°C) for 5% RM825 + CD mixtures as a function of the CD concentration. Data are shown for α -, β -, and γ -CD. In all cases, the viscosity drops with increasing [CD].

Figure 5.2 shows that the sharpest decrease in η_0 is caused by α -CD, with η_0 dropping by a factor of about 500 on addition of 10 mM α -CD. A much smaller drop in η_0 (factor of ~ 5) is observed upon addition of 10 mM of γ -CD. For both α - and γ -CD, the drop in η_0 with increasing CD concentration ([CD]) is approximately exponential

(straight line on the semilog plot). In the case of the β -CD, the magnitude of the viscosity drop is intermediate between that for α - and γ -CD, while the η_0 vs. [CD] relationship is non-exponential. Incidentally, for all these Newtonian liquids, the viscosity η_0 under steady-shear and the complex viscosity η^* under oscillatory shear are nearly identical. For experimental convenience, we prefer to focus on η^* over the rest of this paper; analogous results are available for η .

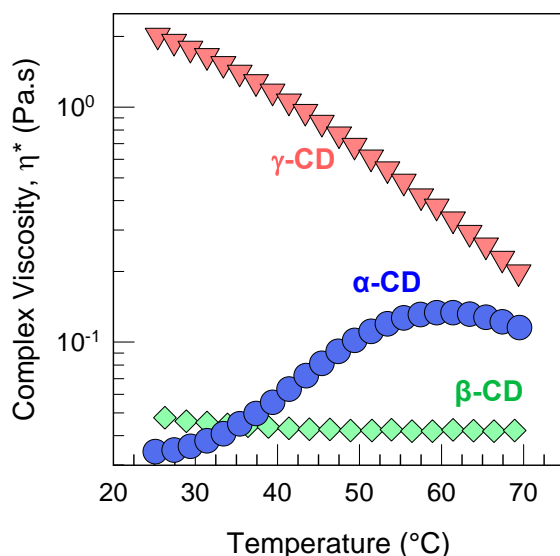


Figure 5.3. Viscosity as a function of temperature for solutions containing 7% RM825 and 14 mM of α -, β -, or γ -CD. The complex viscosity η^* is shown; similar results are available for the steady-shear viscosity. The viscosity decreases with temperature for the β - and γ -CD samples whereas the sample with α -CD shows an increase in viscosity with temperature (thermo-thickening).

As mentioned in the Introduction, the CD-induced decrease in the room-temperature viscosity of HEUR solutions is not surprising and has been observed before by several groups.^{56,58,61,95} The unusual result is that shown by Figure 5.3, which plots the

complex viscosity η^* of RM-825/CD solutions as a function of temperature. Results are compared for three samples, each with 7% RM-825 and 14 mM each of the three different CDs. The β -CD and γ -CD samples both show a decreasing viscosity with increasing temperature, i.e., these solutions become thinner upon heating. In contrast, the combination of RM-825 and α -CD shows a significant increase in viscosity over a range of temperatures (“thermo-thickening”). The above behavior of HEUR/ α -CD mixtures is rather unusual and is the focus of this paper.

Figure 5.4 further describes the temperature-dependent rheology of RM-825/ α -CD solutions over a range of polymer and α -CD concentrations. First, in Figure 5.4a, we study solutions with varying α -CD concentrations while the RM-825 concentration is fixed at 5 wt%. For all samples, the viscosity η^* increases over a range of temperatures followed by a drop in η^* at even higher temperatures. The higher the $[\alpha\text{-CD}]$, the lower the η^* at room temperature – correspondingly, the greater the extent of thermo-thickening (defined as the ratio of peak:initial η^*). Also, the peak in η^* is reached at a lower temperature for a lower $[\alpha\text{-CD}]$: e.g., the peak occurs at 45°C for 6 mM α -CD, 55°C for 8 mM α -CD and 62°C for 10 mM α -CD. Next, in Figure 4b, we show data for solutions over a range of RM-825 concentrations and with the α -CD content being proportionately higher. This allows us to compare solutions with similar initial viscosities at room temperature (around 20–30 mPa.s). All samples exhibit thermo-thickening, with its extent being higher for higher polymer concentrations. The greatest increase in viscosity is for the 7% RM825 + 14 mM α -CD sample for which η^* increases from 33

mPa.s at 25°C to 132 mPa.s at 62°C, which is a net increase by a factor of four. The peak temperature is approximately the same (~ 60°C) for all these samples.

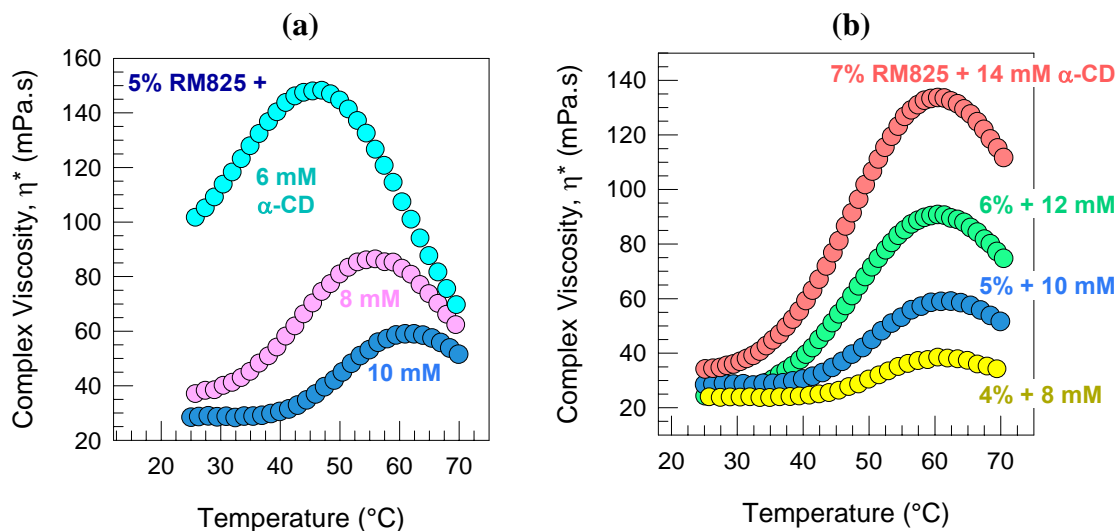


Figure 5.4. Thermo-thickening responses for different compositions of RM825 and α -CD. (a) Constant polymer concentration (5%), varying [α -CD]. (b) Different [polymer] and [α -CD] such that the solutions have approximately the same viscosity at room temperature.

HEUR + α -CD: SANS Studies. The above data provide clear evidence for thermo-thickening in certain HEUR/ α -CD solutions. To probe the underlying mechanism for these unusual results, we conducted SANS experiments on selected samples. Samples were made in D₂O to achieve the necessary contrast between the microstructure and the solvent; these samples were rheologically identical to those in H₂O. Figure 5.5 shows SANS spectra (I vs. q) for four solutions, each containing 5% RM-825 and with α -CD concentrations of 3, 5, 7 and 10 mM. Data are provided at room temperature (25°C) and at a temperature of 50°C, with the latter corresponding to the thermo-thickened state. Together the data reveal a number of systematic trends. First, consider the 3 mM α -CD

sample that shows negligible thermo-thickening: in this case, the curves at 25 and 50°C are nearly identical. In contrast, the remaining samples, which have higher $[\alpha\text{-CD}]$, show increasing differences between their 25 and 50°C spectra. The differences mainly occur at intermediate q (0.01 to 0.1 \AA^{-1}) whereas the curves are almost identical at lower and higher q . Also, with increasing $[\alpha\text{-CD}]$ at a constant temperature of 25°C, the intensity at intermediate q drops and a plateau appears, with the plateau being more pronounced at higher $[\alpha\text{-CD}]$. In other words, increasing $[\alpha\text{-CD}]$ lowers the intensity at intermediate q whereas increasing temperature restores this intensity. An obvious interpretation would be that the drop in intensity upon addition of $[\alpha\text{-CD}]$ corresponds to a *suppression of hydrophobic clustering* (due to complexation of the $\alpha\text{-CD}$ with the hydrophobes on the ends of the HEUR chains) while the increase in intensity with temperature occurs because the *hydrophobic clusters are restored*.

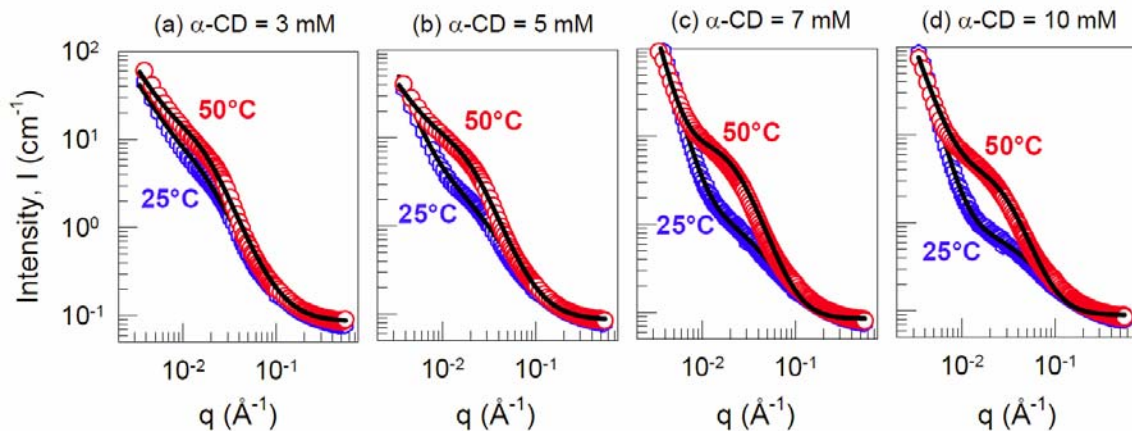


Figure 5.5. SANS data at low (25°C) and high (50°C) temperatures for solutions containing 5% RM825 and different concentrations of $\alpha\text{-CD}$. The solid lines through each curve are fits to eq 5.1.

To obtain further insight, we modeled the SANS data using the following functional form suggested by Hammouda et al.:^{104,105}

$$I(q) = \frac{A}{q^n} + \frac{B}{1 + (q\xi)^m} \quad (5.1)$$

Here, A and B are constants, n and m are power-law indices, and ξ is a correlation length. The model fits the curves in Figure 5.5 very well (fits shown as solid black lines through the data). The above model was originally developed to describe the SANS response from aqueous solutions of PEO.^{104,105} More recently, it has also been applied to SANS data from mixtures of CDs with a class of associating polymers (hydrophobically modified alginate).⁵⁹ The first term in the model (A/q^n) corresponds to Porod-like scattering from large clusters while the second term is a Lorentzian function to describe scattering from individual polymer chains.¹⁰⁵ Thus, the first term describes features in the data at low q , specifically the upturn in intensity, which in our case occurs similarly for all samples and temperatures. It is the second Lorentzian term that accounts for the plateau at intermediate q , and the key parameter here is the correlation length ξ .

Figure 5.6 plots the correlation length ξ as a function of $[\alpha\text{-CD}]$ and for the two temperatures of 25 and 50°C. We interpret ξ as an average size of local heterogeneities (hydrophobic clusters); thus, the larger the ξ the greater the clustering.^{59,105} As expected, ξ decreases with increasing $[\alpha\text{-CD}]$, implying a suppression of hydrophobic clustering. This is consistent with the complexation of polymer hydrophobes by $\alpha\text{-CD}$ molecules. Moreover, the ξ values at 50°C are higher than those at 25°C for all solutions, suggesting that hydrophobe-hydrophobe interactions are reactivated by heat (which in turn implies a

heat-induced weakening of hydrophobe-CD complexes). This result confirms the qualitative arguments put forward above and we will return to this point shortly when we further discuss the mechanism for thermo-thickening.

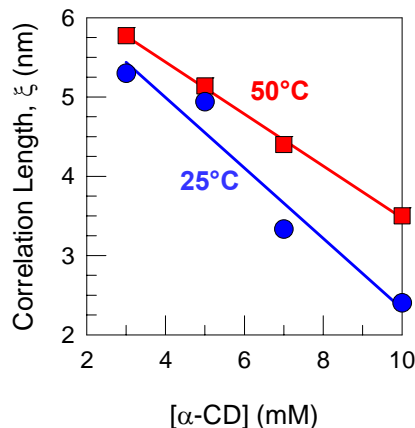


Figure 5.6. Correlation lengths ξ obtained from fits of eq 5.1 to the SANS data in Figure 5.5. The values are shown as functions of the α -CD concentration and for the two different temperatures. Lines through the data are guides for the eye.

HEUR + α -CD + Amphiphile: Rheological Studies. We now describe the effects of adding a surfactant or lipid to HEUR/ α -CD solutions. First, we consider a typical cationic surfactant, CTAB. The term surfactant is used here to imply a *single-tailed* amphiphile that usually forms micelles in water above its critical micelle concentration (cmc). In the case of CTAB, its cmc in deionized water is 0.92 mM.¹⁰⁶ As shown by Figure 5.7, adding CTAB at a concentration above its cmc reversed the CD-induced reduction in room-temperature viscosity as well as the thermo-thickening. The control sample for this experiment was a mixture of 6% RM-825 and 12 mM α -CD: its η^* vs. temperature data is shown for reference. Adding just 5 mM of CTAB increased the η^* at 25°C about 100-fold and η^* decreased monotonically upon heating. Increasing the CTAB content to

20 mM further increased the η^* at 25°C and again the η^* decreased upon heating. These results are to be expected: the added surfactant molecules should competitively bind with the α -CD, thereby liberating a large fraction of the polymer hydrophobes and restoring their associations.^{57,60,61} In addition to CTAB, we have tested other surfactants, including anionic ones like sodium dodecyl sulfate (SDS), and in all cases the surfactant eliminated the thermo-thickening.

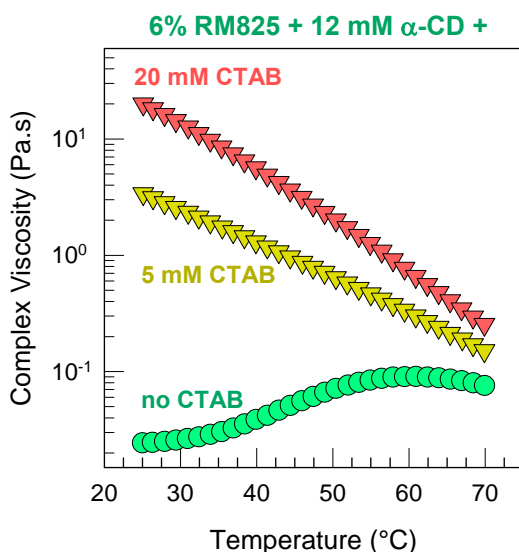


Figure 5.7. Viscosity vs. temperature for solutions of 6% RM825 + 12 mM α -CD in the absence and presence of the cationic surfactant, CTAB. In the presence of CTAB, the response shifts from thermo-thickening to thermo-thinning.

A different result was obtained, however, upon addition of lipids to HEUR/ α -CD solutions. The term lipid refers to *two-tailed* amphiphiles that assemble into vesicles (liposomes) in water. The typical lipid we have studied is lecithin and we have used a standard procedure to make vesicles of lecithin (see Experimental Section). We then combined lecithin vesicles with the HEUR and the α -CD. The control sample again is 6%

RM-825 + 12 mM α -CD, and as seen by Figure 5.8, it shows considerable thermo-thickening (factor of 3.4 increase in η^* with temperature). Adding 10 mM of lecithin vesicles to this sample has negligible effect on the room-temperature viscosity, but the thermo-thickening is enhanced. Further increase in lecithin concentration to 20 mM accentuates the thermo-thickening even more. The overall extent of thermo-thickening, i.e., the ratio of peak:initial η^* is by a factor of 4.6 for the 20 mM lecithin sample. Thus, the addition of lipid vesicles enhances thermo-thickening.

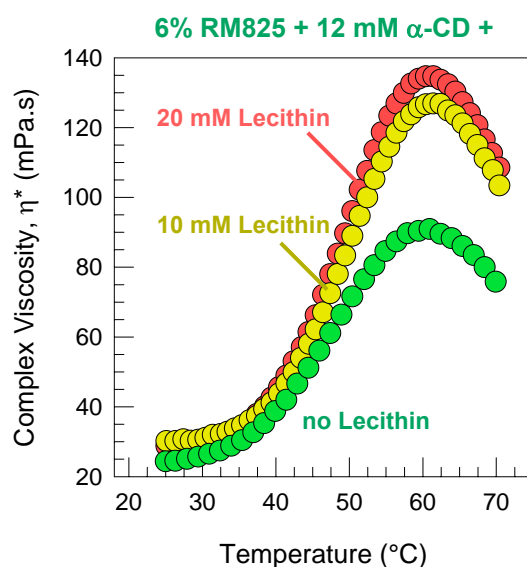


Figure 5.8. Viscosity vs. temperature for solutions of 6% RM825 + 12 mM α -CD in the absence and presence of vesicles of the lipid, lecithin. The presence of lecithin vesicles accentuates the thermo-thickening response.

Thermo-thickening in solutions of HEUR polymers and α -CD is reproducible, as is the enhancement of this effect by addition of lipids. As an example of the robustness of this result, we show data for a different HEUR polymer from a different vendor. This polymer is a commercial, unpurified product from OMG Borchers GmbH and is denoted

by Borchigel PW25. Figure 5.9 presents rheological data for a 5% solution of this polymer combined with 10 mM of α -CD: the data again reveal substantial thermo-thickening. Additionally, we present data for the above sample combined with 10 mM of lecithin vesicles and once again we find that the vesicles accentuate the thermo-thickening. Based on these data, we can generalize the above trends to hold for a range of HEUR polymers.

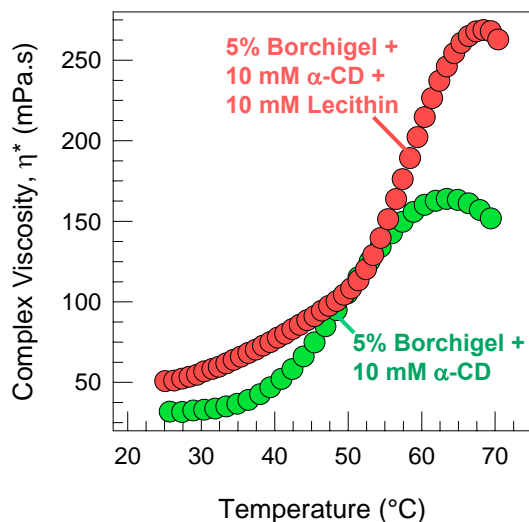


Figure 5.9. Viscosity vs. temperature for solutions of 5% Borchigel PW25 + 10 mM α -CD in the absence and presence of 10 mM lecithin vesicles. This HEUR/ α -CD mixture also shows thermo-thickening and lecithin vesicles again enhance the effect.

Mechanism for Thermo-Thickening. We now attempt to provide sensible explanations for the results described above. Our first result (Figure 5.2) showed that the room-temperature viscosity of HEUR solutions was lowered by all three CDs. This is an expected result and is clearly due to complexation of the hydrophobes on HEUR chain ends by CD molecules. The extent of viscosity reduction follows the trend α -CD > β -CD

> γ -CD (Figure 5.2), which is due to the size of the CD cavity relative to the size of the hydrophobic group.⁵⁵ For hydrophobes $\sim C_{10}$, as is the case here, the same trend has been observed in earlier studies as well.^{55,57} Next, we come to our significant result, which is the observation of thermo-thickening in solutions of HEUR and α -CD, but not in solutions with β - or γ -CD (Figure 5.3). What causes thermo-thickening, and why does it occur only in the case of α -CD? We will now address these questions.

Our SANS data and its corresponding modeling (Figures 5.5 and 5.6) suggested that inclusion complexes between hydrophobes and α -CD molecules get disrupted by heat. The hydrophobes released from the α -CDs can then re-associate with each other, leading to a reactivation of hydrophobic clusters and thereby an increase in solution viscosity with temperature. But why does heat weaken hydrophobe/ α -CD complexes alone and not those with β - or γ -CD? We believe that, at higher temperatures, the PEO *backbone* of the HEUR chains *competes* with the hydrophobic chain ends for forming inclusion complexes with α -CDs.⁹⁵ Complex formation between PEO and α -CD has been corroborated by a number of studies.¹⁰⁷⁻¹⁰⁹ In contrast, β - and γ -CDs do not complex with PEO because their cavities are considerably larger than the cross-section of a PEO chain.¹⁰⁹ Complexation between PEO and α -CD is itself likely to be promoted at higher temperatures because the PEO backbone becomes more hydrophobic^{104,105} and thereby more compatible with the hydrophobic cavity of the α -CD.

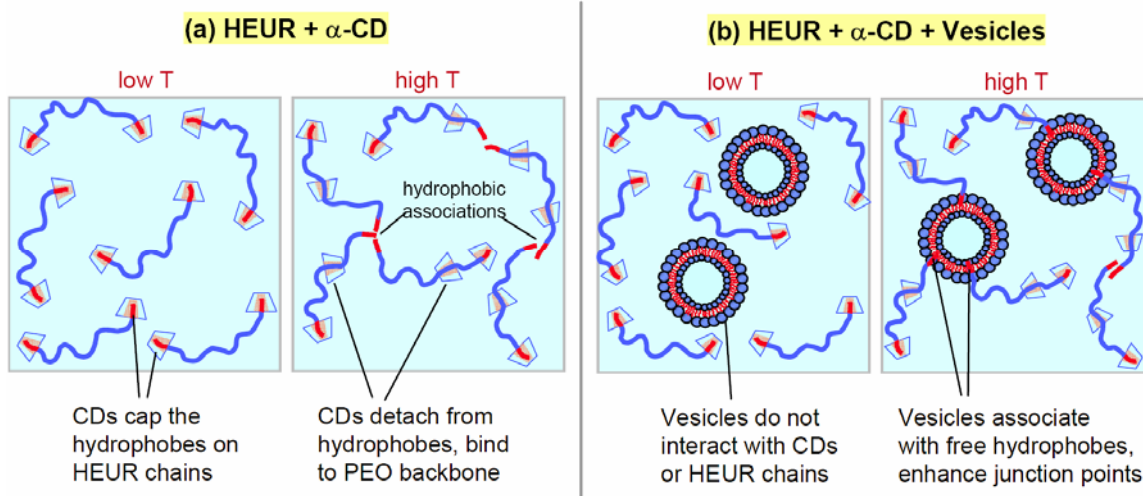


Figure 5.10. (a) Mechanism for thermo-thickening in HEUR/ α -CD mixtures. At low T , the hydrophobes on HEUR chain ends are capped by α -CDs and the viscosity is hence low. Upon heating, some of the α -CDs detach from the hydrophobes and bind to the PEO backbone of the HEUR chains. The liberated hydrophobes associate with each other and thereby enhance the solution viscosity. (b) Mechanism for the enhancement of thermo-thickening by lipid vesicles. The vesicles do not bind to the α -CD and the solution has a low viscosity at low T . Upon heating, some hydrophobes get freed and these can either associate with each other or with the bilayers of the vesicles. The vesicles, in effect, increase the connectivity of HEUR chains and this further enhances the viscosity.

Taken together, we explain thermo-thickening by the schematics in Figure 5.10a. At low temperatures, the α -CD is bound to the hydrophobes on HEUR chain ends and the viscosity is low. At higher temperatures, some of the α -CDs unbind from the hydrophobes and thread onto the PEO backbone of the HEUR chains. This frees up some hydrophobes, which associate with each other and thereby cause an increase in viscosity. It is worth noting that the binding of α -CD with the polymer backbone occurs only in the case of PEO.¹⁰⁸ Other associating polymers such as hydrophobically modified derivatives of chitosan, alginate or hydroxyethyl cellulose (HEC), as well as hydrophobic alkali-soluble emulsion polymers (HASE) do not have backbones that can complex with α -

CD,⁵⁷ as a result, no evidence for thermo-thickening has been reported in past studies (or detected in our laboratory) for mixtures of the above polymers with α -CD.

Next, we discuss why double-tailed lipids accentuate the thermo-thickening of HEUR/ α -CD mixtures (Figure 5.8) whereas single-tailed surfactants revert the viscosity to the typical thermo-thinning trend (Figure 5.7). First, consider single-tailed surfactants: these are known to have high affinities for CDs – for example, the binding constants for CTAB and SDS with α -CD are 99,200 and 21,000 M^{-1} respectively.^{110,111} These surfactants can therefore effectively displace polymer hydrophobes from the cavities of α -CD molecules. The liberated hydrophobes will then associate and give rise to a high solution viscosity at room temperature. As temperature is raised, the progressive disruption of hydrophobic associations leads to thermo-thinning, much like for neat HEUR solutions. In contrast to surfactants, the binding constants of lipids with CDs are very low, i.e., they have weak affinities for CDs. For example, a lipid with two C_7 tails is reported to have binding constants of 550, 1290, and 750 M^{-1} for α , β , and γ -CDs respectively.¹¹² The weaker binding of lipids is because the CDs can typically include only one alkyl chain in their cavities.¹¹² This explains why the HEUR/ α -CD solution retains its low viscosity upon addition of lecithin, i.e., the hydrophobes remain bound to the α -CDs. In turn, the added lecithin will remain in solution in the form of nanosized unilamellar vesicles (Figure 5.10b).

Now, consider the effect of heating a lecithin/HEUR/ α -CD mixture. As discussed above, the α -CD will tend to dissociate from the hydrophobes and instead bind to the

PEO backbone of the HEUR. This will liberate several polymer hydrophobes, which will now be free to interact amongst each other as well as with the unilamellar lecithin vesicles. We hypothesize that some polymer hydrophobes will get embedded in the bilayers of vesicles (Figure 5.10b).¹¹³⁻¹¹⁵ This will enhance the “cross-links” or junction points between the polymer chains, in turn enhancing the thermo-thickening effect. Support for this hypothesis comes from a number of studies on mixtures of associative polymers and vesicles, which have shown viscosity enhancement due to vesicles.¹¹³⁻¹¹⁵ In this context, a higher volume fraction of vesicles will provide more junction points and will thereby permit a higher viscosity to be reached, which is quite consistent with the data in Figure 5.8.

5.4 Conclusions

Aqueous mixtures of HEUR type associating polymers and α -CDs show thermo-thickening, i.e., an increase in viscosity with temperature. The solutions have a low viscosity at room temperature because the hydrophobic end-groups on HEUR chains are sequestered inside the cavities of the α -CDs. As temperature is increased, the increasing affinity of the α -CDs for the PEO backbone of the HEUR causes some of the hydrophobes to be liberated, and the association of these hydrophobes causes thermo-thickening. The effect is not observed with β - and γ -CDs because they do not form inclusion complexes with PEO. Thermo-thickening of HEUR/ α -CD mixtures is accentuated by the addition of lipid vesicles. Lipids (two-tailed amphiphiles) do not bind with α -CD since the cavity in α -CD can accommodate only one hydrophobic tail. As a result, at room temperature, the α -CDs remain bound to the polymer hydrophobes, while

the lipid vesicles are also left intact in solution. Upon heating, some of the polymer hydrophobes disengage from the α -CD as explained above. These free hydrophobes can either connect with each other or can bind to vesicle bilayers. In effect, the vesicles enhance the connectivity of the hydrophobes, which explains why the thermo-thickening effect is enhanced.

Chapter 6

Conclusions and Recommendations

6.1 Conclusions

Previous formulations of PR and TR fluids required synthesis of complex photosensitive molecules, which hindered the widespread use of these fluids. In this dissertation, we have reported two novel formulations of PR fluids and one new class of TR fluids that require no special synthesis and can therefore be easily replicated in any laboratory from inexpensive chemicals. These consist of: a photogelling aqueous fluid (Chapter 3), a photothinning fluid based on a non-polar organic solvent (Chapter 4), and a reversible thermo-thickening aqueous fluid (Chapter 5). Such PR and TR fluids may be of use in a range of applications, such as in sensors and valves in microfluidic devices.

In the first study (Chapter 3), we reported a class of aqueous fluids that exhibited “photogelling”, i.e., a substantial (10,000-fold) increase in fluid viscosity upon exposure to light. This increase in viscosity was triggered by the light-activated growth of wormlike micelles in the sample. The key components in the above fluids were the zwitterionic surfactant, erucyl dimethyl amidopropyl betaine (EDAB) and the photoresponsive molecule, *trans*-ortho-methoxy-cinnamic acid (OMCA), both of which are commercially available. When these two chemicals were combined at high (> 2:1) OMCA:EDAB molar ratios, short cylindrical micelles were formed in aqueous solution.

Upon irradiation by UV light (< 400 nm), OMCA got photoisomerized to its *cis* form, which then desorbed from EDAB micelles. In turn, a transition from short to long, entangled micelles ensued. Support for the above mechanism was provided by zeta-potential and small-angle neutron scattering (SANS) studies.

In the second study (Chapter 4), we extended the concept of PR fluids to non-aqueous systems, and demonstrated a one-way, light-induced viscosity reduction (i.e., photothinning). Here, we created a novel formulation of reverse micellar fluids by mixing the commonly available zwitterionic lipids (e.g., lecithin) with the photosensitive molecule PCA in organic solvents. When the *trans* form of PCA was added to lecithin reverse micelles, the solution became highly viscous and viscoelastic. Upon irradiation with UV light, *trans*-PCA was photoisomerized to *cis*-PCA, which caused the sample to transform into a low viscosity, Newtonian fluid. Using techniques such as SANS and UV-Vis spectroscopy, we were able to show that the light-induced transitions at the molecular level correlated at the microstructural level with a reduction in the length of wormlike micelles.

In our last study (Chapter 5), we reported a reversible thermo-thickening system in which the viscosity increased significantly upon heating. These fluids were mixtures of telechelic associating polymers (HEURs) and cyclodextrins (α -CDs) in water. These results were explained in terms of a competition between the hydrophobic end-caps and the hydrophilic backbone of the polymer for complexation with α -CD molecules. We also demonstrated that the thermo-thickening of HEUR/ α -CD mixtures was accentuated

by the addition of lipid vesicles as they enhanced the connectivity of the polymer hydrophobes at higher temperatures.

6.2 Recommendations for Future Work

We suggest three feasible projects for future work, which would extend the studies conducted in this dissertation as well as explore new concepts and applications.

6.2.1 Reversible PR Fluids

In Chapters 3 and 4, we described two new simple photorheological fluids, which exhibited one way switch in rheology upon UV irradiation, i.e., either gelling or thinning. However the transitions were not reversible. As part of future work, the concept can be extended to develop a reversible PR fluid. For this, alternate photo-additives should be considered that exhibit reversible photoisomerization, such as azobenzene, spiropyran, and photo-acid derivatives. In particular, additives that can promote faster reversible switching of rheological properties would be highly desirable.

6.2.2 Microfluidic Devices Incorporating PR Fluids

Our “smart” PR and TR fluids have an enormous application potential in several emerging technologies, such as micro- and nano-fluidic devices. These stimuli responsive fluids are nano-structured, homogeneous, stable, and single-phase systems that change macroscopic properties by transforming themselves at nanoscale – thus their intrinsic length scale is small enough for use in micro-nano-technologies. Especially, the use of

light as the stimulus permits for a directed control at a precise spatial location (with a resolution on the order of microns). We have already started working on the development of a microfluidic photonic device incorporating our photogelling fluids (EDAB/OMCA) described in Chapter 3. We are collaborating with Dr. Edo Waks and Dr. Benjamin Shapiro's research groups at U. Maryland in this project. The idea is to precisely steer the multiple semiconductor quantum-dots to specific locations in a micro channel by electroosmotic flow control, and then entrap them there by photogelling the media locally to nm accuracy. We have already demonstrated the sequential steering and freezing of three quantum-dots at defined locations in a microchannel. As a part of future work, this study can be extended to more than three q-dots and the system can be further refined and optimized in terms of speed and strength of freezing. Also, the fluids with reversible light induced changes in rheological properties could be especially interesting for such microfluidic applications.

6.2.3 Methods for Writing and Erasing Patterns in Gels with Light

Lastly, we recommend an extremely simple yet effective method (involving no complicated chemistry) of writing and erasing colored 3-D patterns in soft materials, such as polymer-surfactant gels or films. This arose out of some initial experiments that we have conducted in our laboratory with photochromatic molecules, i.e., reversible color change upon UV or visible light irradiation. One material which has attracted a lot of attention in this field is 1',3',3'-trimethyl-6-nitrospiro[1-benzopyran-2,2-indoline], also referred to as Spiropyran (SP). It is a strongly photochromic molecule that undergoes the photochemical change shown in Figure 6.1. The ambient form of SP (left) has an

through a mask, a pink-colored pattern is formed in the gel, corresponding to the regions of the mask that are exposed to the light. The pink color indicates the conversion of the SP into its MC form. Figure 6.2 shows that the patterns over a size scale of millimeters can be formed in the gel. The pattern is maintained as long as the gel is stored in the dark; when exposed to visible light or heat, the merocyanine reverts to its original spiropyran form and the pattern disappears.

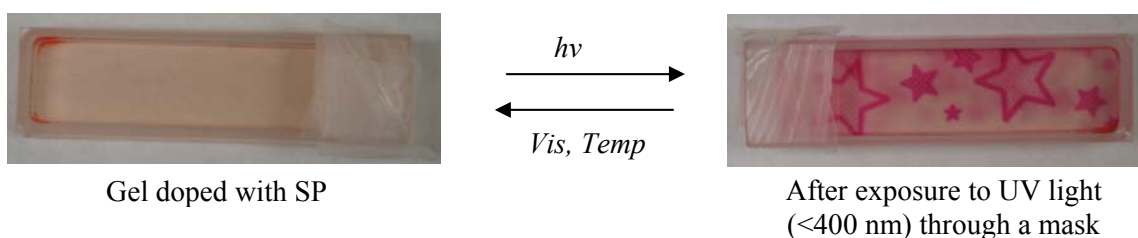


Figure 6.2. Reversibly creating and erasing spatial patterns on a SP-doped gel by irradiating through a mask.

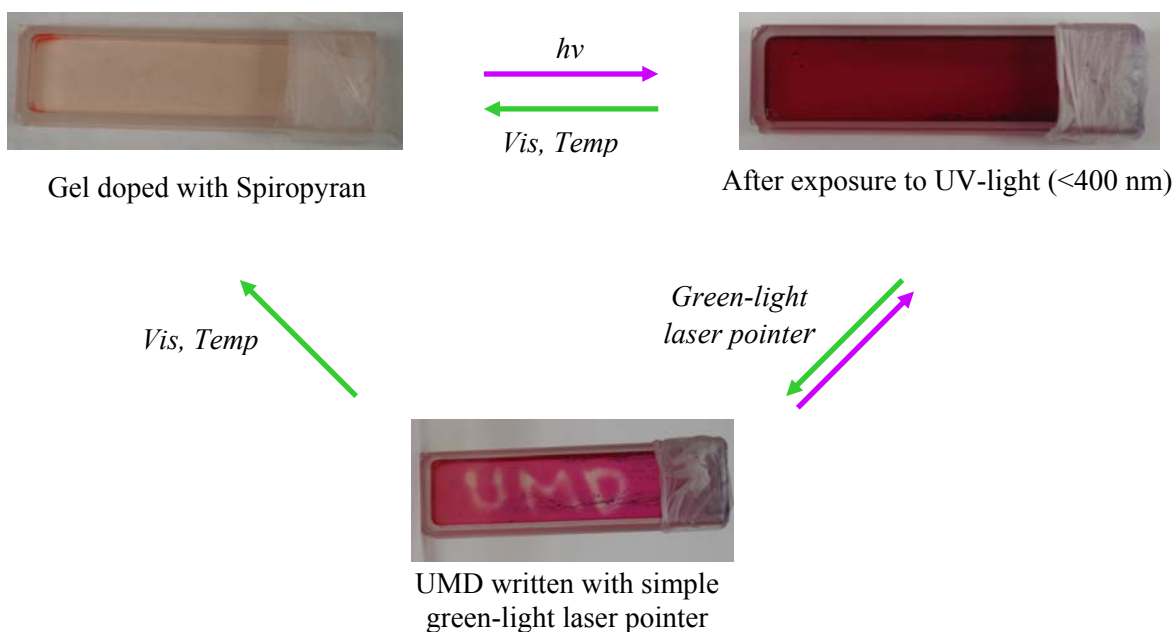


Figure 6.3. Reversibly writing and erasing on SP-doped gel by simple green-light laser pointer.

Working on similar lines, we demonstrate one more interesting experiment in Figure 6.3. Here, as a first step, a colorless SP-doped gel is irradiated uniformly to create a red gel (corresponding to the transformation of SP to MC). We now use a green laser pointer to write patterns onto this gel. As shown in Figure 6.3, we were able to write word “UMD” on this material within few seconds. Again the pattern can be erased simply by exposing the sample to visible or ultraviolet light. Note that, both in Figures 6.2 and 6.3, the patterns are created all the way through the gel – i.e., in three dimensions.

Future work on this project could involve the creation of patterns at much smaller length scales as well as on other types of gels (e.g., gelatin gels containing surfactant). The key idea, again, is that no special synthesis of new molecules would be required – instead, these patternable materials can be created simply by mixing commercial spiropyran with existing gel-forming molecules.

References

- [1] Jeong, B.; Kim, S. W.; Bae, Y. H. "Thermosensitive sol-gel reversible hydrogels." *Advanced Drug Delivery Reviews* **2002**, *54*, 37-51.
- [2] Bromberg, L. E.; Ron, E. S. "Temperature-responsive gels and thermogelling polymer matrices for protein and peptide delivery." *Advanced Drug Delivery Reviews* **1998**, *31*, 197-221.
- [3] Kan, C. W.; Doherty, E. A. S.; Barron, A. E. "A novel thermogelling matrix for microchannel DNA sequencing based on poly-N-alkoxyalkylacrylamide copolymers." *Electrophoresis* **2003**, *24*, 4161-4169.
- [4] Hao, T. "Electrorheological fluids." *Advanced Materials* **2001**, *13*, 1847-+.
- [5] Rankin, P. J.; Ginder, J. M.; Klingenberg, D. J. "Electro- and magneto-rheology." *Current Opinion in Colloid & Interface Science* **1998**, *3*, 373-381.
- [6] Minagawa, K.; Koyama, K. "Electro- and magneto-rheological materials: Stimuli-induced rheological functions." *Current Organic Chemistry* **2005**, *9*, 1643-1663.
- [7] Aminabhavi, T. M.; Agnihotri, S. A.; Naidu, B. V. K. "Rheological properties and drug release characteristics of pH-responsive hydrogels." *Journal of Applied Polymer Science* **2004**, *94*, 2057-2064.
- [8] Bossard, F.; Aubry, T.; Gotzamanis, G.; Tsitsilianis, C. "pH-Tunable rheological properties of a telechelic cationic polyelectrolyte reversible hydrogel." *Soft Matter* **2006**, *2*, 510-516.
- [9] Eastoe, J.; Vesperinas, A. "Self-assembly of light-sensitive surfactants." *Soft Matter* **2005**, *1*, 338-347.
- [10] Vesperinas, A.; Eastoe, J.; Wyatt, P.; Grillo, I.; Heenan, R. K. "Photosensitive gelatin." *Chemical Communications* **2006**, 4407-4409.
- [11] Wolff, T.; Emming, C. S.; Suck, T. A.; Vonbunau, G. "Photorheological Effects in Micellar Solutions Containing Anthracene-Derivatives - a Rheological and Static Low-Angle Light-Scattering Study." *Journal of Physical Chemistry* **1989**, *93*, 4894-4898.
- [12] Lee, C. T.; Smith, K. A.; Hatton, T. A. "Photoreversible viscosity changes and gelation in mixtures of hydrophobically modified polyelectrolytes and photosensitive surfactants." *Macromolecules* **2004**, *37*, 5397-5405.

- [13] Sakai, H.; Orihara, Y.; Kodashima, H.; Matsumura, A.; Ohkubo, T.; Tsuchiya, K.; Abe, M. "Photoinduced reversible change of fluid viscosity." *Journal of the American Chemical Society* **2005**, *127*, 13454-13455.
- [14] Pouliquen, G.; Tribet, C. "Light-triggered association of bovine serum albumin and azobenzene-modified poly(acrylic acid) in dilute and semidilute solutions." *Macromolecules* **2006**, *39*, 373-383.
- [15] Israelachvili, J. N. "Intermolecular and Surface Forces." *Academic Press: New York* **1992**.
- [16] Hoffmann, H. "Fascinating Phenomena in Surfactant Chemistry." *Advances in Colloid and Interface Science* **1990**, *32*, 123-150.
- [17] Israelachvili, J. N.; Mitchell, D. J.; Ninham, B. W. "Theory of Self-Assembly of Hydrocarbon Amphiphiles into Micelles and Bilayers." *Journal of the Chemical Society-Faraday Transactions I* **1976**, *72*, 1525-1568.
- [18] Mitchell, D. J.; Ninham, B. W. "Micelles, Vesicles and Micro-Emulsions." *Journal of the Chemical Society-Faraday Transactions I* **1981**, *77*, 601-629.
- [19] Dreiss, C. A. "Wormlike micelles: where do we stand? Recent developments, linear rheology and scattering techniques." *Soft Matter* **2007**, *3*, 956-970.
- [20] Hoffmann, H. Viscoelastic Surfactant Solutions. In *Structure and Flow in Surfactant Solutions*; Herb, C. A., Prud'homme, R. K., Eds.; American Chemical Society: Washington, DC, 1994; Vol. 578; pp 2-31.
- [21] Berret, J. F. Rheology of Wormlike Micelles. In *Molecular Gels*; Weiss, R. G., Terech, P., Eds.; Springer: Dordrecht, 2005; pp 235-275.
- [22] Cates, M. E.; Candau, S. J. "Statics and Dynamics of Worm-Like Surfactant Micelles." *Journal of Physics-Condensed Matter* **1990**, *2*, 6869-6892.
- [23] Ezrahi, S.; Tuval, E.; Aserin, A. "Properties, main applications and perspectives of worm micelles." *Advances in Colloid and Interface Science* **2006**, *128*, 77-102.
- [24] Yang, J. "Viscoelastic wormlike micelles and their applications." *Current Opinion in Colloid & Interface Science* **2002**, *7*, 276-281.
- [25] Larson, R. G. "The structure and Rheology of Complex Fluids." *Oxford University Press: Oxford* **1999**.
- [26] Appell, J.; Porte, G. "Polymer-Like Behavior of Giant Micelles." *Europhysics Letters* **1990**, *12*, 185-190.

- [27] Candau, S. J.; Hirsch, E.; Zana, R.; Adam, M. "Network Properties of Semidilute Aqueous Kbr Solutions of Cetyltrimethylammonium Bromide." *Journal of Colloid and Interface Science* **1988**, *122*, 430-440.
- [28] Imae, T.; Ikeda, S. "Sphere Rod Transition of Micelles of Tetradecyltrimethylammonium Halides in Aqueous Sodium-Halide Solutions and Flexibility and Entanglement of Long Rodlike Micelles." *Journal of Physical Chemistry* **1986**, *90*, 5216-5223.
- [29] Kern, F.; Lemarechal, P.; Candau, S. J.; Cates, M. E. "Rheological Properties of Semidilute and Concentrated Aqueous-Solutions of Cetyltrimethylammonium Bromide in the Presence of Potassium-Bromide." *Langmuir* **1992**, *8*, 437-440.
- [30] Rehage, H.; Hoffmann, H. "Viscoelastic Surfactant Solutions - Model Systems for Rheological Research." *Molecular Physics* **1991**, *74*, 933-973.
- [31] Harrison, D.; Szule, R.; Fisch, M. R. "Solution behavior of the zwitterionic surfactant octadecyldimethylbetaine." *Journal of Physical Chemistry B* **1998**, *102*, 6487-6492.
- [32] Hashimoto, K.; Imae, T. "Rheological Properties of Aqueous-Solutions of Alkyldimethylamine and Oleyldimethylamine Oxides - Spinnability and Viscoelasticity." *Langmuir* **1991**, *7*, 1734-1741.
- [33] Lopez-Diaz, D.; Garcia-Mateos, I.; Velazquez, M. M. "Synergism in mixtures of zwitterionic and ionic surfactants." *Colloids and Surfaces a-Physicochemical and Engineering Aspects* **2005**, *270*, 153-162.
- [34] Ono, Y.; Shikata, T. "Dielectric behavior of aqueous micellar solutions of betaine-type surfactants." *Journal of Physical Chemistry B* **2005**, *109*, 7412-7419.
- [35] Shikata, T.; Itatani, S. "Viscoelastic behavior of aqueous threadlike micellar solutions of oleyldimethylamineoxide." *Colloid and Polymer Science* **2003**, *281*, 447-454.
- [36] Weers, J. G.; Rathman, J. F.; Axe, F. U.; Crichlow, C. A.; Foland, L. D.; Scheuing, D. R.; Wiersema, R. J.; Zielske, A. G. "Effect of the Intramolecular Charge Separation Distance on the Solution Properties of Betaines and Sulfobetaines." *Langmuir* **1991**, *7*, 854-867.
- [37] Tung, S.-H. Self-Assembly of Amphiphilic Molecules in Organic Liquids Doctor of Philosophy, University of Maryland, **2007**.
- [38] Larson, R. G. *The Structure and Rheology of Complex Fluids*; Oxford University Press: New York, **1998**.

- [39] Harrison, W. J.; McDonald, M. P.; Tiddy, G. J. T. "Phase-Behavior and Mesophase Formation in the Lithium Phenylstearate + 1-Phenylheptane System." *Journal of Physical Chemistry* **1991**, *95*, 4136-4140.
- [40] Hellweg, T.; Eimer, W. "The micro-structures formed by Ni²⁺-AOT/cyclohexane/water microemulsions: a light scattering study." *Colloids and Surfaces a-Physicochemical and Engineering Aspects* **1998**, *136*, 97-107.
- [41] Scartazzini, R.; Luisi, P. L. "Organogels from Lecithins." *Journal of Physical Chemistry* **1988**, *92*, 829-833.
- [42] Steytler, D. C.; Jenta, T. R.; Robinson, B. H.; Eastoe, J.; Heenan, R. K. "Structure of reversed micelles formed by metal salts of bis(ethylhexyl) phosphoric acid." *Langmuir* **1996**, *12*, 1483-1489.
- [43] Yu, Z. J.; Neuman, R. D. "Giant Rodlike Reversed Micelles Formed by Sodium Bis(2-Ethylhexyl) Phosphate in N-Heptane." *Langmuir* **1994**, *10*, 2553-2558.
- [44] Shchipunov, Y. A.; Shumilina, E. V. "Lecithin Bridging by Hydrogen-Bonds in the Organogel." *Materials Science and Engineering C-Biomimetic Materials Sensors and Systems* **1995**, *3*, 43-50.
- [45] Willard, D. M.; Riter, R. E.; Levinger, N. E. "Dynamics of polar solvation in lecithin/water/cyclohexane reverse micelles." *Journal of the American Chemical Society* **1998**, *120*, 4151-4160.
- [46] Saltiel, J. S., D. F. J. K., Dong-Hoon ; Park, Kyung-Mi. "Cis-Trans Isomerization of Alkenes." *In CRC Handbook of Organic Photochemistry and Photobiology*, Horspool, W. M.; Song, P.-S., Eds. CRC Press, Inc.: New York **1995**, *2*.
- [47] Dou, Y. S.; Allen, R. E. "Detailed dynamics of a complex photochemical reaction: Cis-trans photoisomerization of stilbene." *Journal of Chemical Physics* **2003**, *119*, 10658-10666.
- [48] Waldeck, D. H. "Photoisomerization Dynamics of Stilbenes." *Chemical Reviews* **1991**, *91*, 415-436.
- [49] Rau, H. Photoisomerization of Azobenzenes. *In Photochemistry and Photophysics*; Rabek, J. F., Ed.; CRC Press: Boca Raton, FL, **1990**; Vol. 2.
- [50] Kumar, G. S.; Neckers, D. C. "Photochemistry of Azobenzene-Containing Polymers." *Chemical Reviews* **1989**, *89*, 1915-1925.
- [51] Suginome, H. "E,Z-Isomerization of Imines, Oximes, and Azo Compounds." *In CRC Handbook of Organic Photochemistry and Photobiology*, Horspool, W. M.; Song, P.-S., Eds. CRC Press, Inc.: New York **1995**, 824-840.

- [52] Mohan, J. "Organic Spectroscopy Principles and Applications 2nd edition. Alpha Science International Ltd.: India." **2004**.
- [53] Galant, C.; Wintgens, W.; Amiel, C.; Auvray, L. "A reversible polyelectrolyte involving a beta-cyclodextrin polymer and a cationic surfactant." *Macromolecules* **2005**, *38*, 5243-5253.
- [54] Szejtli, J. "Introduction and general overview of cyclodextrin chemistry." *Chemical Reviews* **1998**, *98*, 1743-1753.
- [55] Tonelli, A. E. "Nanostructuring and functionalizing polymers with cyclodextrins." *Polymer* **2008**, *49*, 1725-1736.
- [56] Karlson, L.; Thuresson, K.; Lindman, B. "Cyclodextrins in hydrophobically modified poly(ethylene glycol) solutions: Inhibition of polymer-polymer associations." *Langmuir* **2002**, *18*, 9028-9034.
- [57] Abdala, A. A.; Tonelli, A. E.; Khan, S. A. "Modulation of hydrophobic interactions in associative polymers using inclusion compounds and surfactants." *Macromolecules* **2003**, *36*, 7833-7841.
- [58] Liao, D.; Dai, S.; Tam, K. C. "Rheological properties of hydrophobic ethoxylated urethane (HEUR) in the presence of methylated beta-cyclodextrin." *Polymer* **2004**, *45*, 8339-8348.
- [59] Burckbuchler, V.; Kjoniksen, A. L.; Galant, C.; Lund, R.; Amiel, C.; Knudsen, K. D.; Nystrom, B. "Rheological and structural characterization of the interactions between cyclodextrin compounds and hydrophobically modified alginate." *Biomacromolecules* **2006**, *7*, 1871-1878.
- [60] Talwar, S.; Harding, J.; Oleson, K. R.; Khan, S. A. "Surfactant-mediated modulation of hydrophobic interactions in associative polymer solutions containing cyclodextrin." *Langmuir* **2009**, *25*, 794-802.
- [61] Liao, D. S.; Dai, S.; Tam, K. C. "Influence of anionic surfactant on the rheological properties of hydrophobically modified polyethylene-oxide/cyclodextrin inclusion complexes." *Journal of Rheology* **2009**, *53*, 293-308.
- [62] Challa, R.; Ahuja, A.; Ali, J.; Khar, R. K. "Cyclodextrins in drug delivery: An updated review." *Aaps Pharmscitech* **2005**, *6*, E329-E357.
- [63] Annable, T.; Buscall, R.; Ettelaie, R.; Whittlestone, D. "The rheology of solutions of associating polymers - Comparison of experimental behavior with transient network theory." *Journal of Rheology* **1993**, *37*, 695-726.

- [64] Winnik, M. A.; Yekta, A. "Associative polymers in aqueous solution." *Current Opinion in Colloid & Interface Science* **1997**, *2*, 424-436.
- [65] Menchen, S.; Johnson, B.; Winnik, M. A.; Xu, B. "Flowable networks as equilibrium DNA sequencing media in capillary columns." *Chemistry of Materials* **1996**, *8*, 2205-&.
- [66] Macosko, C. W. *Rheology: Principles, Measurements and Applications*; VCH Publishers: New York, 1994.
- [67] Morrison, F. A. *Understanding Rheology*; Oxford University Press: New York, 2001.
- [68] Zemb, T. L., P. "Neutron, X-Ray and Light Scattering: Introduction to an Investigative Tool for Colloidal and Polymeric Systems." *Elsevier: Amsterdam* **1991**.
- [69] Paulusse, J. M. J.; Sijbesma, R. P. "Molecule-based rheology switching." *Angewandte Chemie-International Edition* **2006**, *45*, 2334-2337.
- [70] Tomatsu, I.; Hashidzume, A.; Harada, A. "Photoresponsive hydrogel system using molecular recognition of alpha-cyclodextrin." *Macromolecules* **2005**, *38*, 5223-5227.
- [71] Ketner, A. M.; Kumar, R.; Davies, T. S.; Elder, P. W.; Raghavan, S. R. "A simple class of photorheological fluids: Surfactant solutions with viscosity tunable by light." *Journal of the American Chemical Society* **2007**, *129*, 1553-1559.
- [72] Wolff, T.; Emming, C. S.; Suck, T. A.; Von Bunau, G. "Photorheological Effects in Micellar Solutions Containing Anthracene-Derivatives - a Rheological and Static Low-Angle Light-Scattering Study." *Journal of Physical Chemistry* **1989**, *93*, 4894-4898.
- [73] Cates, M. E.; Candau, S. J. "Statics and Dynamics of Worm-Like Surfactant Micelles." *Journal of Physics-Condensed Matter 0he,England Univ Strasbourg 1,Spectrometrie & Imagerie Ultrasonores Lab,F-67070 Strasbourg,France* **1990**, *2*, 6869-6892.
- [74] Kumar, R.; Kalur, G. C.; Ziserman, L.; Danino, D.; Raghavan, S. R. "Wormlike micelles of a C22-tailed zwitterionic betaine surfactant: From viscoelastic solutions to elastic gels." *Langmuir* **2007**, *23*, 12849-12856.
- [75] Glatter, O. "New Method for Evaluation of Small-Angle Scattering Data." *Journal of Applied Crystallography* **1977**, *10*, 415-421.

- [76] Hiemenz, P. C.; Rajagopalan, R. *Principles of Colloid and Surface Chemistry, 3rd Ed.*; Marcel Dekker: New York, 1997.
- [77] Pedersen, J. S. "Analysis of small-angle scattering data from colloids and polymer solutions: modeling and least-squares fitting." *Advances in Colloid and Interface Science* **1997**, *70*, 171-210.
- [78] Hubbard, F. P.; Santonicola, G.; Kaler, E. W.; Abbott, N. L. "Small-angle neutron scattering from mixtures of sodium dodecyl sulfate and a cationic, bolaform surfactant containing azobenzene." *Langmuir* **2005**, *21*, 6131-6136.
- [79] Hassan, P. A.; Fritz, G.; Kaler, E. W. "Small angle neutron scattering study of sodium dodecyl sulfate micellar growth driven by addition of a hydrotropic salt." *Journal of Colloid and Interface Science* **2003**, *257*, 154-162.
- [80] Imae, T.; Tsubota, T.; Okamura, H.; Mori, O.; Takagi, K.; Itoh, M.; Sawaki, Y. "Photocyclodimerization of Cinnamic Acid on a Reaction Matrix - Structural Effect of Molecular Assemblies Constructed by Amphiphilic Compounds." *Journal of Physical Chemistry* **1995**, *99*, 6046-6053.
- [81] Eastoe, J.; Sanchez-Dominguez, M.; Wyatt, P.; Heenan, R. K. "A photo-responsive organogel." *Chemical Communications* **2004**, 2608-2609.
- [82] Murata, K.; Aoki, M.; Suzuki, T.; Harada, T.; Kawabata, H.; Komori, T.; Ohseto, F.; Ueda, K.; Shinkai, S. "Thermal and Light Control of the Sol-Gel Phase-Transition in Cholesterol-Based Organic Gels - Novel Helical Aggregation Modes as Detected by Circular-Dichroism and Electron-Microscopic Observation." *Journal of the American Chemical Society* **1994**, *116*, 6664-6676.
- [83] Luisi, P. L. S., R.; Haering, G.; Schurtenberger, P. "Organogels from Water-in-Oil Microemulsions." *Colloid and Polymer Science* **1990**, *268*, 356-374.
- [84] Schurtenberger, P. M., L. J.; King, S. M.; Lindner, P. "Cylindrical Structure and Flexibility of Polymer-Like Lecithin Reverse Micelles." *Journal of Physical Chemistry* **1991**, *95*, 4173-4176.
- [85] Schurtenberger, P. S., R.; Luisi, P.L. "Viscoelastic Properties of Polymer-Like Reverse Micelles." *Rheologica Acta* **1989**, *28*, 372-381.
- [86] Schurtenberger, P. S., R.; Magid, L. J.; Leser, M. E.; Luisi, P. L. "Structural and Dynamic Properties of Polymer-Like Reverse Micelles." *Journal of Physical Chemistry* **1990**, *94*, 3695-3701.
- [87] Shchipunov, Y. A. "Lecithin organogel - A micellar system with unique properties." *Colloids and Surfaces a-Physicochemical and Engineering Aspects* **2001**, *183*, 541-554.

- [88] Snook, M. E.; Fortson, P. J.; Chortyk, O. T. "Gel Chromatography for the Isolation of Phenolic-Acids from Tobacco Leaf." *Analytical Chemistry* **1981**, *53*, 374-377.
- [89] Takeshita, K.; Hirota, N.; Terazima, M. "Enthalpy changes and reaction volumes of photoisomerization reactions in solution: azobenzene and p-coumaric acid." *Journal of Photochemistry and Photobiology a-Chemistry* **2000**, *134*, 103-109.
- [90] Nollet, L. M. L. "Food analysis by HPLC." *Published by CRC Press* **2000**.
- [91] Kort, R.; Vonk, H.; Xu, X.; Hoff, W. D.; Crielaard, W.; Hellingwerf, K. J. "Evidence for trans-cis isomerization of the p-coumaric acid chromophore as the photochemical basis of the photocycle of photoactive yellow protein." *Febs Letters* **1996**, *382*, 73-78.
- [92] Kumar, R.; Raghavan, S. R. "Photogelling fluids based on light-activated growth of zwitterionic wormlike micelles." *Soft Matter* **2009**, *5*, 797-803.
- [93] Tung, S. H.; Huang, Y. E.; Raghavan, S. R. "A new reverse wormlike micellar system: Mixtures of bile salt and lecithin in organic liquids." *Journal of the American Chemical Society* **2006**, *128*, 5751-5756.
- [94] Islam, M. F.; Jenkins, R. D.; Bassett, D. R.; Lau, W.; Ou-Yang, H. D. "Single chain characterization of hydrophobically modified polyelectrolytes using cyclodextrin/hydrophobe complexes." *Macromolecules* **2000**, *33*, 2480-2485.
- [95] Liao, D. S.; Dai, S.; Tam, K. C. "Rheological properties of a telechelic associative polymer in the presence of alpha- and methylated beta-cyclodextrins." *Journal of Physical Chemistry B* **2007**, *111*, 371-378.
- [96] Jeong, B.; Kibbey, M. R.; Birnbaum, J. C.; Won, Y. Y.; Gutowska, A. "Thermogelling biodegradable polymers with hydrophilic backbones: PEG-g-PLGA." *Macromolecules* **2000**, *33*, 8317-8322.
- [97] Bossard, F.; Tsitsilianis, C.; Yannopoulos, S. N.; Petekidis, G.; Sfika, V. "A novel thermothickening phenomenon exhibited by a triblock polyampholyte in aqueous salt-free solutions." *Macromolecules* **2005**, *38*, 2883-2888.
- [98] Nair, L. S.; Starnes, T.; Ko, J. W. K.; Laurencin, C. T. "Development of injectable thermogelling chitosan-inorganic phosphate solutions for biomedical applications." *Biomacromolecules* **2007**, *8*, 3779-3785.
- [99] Kalur, G. C.; Frounfelder, B. D.; Cipriano, B. H.; Norman, A. I.; Raghavan, S. R. "Viscosity increase with temperature in cationic surfactant solutions due to the growth of wormlike micelles." *Langmuir* **2005**, *21*, 10998-11004.

- [100] Davies, T. S.; Ketner, A. M.; Raghavan, S. R. "Self-assembly of surfactant vesicles that transform into viscoelastic wormlike micelles upon heating." *Journal of the American Chemical Society* **2006**, *128*, 6669-6675.
- [101] Kidowaki, M.; Zhao, C. M.; Kataoka, T.; Ito, K. "Thermoreversible sol-gel transition of an aqueous solution of polyrotaxane composed of highly methylated alpha-cyclodextrin and polyethylene glycol." *Chemical Communications* **2006**, 4102-4103.
- [102] Kamibayashi, M.; Ogura, H.; Otsubo, Y. "Viscosity behavior of silica suspensions flocculated by associating polymers." *Journal of Colloid and Interface Science* **2005**, *290*, 592-597.
- [103] Kamibayashi, M.; Ogura, H.; Otsubo, Y. "Rheology of complex suspensions flocculated by associating polymers." *Journal of Rheology* **2006**, *50*, 1009-1023.
- [104] Hammouda, B.; Ho, D.; Kline, S. "SANS from poly(ethylene oxide)/water systems." *Macromolecules* **2002**, *35*, 8578-8585.
- [105] Hammouda, B.; Ho, D. L.; Kline, S. "Insight into clustering in poly(ethylene oxide) solutions." *Macromolecules* **2004**, *37*, 6932-6937.
- [106] Brackman, J. C.; Engberts, J. "Influence of polymers on the micellization of cetyltrimethylammonium salts." *Langmuir* **1991**, *7*, 2097-2102.
- [107] Harada, A.; Kamachi, M. "Complex formation between poly(ethylene glycol) and alpha-cyclodextrin." *Macromolecules* **1990**, *23*, 2821-2823.
- [108] Harada, A.; Li, J.; Kamachi, M. "Preparation and properties of inclusion complexes of poly(ethylene glycol) with alpha-cyclodextrin." *Macromolecules* **1993**, *26*, 5698-5703.
- [109] Harada, A.; Takashima, Y.; Yamaguchi, H. "Cyclodextrin-based supramolecular polymers." *Chemical Society Reviews* **2009**, *38*, 875-882.
- [110] Mwakibete, H.; Cristantino, R.; Bloor, D. M.; Wynjones, E.; Holzwarth, J. F. "Reliability of the experimental methods to determine equilibrium-constants for surfactant cyclodextrin inclusion complexes." *Langmuir* **1995**, *11*, 57-60.
- [111] Tsianou, M.; Alexandridis, P. "Control of the rheological properties in solutions of a polyelectrolyte and an oppositely charged surfactant by the addition of cyclodextrins." *Langmuir* **1999**, *15*, 8105-8112.
- [112] Funasaki, N.; Ishikawa, S.; Neya, S. "Binding of short-chain lecithin by beta-cyclodextrin." *Langmuir* **2002**, *18*, 1786-1790.

- [113] Meier, W.; Hotz, J.; GuntherAusborn, S. "Vesicle and cell networks: Interconnecting cells by synthetic polymers." *Langmuir* **1996**, *12*, 5028-5032.
- [114] Ashbaugh, H. S.; Boon, K.; Prud'homme, R. K. "Gelation of "catanionic" vesicles by hydrophobically modified polyelectrolytes." *Colloid and Polymer Science* **2002**, *280*, 783-788.
- [115] Lee, J. H.; Gustin, J. P.; Chen, T. H.; Payne, G. F.; Raghavan, S. R. "Vesicle-biopolymer gels: Networks of surfactant vesicles connected by associating biopolymers." *Langmuir* **2005**, *21*, 26-33.